

The Taurus Spitzer Survey: New Candidate Taurus Members Selected Using Sensitive Mid-Infrared Photometry

L. M. Rebull¹, D. L. Padgett¹, C.-E. McCabe¹, L. A. Hillenbrand², K. R. Stapelfeldt³, A. Noriega-Crespo¹, S. J. Carey¹, T. Brooke¹, T. Huard⁴, S. Terebey⁵, M. Audard^{6,7}, J.-L. Monin⁸, M. Fukagawa⁹, M. Güdel¹⁰, G. R. Knapp¹¹, F. Menard⁸, L. E. Allen¹², J. R. Angione^{3,5}, C. Baldovin-Saavedra^{6,7}, J. Bouvier⁸, K. Briggs¹⁰, C. Dougados⁸, N. J. Evans¹³, N. Flagey¹, S. Guieu¹, N. Grosso¹⁴, A. M. Glauser^{10,15}, P. Harvey¹³, D. Hines¹⁶, W. B. Latter¹⁷, S. L. Skinner¹⁸, S. Strom¹², J. Tromp⁵, S. Wolf¹⁹

ABSTRACT

We report on the properties of pre-main-sequence objects in the Taurus molecular clouds as observed in 7 mid- and far-infrared bands with the Spitzer Space Telescope. There are 215 previously-identified members of the Taurus star-forming region in our ~ 44 square degree map; these members exhibit a range of Spitzer colors that we take to define young stars still surrounded by circumstellar dust (noting that $\sim 20\%$ of the bonafide Taurus members exhibit no detectable dust excesses). We looked for new objects in the survey field with similar Spitzer properties, aided

¹Spitzer Science Center/Caltech, M/S 220-6, 1200 E. California Blvd., Pasadena, CA 91125 (luisa.rebull@jpl.nasa.gov)

²Department of Astronomy, California Institute of Technology

³Jet Propulsion Laboratory

⁴University of Maryland, College Park

⁵California State University, Los Angeles

⁶ISDC Data Center for Astrophysics, University of Geneva, Ch. d'Ecogia 16, CH-1290 Versoix, Switzerland

⁷Observatoire de Genève, University of Geneva, Ch. des Maillettes 51, 1290 Versoix, Switzerland

⁸Laboratoire d'Astrophysique de Grenoble, Université de Grenoble – CNRS, UMR 5571, Grenoble, France

⁹Department of Earth and Space Science, Graduate School of Science, Osaka University, 1-1 Machikaneyama, Toyonaka, Osaka 560-0043 Japan Nagoya University, Japan

¹⁰ETH Zurich, Institute of Astronomy, 8093 Zurich, Switzerland

¹¹Princeton University

¹²NOAO, Tucson, AZ

¹³University of Texas, Austin

¹⁴Observatoire astronomique de Strasbourg, Université de Strasbourg, CNRS, INSU, 11 rue de l'Université, 67000 Strasbourg, France

¹⁵UK Astronomy Technology Centre, Royal Observatory, Edinburgh EH9 3HJ, UK

¹⁶Space Science Institute

¹⁷NASA Herschel Science Center, IPAC, Pasadena, CA 91125

¹⁸CASA, University of Colorado, Boulder, CO 80309-0389

¹⁹University of Kiel, Institute of Theoretical Physics and Astrophysics, Leibnizstrasse 15, 24098 Kiel, Germany

by extensive optical, X-ray, and ultraviolet imaging, and found 148 candidate new members of Taurus. We have obtained follow-up spectroscopy for about half the candidate sample, thus far confirming 34 new members, 3 probable new members, and 10 possible new members, an increase of 15-20% in Taurus members. Of the objects for which we have spectroscopy, 7 are now confirmed extragalactic objects, and one is a background Be star. The remaining 93 candidate objects await additional analysis and/or data to be confirmed or rejected as Taurus members. Most of the new members are Class II M stars and are located along the same cloud filaments as the previously-identified Taurus members. Among non-members with Spitzer colors similar to young, dusty stars are evolved Be stars, planetary nebulae, carbon stars, galaxies, and AGN.

Subject headings: stars: formation – stars: circumstellar matter – stars: pre-main sequence – infrared: stars

1. Introduction

A complete inventory of all the coeval stars in a young stellar association, cluster, or group (hereafter “association”) enables studies of the initial mass function (IMF), disk fraction, and stellar rotational properties, among other pursuits. Information from associations with a range of ages enables understanding of the overall formation and evolution of young stars, including the change with time of disk fraction and stellar rotation rate. However, identifying all of the member stars of a given young association can be quite difficult. (By “member,” we mean objects that are clearly young, close to the same age, and often still associated with their natal cloud.) Finding all such members requires that one employ multiple observational techniques. These methods include but are not limited to X-ray surveys (e.g., Alcalá et al. 1996, Wolk et al. 2006), H α surveys (e.g., Ogura et al. 2002), variability surveys (e.g., Carpenter et al. 2001, Rebull 2001), ultraviolet (UV) surveys (e.g., Rebull et al. 2000), and infrared (IR) surveys (e.g., Jørgensen et al. 2006, Rebull et al. 2007). At each wavelength, we can use the fact that stellar youth implies more flux at a given radiometric band (X-rays, H α , UV, IR), or more flux variability, than older stars of comparable mass, allowing separation of association members from field contaminants. When we combine the information from surveys in multiple wavelengths, we must remember that the influence of extinction due to circumstellar matter and/or the molecular cloud is vastly different at different wavelengths; extinction affects UV and optical wavelengths much more strongly than IR. For young associations, many, but not all, legitimate members are identifiable using just one or a few survey methods.

There are advantages and disadvantages to studying nearby young associations. Identification of young members in an association is made easier if the objects are located at smaller heliocentric distances and therefore brighter on the whole. This is especially the case for low-mass members with very low luminosities; a complete census of these stars and brown dwarfs can be made only for very nearby star-forming regions. On the other hand, nearby star-forming molecular clouds cover large areas of sky and therefore require large investments of observing time. At just 137 pc (with a depth of ~ 20 pc; Torres et al. 2007, 2009), the Taurus star-forming region is one of the closest large cloud complexes with hundreds of low-mass stars, ongoing star formation, and objects ranging in age up to ~ 5 Myr. Studies of Taurus objects have significantly influenced our basic understanding of the star-formation process for decades (e.g., Herbig & Rao 1972, Kenyon et al. 2008). However, the Taurus Molecular Cloud is close enough that it subtends more than 100 square degrees of sky; surveying all or even most of it is difficult within typical telescope time allocations.

Infrared surveys led to the discovery that some stars have infrared excesses, interpreted as circumstellar

matter (e.g., Aumann et al. 1984, Beichman et al. 1986). Most if not all low-mass stars form with circumstellar accretion disks, resulting in IR excesses for as long as the dusty circumstellar material survives (e.g., Hernandez et al. 2007). By using IR to survey a star-forming region, the stars with IR excesses are relatively easily distinguished from stars without such excesses. The Spitzer Space Telescope (Werner et al. 2004) provides an excellent platform for surveying star-forming regions in the mid-IR and far-IR, enabling stars with IR excesses to be identified; the member stars which do not have IR excesses must be recovered using different techniques such as the ones listed above. Because Spitzer relatively efficiently maps large regions of sky, it is a particularly useful tool for surveying large star forming regions.

We have conducted a large multi-wavelength imaging and spectroscopic survey of the Taurus Molecular Cloud (TMC) in order to test if our inventory of Taurus members with infrared excesses is, in fact, complete. The Spitzer imaging component is referred to as the Taurus Spitzer Survey, and is described by Padgett et al. (2008; hereafter P08) and Padgett et al. (2009; hereafter P09). It covers ~ 44 square degrees from 3.6 to 160 μm and is a Spitzer Legacy Project, so enhanced data products have been delivered back to the Spitzer Science Center (SSC), including the catalogs on which this present paper is based. In addition to the Spitzer component, there are four other major components to our Taurus survey. XMM-Newton was used by the XMM-Newton Extended Survey of the Taurus Molecular Cloud (XEST) program (e.g., Güdel et al. 2007 and references therein), which mapped ~ 5 square degrees, most of which was also mapped by the Spitzer observations; the XEST data include X-ray imaging but also include ultraviolet data from the XMM-Newton Optical Monitor (Audard et al. 2007). XEST was deliberately pointed towards aggregates of previously identified Taurus members. In the optical, the Canada-France-Hawaii Telescope (CFHT) survey (Monin et al. in preparation; Güdel, Padgett, & Dougados 2007) mapped ~ 28 square degrees (all of which are encompassed by the Spitzer area), and the Sloan Digital Sky Survey (SDSS) (Finkbeiner et al. 2004; Padmanabhan et al. 2008) mapped ~ 48 square degrees in two perpendicular strips, about half of which overlaps the Spitzer area. Finally, the Five College Radio Astronomy Observatory (FCRAO) millimeter wavelength survey (Goldsmith et al. 2008) mapped ~ 100 square degrees in the CO(1-0) line, covering the Spitzer survey area entirely. The relative coverages of these surveys is shown in P09. Our extended collaboration has already begun to use this rich dataset to search for new members of Taurus; Scelsi et al. (2007,2008) identified new candidate members using the XEST data, and Guieu et al. (2006, 2007) identified new brown dwarf members using the CFHT data to study their disk properties using the Spitzer data. Ongoing investigations include searches for members via emission line spectra (Knapp et al., in prep), Herbig-Haro (HH) objects (Stapelfeldt et al. in prep), and transition disks (McCabe et al. in prep).

In this paper, we select new candidate Taurus members with infrared excesses using Spitzer and Two-Micron All-Sky Survey (2MASS; Skrutskie et al. 2006) data. We construct color-magnitude and color-color diagrams for point sources, then use the locations of previously-identified young stars in these diagrams to select new candidate members with infrared excesses. To discard obvious extragalactic sources, we examine the source morphology in all available bands of the multiwavelength Taurus survey. We construct spectral energy distributions (SEDs) from the photometry over all available bands, again discarding objects we believe to be galaxies. Follow-up spectroscopy has been obtained to assess whether or not our new candidate Taurus objects are likely Taurus members. We also present Spitzer flux densities for the 215 previously-identified members found in the region covered by our Spitzer survey. Note that (a) the 215 previously-identified objects include those members without infrared excesses identified via other mechanisms; (b) the 215 previously-identified objects are those covered by our Spitzer map – there are other legitimate Taurus members outside the region we observed, such as in L1551; (c) our new candidate member list is necessarily just those with IR excesses and exclusively within the regions covered by our Spitzer observations. Some objects are resolved in one or more of the Spitzer images, and extended source photometry may be a better representation of

the complete flux from the object; many of the extended sources are discussed individually in other papers (e.g., Tobin et al. 2008, Stapelfeldt et al. in prep)

The observations, data reduction, and ancillary data are described in §2. Section 3 describes our young stellar object (YSO) selection process which is based on the colors of previously-identified Taurus members, also presented here. We describe 34 objects that we have, thus far, identified as new members of Taurus (plus 3 probable new members and 10 possible new members) in §4 and discuss the properties of the new objects in conjunction with (and comparison to) the previously-identified members of Taurus. Finally, we summarize our main points in §5. The Appendix contains spectral energy distributions and discussion of some specific objects.

2. Observations, Data Reduction, and Ancillary Data

2.1. Spitzer data

P08 and P09 present a comprehensive discussion of the Spitzer data acquisition, reduction, and band-merging to the 2MASS data. In summary, we conducted the observations using IRAC (Infrared Array Camera; 3.6, 4.5, 5.8, & 8 μm ; Fazio et al. 2004) and MIPS (Multi-band Imaging Photometer for Spitzer; 24, 70, & 160 μm ; Rieke et al. 2004) in two epochs to enable removal of asteroids from the final point-source catalog. The observations were spread over three observing programs and three years, 2005 to 2007.

For IRAC, we used MOPEX (MOsaicking and Point source EXtractor; Makovoz & Marleau 2005) to find the sources, and IDL to perform aperture photometry at those locations. With our IRAC observations, we sacrificed redundancy for spatial coverage, and obtained just 2 IRAC frames per position (total integration time of 25.2 seconds), so instrumental artifacts are abundant. We discarded single-band (apparent) detections as likely artifacts. Objects that we measured to be brighter than the 0.6 sec saturation limits (630, 630, 4600, and 2500 mJy at the four IRAC channels) we took to be saturated, and these appear as lower limits in our catalog. The zero-points we used to convert between flux densities and magnitudes were as found in the IRAC Data Handbook on the SSC website: 280.9, 179.7, 115.0, and 64.13 Jy for IRAC’s four channels, respectively.

For MIPS, we used MOPEX point-response-function (PRF) fitting photometry at 24 and 70 μm . The total integration time at 24 μm was 30 seconds per position; the MIPS scan legs were interleaved to provide complete coverage at 70 μm , and a total integration time of 15 seconds per position. We took objects brighter than 4.7 Jy at 24 μm and 6.5 Jy at 70 μm to be saturated (or at least non-linear). These objects appear in our catalog as having lower flux density limits. Following the MIPS Data Handbook on the SSC website, the zero-points that convert between flux densities and magnitudes are 7.14 and 0.775 Jy for MIPS-24 and 70.

The observations at 160 μm present special challenges. All of the things that can affect the other bands (such as saturation, extended emission, confusion with the cloud background and nearby objects – whether they be Taurus or background objects – and instrumental artifacts), also affect this band. Because the Taurus cloud emission and instrumental effects are both very strong, and because the resolution is the poorest of all the Spitzer bands, these items are of particular concern at this bandpass. Additionally, due to scattered data gaps in our 160 μm map (see P08,P09), measurements (or limits) at 160 μm are missing or compromised for some sources. MOPEX does not detect any point sources automatically at 160 μm , because all detected point-like objects appear to be slightly resolved. For ~ 100 objects that were apparent by eye in

the 160 μm image (or for which limits were of interest for this paper), we performed aperture photometry on the cleaned image which was smoothed by a 4 pixel median filter to minimize the influence of holes in the map and image artifacts. We used a $32''$ aperture, an annulus from 64-128'', and an aperture correction of 1.97 (valid for temperatures between 500 and 2000 K¹). Based on a comparison of the flux densities obtained from the filtered image and the unfiltered image, we took the flux density uncertainties to be 20% below 5 Jy and 30% for higher flux densities. Some objects that fell in regions with too many missing flux density values (from saturation or gaps in the map) are not retrievable and thus do not have a measurement (or limits); in essence, they are off the edge of the map. Visual inspection of each 160 micron source was used in order to determine whether the object was clearly detected as a single point source, confused with another nearby source, or contaminated by data dropouts and/or saturation issues which would cause the reported flux density to be a lower limit; these are indicated in the data tables below. The zero-point for MIPS-160 is 0.159 Jy, again from the MIPS Data Handbook on the SSC website.

We extracted JHK_s data from the 2MASS point source catalog for our region, retaining flux densities only for those objects with high-quality 2MASS data flags. There were a handful of objects of interest for this paper for which we made the following manual modifications, and therefore these modified values were used for the color-magnitude diagrams (CMDs) and spectral energy distributions (SEDs) below. Measurements for five objects did not meet the data flag criteria we imposed on the 2MASS catalog, but their as-reported flux densities were completely consistent with the rest of their SED, so we adopted their measurements as good detections; these objects are SST Tau 041542.7+290959, 041542.7+290959, 042517.6+261750, 043835.4+261041, and 043354.7+261327. Flux densities for one or more bands for the following previously-identified Taurus members do not exist in the point source catalog, and thus the flux densities used below were taken from the extended source catalog: SST Tau 042757.3+261918, 044112.6+254635, 043535.3+240819, and 043316.5+225320.

We bandmerged all the available point sources between 2 and 70 microns using position matching alone, with a wavelength-dependent maximum matching radius. Sources between 2 and 8 μm were matched over a radius of $1''$, and at 24 μm , the matching radius to the rest of the catalog was $2''$. All matching radii are values empirically determined by inspection of histograms of nearest neighbors between bands, and spot-checking individual sources; histograms of positional offsets and additional discussion appears in P09. We pre-merged the 24 and 70 μm catalogs before merging to the rest of the catalog using an empirically-determined radius of $10''$. Because the spatial resolution of the 70 μm images is so much worse than the 2 μm images, often more than one NIR (or optical) source can be matched to the 70 μm source; however, it is extremely likely that if we detect a source at 70 μm , it will also appear at 24 μm , so by implementing the pre-merge of 24 and 70 μm , we are preferentially matching the 70 μm sources to a likely physical match.

We include here a brief aside on the accuracy of blind merging by position. In the generic case of surveys across wavelengths, relative astrometric accuracy and spatial resolution is paramount. In our case of a catalog primarily driven by Spitzer+2MASS sources, astrometric accuracy is not the dominant source of error, since each instrument is internally consistent and calibrated to the 2MASS coordinate system. For many star-forming regions studied with Spitzer, e.g., many of those observed by the Cores-to-Disks (c2d; Evans et al. 2003) and Gould’s Belt (Allen et al. in preparation) projects, the source surface density is high enough that blind merging by position causes an unacceptable rate of false matches, and multiple short-wavelength sources should in reality be assigned to a single long-wavelength source. However, the source

¹The dust we see at 160 μm is likely to be cooler than this, but the aperture correction changes only by 0.7% between this temperature range and 50 K, well within the uncertainties.

surface density in Taurus is low enough (~ 4 sources per square arcminute, compared to ~ 20 in some star-forming regions) that source confusion in general is not as much of a concern. On the other hand, in Taurus, many objects are known to be close binaries, and we do not apportion the flux density we observe between the two objects; for close binaries, we have treated the object as single here. In any case, in three of the objects investigated in detail for this paper ($<1\%$ of the objects investigated, $<0.5\%$ of the total number of $70\ \mu\text{m}$ sources in the entire catalog), we determined by individual inspection that the $24/70$ flux densities were incorrectly matched to a nearby faint short-wavelength source, rather than the correct, bright, slightly farther away, short-wavelength source. In these cases, we manually tweaked the flux assignment; the position change is well within the expected uncertainties between the long- and short-wavelength catalogs. We are confident that for the large majority of the sources in our entire catalog, our blind merging by position works, but for any particular source not discussed here, the images and the flux assignment in our delivered catalogs should be carefully scrutinized.

In creating our Spitzer-centric catalog, we dropped any object without a Spitzer detection (e.g., sources off the edges of our maps) before proceeding and after each additional merging step below (e.g., when combining the SDSS catalog and the Spitzer catalog, we did not retain SDSS-only sources from off the edges of our map or whose SED falls so rapidly that they are too faint for our shallow Spitzer survey). There are nearly 700,000 sources in the catalog with Spitzer flux densities in at least one band. This does not include the asteroids, which will be discussed by Hines et al., in preparation. It also does not include sources that are substantially extended (except at $160\ \mu\text{m}$, see below); many of those will be covered by Stapelfeldt et al., in preparation. The vast majority of the $\sim 700,000$ sources are well behind the Taurus Molecular Cloud. Sources which are members are generally expected to be bright in the shorter bands and detected in multiple bands.

P09 discusses the survey sensitivity in detail. In summary, the 3.6 and $4.5\ \mu\text{m}$ sensitivities are quite comparable, and 98% of the objects detected in $3.6\ \mu\text{m}$ are also detected at $4.5\ \mu\text{m}$. The 5.8 and $8\ \mu\text{m}$ channels are much less sensitive; only 22% of the objects detected at $3.6\ \mu\text{m}$ are also detected at $5.8\ \mu\text{m}$, and just 17% of the objects detected at $3.6\ \mu\text{m}$ are also detected at $8\ \mu\text{m}$ (where nebulosity can also be a factor in point source identification and extraction). Our 24 , 70 , and $160\ \mu\text{m}$ sensitivity is a strong function of position in the image because of nebular and high Zodiacal dust emission contributions to the background. In part because of the varying background but also because of the effective sensitivity of the instrument to photospheres at the distance of Taurus given our exposure times, just 1.4% of the objects detected at $3.6\ \mu\text{m}$ are also detected at $24\ \mu\text{m}$, and just 0.15% are detected at $70\ \mu\text{m}$. The faintest independent $24\ \mu\text{m}$ detection is ~ 10 th mag ($\sim M2$ spectral type photosphere at Taurus age and distance), and the histogram of detections turns over at ~ 9.3 mags (e.g., there is a steep fall-off between $[24]\sim 9.3$ and 10 , where the bracket notation denotes the magnitude at that band). Similarly, at $70\ \mu\text{m}$, the faintest object is $[70]\sim 3.5$, and a more typical value is 2.5 - 2.7 (note that $70\ \mu\text{m}$ is much more strongly affected by nebular emission and instrumental effects than $24\ \mu\text{m}$). Only O or B photospheres would be that bright at the distance of Taurus, so we can only detect legitimate Taurus objects at 70 (or 160) μm which have substantial IR excesses.

A full completeness analysis is given by P09, but as another independent way of assessing our completeness, we examined by hand each of the images at each of the Spitzer bands for each of the previously identified Taurus members and new candidate Taurus members discussed here (see §3.1.1 and §3.1). If the object could be seen in the image but a flux density was not initially reported at that band, we made a manual assessment of the flux density or upper/lower limit, as appropriate. For IRAC, ~ 1 - 2% (depending on the band) of the previously identified Taurus members and ~ 4 - 11% of the new candidate members were missing photometry and were filled in manually (having lower signal-to-noise). The most common band in

which flux densities were erroneously missing (e.g., not in the automatically generated catalog but visible in the images) was $5.8 \mu\text{m}$, which is not particularly surprising, as this is the least sensitive of the IRAC bands. For MIPS, $\sim 9\%$ of the previously identified Taurus members were missing photometry in either 24 or $70 \mu\text{m}$, and $\sim 6\%$ of the new candidate objects were missing photometry at 24 or $70 \mu\text{m}$. The lower fraction of missing photometry in the new candidate objects as compared to the previously identified objects is a reflection of the fact that our selection mechanism is somewhat biased towards objects with MIPS detections; see §4.1 below.

Many sources detected at shorter wavelengths are undetected at longer wavelengths, and it is important for our science analysis to obtain upper limits for our sources in the Spitzer photometric bands. For the list of coordinates of previously identified and new candidate Taurus members, at $24 \mu\text{m}$, we used MOPEX to look for a source whose photometry could be obtained via PRF-fitting at that location. If an object was detected, we took a weighted average flux density based on all detections (e.g., between epochs and tiles). If the final signal-to-noise ratio (SNR) was <3 , we took the error to be the 1σ upper limit, and multiplied by 3 to get the 3σ limits found in the data tables below and SEDs in §A. If the PRF fitting failed, we performed aperture photometry at the location of the object (at each tile and epoch available), and took a weighted average of all the resultant positive aperture flux densities. If that average had a SNR >3 , we took that weighted average to be a detection. For all objects that had SNR <3 , we took the upper limit to be the 1σ limit (and multiplied by 3 to get the 3σ limits found in the data tables and SEDs below). If all the measured aperture flux densities were negative, we took the 1σ limit to be the straight average of the errors (and multiplied by 3 to get the 3σ limits found in the tables and SEDs below). Finally, still at $24 \mu\text{m}$, the objects that cannot be resolved from a companion are reported as simply unknown, where the presence of a companion is known from shorter-wavelength higher-spatial-resolution observations. At $70 \mu\text{m}$, some objects are unresolved from a nearby object and are impossible to estimate (again, where the presence of a companion is known from shorter-wavelength higher-spatial-resolution observations). Upper limits at $70 \mu\text{m}$ for all remaining undetected sources were obtained by performing aperture photometry at the expected source location, using a $35''$ aperture and a multiplicative aperture correction of 1.22, as discussed in the MIPS Data Handbook, available at the SSC website. These $1\text{-}\sigma$ errors were multiplied by 3 to get the $3\text{-}\sigma$ errors shown in the Tables and Figures here. Upper limits at $160 \mu\text{m}$ were individually assessed using aperture photometry on the uncertainty image using the same parameters as for detected sources above ($32''$ aperture, an annulus from $64\text{-}128''$, and an aperture correction of 1.97) to obtain $1\text{-}\sigma$ errors, and then multiplied by 3 to get the $3\text{-}\sigma$ errors shown in the Tables and Figures here.

2.2. Complementary survey photometric data

In §2.1, above, we discussed merging the 2MASS and Spitzer data. We also need to match our catalog to the other Taurus surveys, listed in §1 above. Again, we match by position, with a radial offset tolerance customized empirically to each band or catalog.

The extracted CFHT point sources (see Monin et al. in preparation or Guieu et al. 2006 for more details on the extraction process; also see Monin et al. 2007 or Guieu 2008) are merged first to 2MASS. Sources that are CFHT-only are then dropped in order to remove objects that are very statistically likely to be instrumental artifacts. The CFHT sources are then merged to the Spitzer catalog. The CFHT I bandpass is converted to Cousins I via the following equation:

$$I_C = I_{CFHT} - 0.531 \times (I_{CFHT} - z_{CFHT}) - 0.278 \quad (1)$$

and then converted to flux densities using the Cousins I zero-point from Bessell (1979), $2.55 \times 10^{-23} \text{ W m}^{-2} \text{ Hz}^{-1}$. For these points, we use the I_C effective wavelength of $0.79 \mu\text{m}$. About 138,000 of the point sources in our catalog have CFHT I_C magnitudes (20% of the entire catalog).

The SDSS photometry arrives from the SDSS pipeline with photometric measurements in *ugriz* in flux density units of nanomaggies², which can be converted to the same flux density units as the rest of the catalog data. We retained only those flux density measurements with good quality flags, and we merged the source lists for each of the SDSS tiles to each other by position to remove duplicates before merging to the master Spitzer catalog. The effective wavelengths are 3590, 4810, 6230, 7640, and 9060 Å for *ugriz*, respectively. We also made note of whether the object appearing in the SDSS images was flagged by the pipeline as extended or not. There are SDSS z -band flux densities for about 300,000 objects in our catalog (45% of the entire catalog). There are 6400 spectra available from SDSS, about 3400 of which overlap the Spitzer survey region; for each object, we matched by position to our Spitzer catalog, and accepted the spectral classification produced by the SDSS pipeline as a spectral classification of the object, unless another spectral classification was available in the literature (see below).

There are ~ 1000 objects in our catalog (0.1% of the entire catalog) with X-ray measurements from the XEST survey (Güdel et al. 2007). The XEST catalog includes flux densities from the XMM-Newton Optical Monitor (OM). The OM has a field of view comparable to, but not exactly identical to, the main X-ray field of view; see Audard et al. (2007) for more discussion of the XEST-OM sample. These data are in one of three ultraviolet bandpasses (U , UVW1, or UVW2). To convert these values to flux densities, we used the following equation, found in the XMM-Newton OM calibration document (Chen et al. 2004):

$$F_\nu = 10^{(0.4(Z-m))} \times f \times \lambda^2 / c \times 10^{23} \quad (2)$$

where m is the reported magnitude (and F_ν the flux density) for a given object, $Z = 18.259$, 17.204 , and 14.837 , and $f = 1.94 \times 10^{-16}$, 4.76×10^{-16} , and $5.71 \times 10^{-15} \text{ ergs cm}^{-2} \text{ s}^{-1} \text{ Å}^{-1} \text{ counts}^{-1} \text{ sec}$ for U , UVW1, and UVW2 (respectively). In the equation, λ is in units of Å, and c is $3 \times 10^{18} \text{ Å s}^{-1}$. The effective wavelengths are 0.344 , 0.291 , and $0.212 \mu\text{m}$ for U , UVW1, and UVW2. There are ~ 1600 objects with XMM-Newton OM flux densities in our catalog (0.2% of the entire catalog).

We note that many of the X-ray detected XEST sources are likely background galaxies (see Güdel et al. 2007) and that XEST included regions not covered by our map, such as L1551.

The XEST team assembled a catalog of supporting data from the literature, such as optical photometric measurements, for all of the previously-identified Taurus members (see §3.1.1 below); we have included these photometric points in our database, converting Johnson magnitudes to flux densities using zero-points available in the literature (e.g., Cox 2001 and references therein).

The SEDs presented in this paper use all of these supporting data where available (except for the X-ray fluxes), and are presented as λF_λ in cgs units ($\text{erg s}^{-1} \text{ cm}^{-2}$), against λ in microns.

²In SDSS, a “maggy” is the ratio of the flux density of the object to a standard flux density. The Sloan magnitudes are AB magnitudes, as opposed to Vega magnitudes. In the AB system, a flat spectrum object with 3631 Jy at each band should have every magnitude equal to zero, and all maggies equal to one. Flux densities returned by the Sloan pipeline are nanomaggies, and can be converted to μJy . For more discussion, see Padmanabhan et al. (2008).

2.3. Spectroscopy

We obtained follow-up spectroscopy for $\sim 75\%$ of the candidate YSOs discussed in this paper. Some previously identified Taurus members missing spectral types in our database (as discussed in §3.1.1 below) were also observed. Data were obtained over six runs between 2007 and 2009 at Keck and the Palomar 200". Most of the $\gtrsim 200$ spectra are low-resolution optical, obtained with the Double Spectrograph at Palomar (30 Nov - 3 Dec 2008) or LRIS at Keck (Feb 2007). Many spectra were taken in the infrared with Triplespec at Palomar (21-24 Nov 2008 and 21 Dec 2008) or NIRSPEC at Keck (Dec 2007 and Feb 2008). The infrared spectra will be discussed in a forthcoming paper; the optical spectra are discussed here.

The optical spectra from Palomar are taken in two segments, blue and red; the blue covered ~ 3710 - 5660 Å at ~ 2 Å/px and the red, ~ 6230 - 8720 Å at ~ 2.5 Å/px. Instrument settings were a 316 lines mm^{-1} grating blazed at 7500 Å and used at grating angle 24.75° for the red side, and a 300 lines mm^{-1} grating blazed at 3900 Å and used at grating angle 23.12° for the blue side. LRIS at Keck is also a double-barreled spectrograph which we used with a 400 lines mm^{-1} grism blazed at 3400 Å in the blue and a 400 lines mm^{-1} grating blazed at 8500 Å and positioned at grating angle 23.49° in the red. We obtained continuous wavelength coverage from the blue atmospheric cutoff to ~ 9400 Å at 1.86 Å px^{-1} . The Double Spectrograph and LRIS data were both reduced using the Image Reduction and Analysis Facility (IRAF)³ ccdred and onedspec packages. Images were trimmed, bias-subtracted, and flattened prior to spectral extraction with the IRAF task `apall`. Wavelength calibration was performed using a Fe-Th-Ar lamp in the blue and Th-Ar lamp in the red. The wavelength solution was applied using the IRAF task `dispcor`. The white dwarf Feige 34 was observed each night, providing an approximate flux calibration reference for all the scientific targets.

Spectral classification was obtained via visual examination of each spectrum and comparison to a standard grid composed of >60 stars ranging in types from B8 to M9. Four authors performed the classification independently to achieve an estimated accuracy of roughly a subclass.

The red spectra included $\text{H}\alpha$. For each spectrum, we used IRAF to measure an equivalent width for $\text{H}\alpha$, following the usual convention where negative values indicate emission (see §4.1). We also noted if the Ca IR triplet was in emission at the time of observation; this is indicated in the data tables below.

The spectroscopic data are sufficient to rule out redshifted galaxies, to classify stars, and to find stars with $\text{H}\alpha$ in emission. However, our data are of insufficient resolution to, e.g., detect the presence of lithium, or determine surface gravities for most types. Section 4.1 discusses an analysis similar to that presented by Slesnick et al. (2008) which uses the TiO 8465 Å index and Na 8190 Å index to determine an estimate of the surface gravity of the star. Additional follow-up data will be required to assess membership for stars with no $\text{H}\alpha$ in emission and a small IR excess at Spitzer bands, and/or types earlier than M1 where the gravity analysis is not applicable.

³IRAF is distributed by the National Optical Astronomy Observatories, which are operated by the Association of Universities for Research in Astronomy, Inc., under cooperative agreement with the National Science Foundation.

3. YSO candidate selection

3.1. Overview of YSO selection process

First, we establish two comparison samples from the literature, and then we discuss the process by which we selected new candidate YSOs in Taurus.

3.1.1. *Template sample of previously-identified Taurus members*

We first informed our search for new Taurus members by determining the regions of color space occupied by previously identified Taurus members. By “Taurus member,” we mean an object that is confirmed via multiple mechanisms to be young and associated with the Taurus Molecular Cloud and the other Taurus members, e.g., sharing communal properties such as stellar activity. By “previously identified,” we mean identified as a member by other authors in the literature using data sets other than the Taurus Spitzer Legacy Survey. However, in order to appear in our catalog, the object must be within the region we mapped with Spitzer. There are legitimate Taurus members outside our region, including, e.g., those in the L1551 region.

The core of our sample of previously-identified Taurus members is the list assembled by the XEST team for their analysis (see Güdel et al. 2007 and references therein). We have updated this list with more recently confirmed objects (e.g., Scelsi et al. 2008), as well as scattered additional previously-identified Taurus members found in the literature. Kenyon et al. (2008) also report previously identified Taurus objects, with ~ 30 more objects in our Spitzer field of view, which we have also included (but see Appendix B.7 for one object from Kenyon et al. (2008) which we rejected). We have thus defined our sample of previously identified Taurus members as basically an updated XEST+Kenyon et al. list convolved with our survey coverage. There are 215 previously-identified Taurus members in our Spitzer maps. There are ~ 100 more objects from Kenyon et al. which are outside our mapped region. Binary objects that are unresolved in any of our Spitzer maps are regarded here as a single object (e.g., FS Tau Aab, whose separation is $< 1''$). We discuss the overall Spitzer properties of this list in some detail below. We note here that all of these 215 previously-identified Taurus members were detected by Spitzer, but not all of them have IR excesses; this list includes the young stars without IR excesses (e.g., mostly weak-lined T Tauri stars, WTTS) discovered by other means.

Hartmann et al. (2005) report IRAC observations of a set of previously identified members covered by IRAC guaranteed time observation (GTO) team observations. This region of the sky is also covered by our shallower map, to the same depth as the rest of our survey. Our photometry agrees within the errors expected from photometry methodology and from the intrinsic variability of the stars.

We do not include the objects reported by Luhman et al. (2006, 2009a,b) as previously known objects because they were found with an independent analysis of the same data used here – our Taurus Legacy data, in part along with the XEST data – and the derived values agree.

Scelsi et al. (2008) present spectroscopic follow-up on potential new Taurus members discovered by the XEST survey (Scelsi et al. 2007). Three confirmed new Taurus members from Scelsi et al. (2008) were independently discovered and confirmed by us using Spitzer data (SST Tau 043456.9+225835 = XEST 08-003, SST Tau 043542.0+225222 = XEST 08-033, and SST Tau 042215.6+265706 = XEST 11-078). Since we report these in the list of new Taurus members, these do not appear in the list of previously identified

Taurus members; they are noted in the tables below. The new members reported there that we did not rediscover are included in our list of previously identified Taurus members. A complete discussion of the Spitzer properties of all of the candidate members found using XEST X-rays that were presented by Scelsi et al. (2007) will appear in Audard et al., in preparation.

3.1.2. *Template sample of non-members*

Aside from previously-identified Taurus members, there are a large variety of other previously-identified objects in our survey region. Many of these are clearly not Taurus members, but some are more ambiguous. The previously-identified objects include known extragalactic objects, named objects of unknown nature, confirmed non-members, and potential (unconfirmed) members of Taurus.

To construct this list, we first searched in SIMBAD over our entire field to obtain a list of ~ 8000 known objects. For objects that did not already have high-precision coordinates, we went back to the original article reporting the discovery of the object and attempted re-identification of the object using finding charts and 2MASS images. If no finding charts were available, the brightest close object from 2MASS was assigned to the object’s name. Some objects are not recoverable, but most were identified; nearly 90% of the entire ~ 8000 -object list has high-accuracy coordinates in the end. New coordinates were reported back to the SIMBAD team for inclusion in their database.

We also included the results from several papers from the literature reporting specifically confirmed non-members. These confirmed non-members can be candidate member objects from other Taurus surveys such as Luhman et al. (2006) or Scelsi et al. (2008), that failed a spectroscopic test for membership. They can also be spectroscopically confirmed background giants from studies of the ISM (e.g., studies of the Taurus dark cloud). These confirmed non-members have not necessarily been ingested into SIMBAD, since they were not the primary scientific result of the paper. Note that we did not list as non-members those objects merely assumed but not confirmed (via spectroscopy) to be background giants.

We merged this list by position with our master catalog to identify objects seen in our survey. For each object for which a match was found in our catalog, we went back to the original literature in an attempt to identify it as a known extragalactic object, a named object of unknown nature (e.g., objects from an all-sky survey where no specific follow-up has been done), a confirmed non-member (as defined immediately above), or a potential (unconfirmed) member of Taurus. In the case of objects from the literature listed as potential but unconfirmed Taurus members, we noted and bookkept these objects separately, and we mention them where relevant below; some are indeed recovered here by our Spitzer-based searches for YSOs.

Thus, the sample of Taurus non-members is certainly biased and far from comprehensive and is *defined* to include mixtures of stars, other Galactic objects (such as planetary nebulae), and extragalactic objects. This sample can be indicative of some typical colors to expect from a variety of types of infrared-bright non-member objects.

As a further diagnostic for non-members (including extragalactic objects), we merged by position to the 2MASS extended object catalog. Objects in this catalog are likely but not guaranteed to be all extragalactic objects – 11 (out of 215) previously identified Taurus members are also 2MASS extended objects (due to, e.g., scattered light from extended dust structures), but 107/148 previously-known galaxies are 2MASS extended objects. 2MASS extended object identifications, if relevant, are noted in the data tables and SEDs below.

3.1.3. *The Process*

In order to find new candidate Taurus members, we first examined various color-color and color-magnitude spaces using our entire Taurus catalog, highlighting the locations of the previously identified objects (both members and non-members). We compared these diagrams to discussions in the literature also seeking to identify YSOs from Spitzer photometric measurements (e.g., Allen et al. 2004, Padgett et al. 2008b, Rebull et al. 2007, Harvey et al. 2007, Gutermuth et al. 2008). There is no single color selection criterion that is 100% reliable in separating members from non-member contaminants. Exactly which color selection criteria work best can be a strong function of the relative bandpass sensitivities and saturations, since 2MASS, IRAC, and MIPS do not all detect the same faintest objects (due not only to sensitivities but also degree of interstellar reddening and embeddedness of the young protostellar objects), or saturate for the same brightest objects. After extensive empirical investigation using diagrams from the literature as well as new diagrams, we selected four color-magnitude diagrams (CMDs) and one color-color diagram (CCD) which provided the best diagnostics for YSOs, and we used them to construct an initial list of new candidate YSOs. In each diagram, we define regions most likely to harbor YSO candidates, and regions most likely to contain galaxies or other non-members; these are listed in detail in §3.1.5.

By imposing these color selections, we are selecting objects that have infrared excesses (e.g., flux densities above that expected for a photosphere) and whose overall brightness is consistent with objects at the Taurus distance. We interpret these excess objects as dusty objects, with circumstellar disks and/or envelopes. We do not select objects without infrared excesses.

One aspect of our survey which makes it different from many of the Spitzer-based surveys in the literature is our extensive optical imaging. While the SDSS and CFHT imaging data do not cover every square arcminute of the Spitzer maps, they cover most of it. The SDSS spatial resolution is only slightly better than the IRAC resolution at $\sim 1.4''$, but the CFHT data has much better spatial resolution at $\sim 0.6 - 0.8''$. We examined the images at all available bands for each of the nearly 900 objects meeting the color-color or color-magnitude criteria (plus many more objects in the process of establishing these color spaces). At any band, if the object is a resolved galaxy, or projected in the vicinity of a galaxy cluster, we dropped it from further consideration. Some of the objects that are resolved are actually previously-identified YSOs. Many of the objects that have Spitzer colors similar to YSOs turn out to be resolved galaxies when examined with SDSS or CFHT. These optical imaging data have been crucial to our ability to distinguish galaxies from YSO candidates.

If the candidate object meets the color criteria in any one of the color-magnitude spaces we investigated and passes the imaging/spatial resolution test, we regard it as a provisional YSO candidate, pending additional scrutiny discussed below. Objects meeting the color criteria but failing the imaging/spatial resolution test are “candidate non-members” and appear separately in the Figures below.

3.1.4. *Gradations of Confidence for YSO candidates*

Previously identified Taurus members tend to be bright, because previous infrared (and optical) surveys were shallower than our surveys. True new Taurus members are also likely to be generally bright. Very red (embedded or cool) objects could also be members, especially since this survey goes fainter in the infrared than any prior survey of the region (excepting the Spitzer GTO observations in the various core regions, Hartmann et al. 2005). However, the fainter objects are also statistically more likely to be galaxies, especially over our survey area of more than 44 square degrees at -15° galactic latitude. Thus, we specifically focused

our attention on bright and/or red objects meeting our color selection criteria. Faint red objects meeting our color selection criteria were also considered but are statistically more likely to be galaxies than YSO Taurus members.

In addition to the easily quantifiable Spitzer magnitude and color criteria, we also individually assessed each candidate YSO using qualitative judgments. These include but are not limited to: morphology in imaging data in each available band; relative brightness at all bands from U to $160\ \mu\text{m}$ (e.g., infrared excess, but optical too bright to be a Taurus member); amplitude of excess; shape of SED; apparent (projected) proximity to other previously identified Taurus members; apparent (projected) proximity to clearly-identifiable galaxies (e.g., appearing to be part of a galaxy cluster); resolvable spiral arms or tidal tails; previous identifications (e.g., with the 2MASS extended source catalog); estimated A_V from the $160\ \mu\text{m}$ map (e.g., objects seen in high extinction regions are likely Taurus members); and star counts (a similar criterion to proximity to galaxies or estimated A_V). These assessments were done over several weeks by groups of co-authors and resulted in increased appreciation of the range of contaminants, and more objects being identified as new likely galaxies. (See the Appendix discussion on “ $8\ \mu\text{m}$ pop-up objects,” §B.7, for an example of a class of objects we rejected.) We looked critically at the shape of the excess above the photosphere, and if the excess appeared only at one band (8 or $24\ \mu\text{m}$), we retained the object as a YSO candidate only if it was more than 4σ above the photosphere (see §B.5 for many of the rejected low-significance sources). For the surviving YSO candidates, based on all of the available information from any wavelength (spectroscopic as well as photometric, plus derived information such as placement in a theoretical Hertzsprung-Russell Diagram – see §4.6) as well as all the criteria listed above, we assigned a letter grade, A/B/C, with grades of “A” as more likely members than those with grades of “C.”

These qualitative criteria can fail to recover some of the previously-identified Taurus members. Several of the previously-identified Taurus members do not have IR excesses and are therefore not recoverable by our search. Seven of the previously-identified Taurus members (e.g., 042146.3+265929 or 042307.7+280557) would probably have been rejected because in the optical images, these objects are in front of a field of galaxies, i.e., they appear to be part of a galaxy cluster, and are not in a high A_V region. One additional previously identified member, the well-known edge-on disk IRAS 04302+2247 (=SST Tau 043316.5+225320), was temporarily identified as a galaxy because its appearance was so unusual in the optical image. While our process is clearly imperfect, we are confident that, working as a group and using all of the available multi-wavelength information, we have identified a reasonably high-confidence sample of candidate Taurus members present in our photometric catalog.

Our approach for finding YSOs is customized to our data set. This labor-intensive process is not one that can be blindly applied to other regions, even regions where similar extensive supporting optical data are available. While our color selection can be easily applied to any Spitzer+2MASS catalog, the manual examination of each object is not necessarily easily duplicated and certainly automating this process is not currently possible. However, because our survey is wide-area, and the contamination rate is high, this process is unavoidable and has been crucial to our YSO selection. The time we spent in vetting the candidate list enabled more efficient use of our follow-up spectroscopic telescope time, e.g., there was little time wasted in taking spectra of contaminants.

3.1.5. The Figures and Sample Selection Criteria

The color-color and color-magnitude spaces we have chosen to use (see §3.1.3 for overview) are the following: [24] vs. [24]–[70] (§3.2.1), K_s vs. K_s –[24] (§3.2.2), [8] vs. [8]–[24] (§3.2.3), [4.5] vs. [4.5]–[8] (§3.2.4), and finally, [3.6]–[4.5] vs. [5.8]–[8] with an additional [3.6] brightness cutoff (§3.2.5). Table 1 summarizes the details of the sample selection criteria for each parameter space. Our final selection includes objects selected in any of these parameter spaces (not just objects selected in all of them); this will be discussed in more detail in §4.1. (We explicitly compare this selection method to others from the literature in §4.7 below.) We discuss each of these parameter spaces, in the order given above and in Table 1, in §3.2.1–3.2.5; for each, there is a figure (Figures 1–5) consisting of 6 panels. Each of the panels contains either a subsample or a comparison sample to clearly demonstrate our selection techniques. In the remainder of this section, we discuss each of the panels in introductory terms only.

In the upper left of each Figure is the SWIRE (Spitzer Wide-area Infrared Extragalactic Survey; Lonsdale et al. 2003) ELAIS N1 extragalactic field⁴ (the c2d reduction – see Evans et al. 2007 – is used here, as in Rebull et al. 2007 and Padgett et al. 2008b). The ELAIS N1 field is a ~ 6 square degree field centered on 16h08m44s +56d26m30s (J2000), or galactic coordinates (l, b) of 86.95, +44.48 (to be compared with the Taurus map center of $l, b \sim 173, -15$). The SWIRE sample is expected to be essentially entirely galaxies and foreground stars, and as such provides a visual guide to the locations where such objects appear in the corresponding diagram. Note that this is just the ~ 6 square degree field, as observed; it has *not* been scaled up to represent ~ 44 square degrees of Taurus data, because in this case we are primarily interested in the range of colors sampled by the galaxies, not the overall numbers. As we will see below, many newly discovered extragalactic objects in our survey have colors very similar to many certifiable YSOs, and different than the colors of objects found in SWIRE. Note also the Galactic latitude difference; this difference in Galactic latitude is likely to dominate the source counts in IRAC bands 1 and 2. More discussion of relative source counts will appear in P09.

In the upper right panel of each Figure, our entire Taurus catalog is represented, so that various subsamples can be seen in the context of the larger catalog. The Taurus catalog is expected to consist of YSOs, foreground/background stars (and other non-stellar galactic objects such as planetary nebulae), and background galaxies (recall that the asteroids have already been removed). To first order, then, the objects in the Taurus catalog that do not resemble the objects found in SWIRE are the YSOs. However, the

⁴VizieR Online Data Catalog, II/255 (J. Surace et al., 2004)

Table 1. Sample Selection Criteria

sample selected via...	YSO selection	faint flag
24/70 CMD	either [24]<7 OR [24]–[70]>6	[24]>7
K_s /24 CMD	K_s <14 AND K_s –[24]>1	K_s >13.5
8/24 CMD	[8]–[24]>0.5 AND (([8]–[24]<4 and [8]<10) or ([8]–[24]≥ 4 and [8]<2.5×([8]–[24])))	[8]>9.5
4.5/8 CMD	[4.5] < 6 AND ([4.5] ≥ 6 and [4.5] ≤ 11.5 and [4.5]–[8] > 0.4) OR ([4.5] > 11.5 and [4.5] < 0.6944×([4.5]–[8])+11.22)	[4.5]>11
IRAC CCD	[3.6]–[4.5]> 0.15 and [5.8]–[8]> 0.3 and [3.6] < 13.5	...

populations are not necessarily well-separated, as can be seen in the remaining panels of the Figures.

The remaining 4 panels in each Figure are subsets of the Taurus catalog. The second row of plots contains YSOs, both the previously identified Taurus members (left) and new candidate Taurus members (right), those selected by that particular diagram (+) as well as others selected from other diagrams (grey dots). The distribution of previously identified Taurus members includes those selected based on infrared excess and those selected via other mechanisms, and thus includes objects without IR excesses; of course, we will not find objects like the latter using Spitzer. Note also that the distribution of previously identified Taurus members often includes objects that have colors resembling galaxies. This is not surprising, since the galaxies are indeed undergoing star formation; thus, these color selection mechanisms are successfully finding star formation, just not necessarily in Taurus. The set of new candidate Taurus members is constructed from a color and magnitude cut on the entire sample, and then examining all of the available data for each of the candidates, dropping the likely galaxies (§3.1.4).

The third and final row contains the distributions for non-members, both previously identified and newly identified here. The left panel is the sample of previously identified non-members which, as discussed in §3.1.2, includes stars identified via proper motions, background giants, and galaxies identified in the literature. The last panel is the sample of all objects identified as possibly YSOs based on Spitzer colors but then rejected as such, based primarily on inspection of the optical images and SEDs; see §3.1.4. Objects which passed all the other tests to be YSO candidates but failed the spectroscopic test (see §2.3) are indicated in the last two panels of the Figures by grey stars. (Note that, having been selected by the other tests, they *also* appear in the 4th panel as candidate YSOs.)

Thus, for the color-magnitude or color-color space represented by each Figure, one can examine and compare the distribution of galaxies (SWIRE, previously identified non-members, new non-members), the distribution of YSOs (previously identified Taurus members), the distribution of foreground/background stars (SWIRE, previously identified non-members), and the distribution of new candidate Taurus members.

Table 2. Sample properties I.^a

sample	24/70 CMD	$K_s/24$ CMD	8/24 CMD	4.5/8 CMD	IRAC CCD	ANY objects identified	objects identified in <i>ALL</i> diag.
initial sample size	447	357	381	334	266	883	103
Entire sample							
# previously identified YSOs (all)	89	135	124	102	102	144	65
(% out of CMD selection)	19	37	32	30	38	16	63
(% out of 215 previously identified YSO sample)	41	63	58	47	47	67	30
# new candidate YSOs (all)	34	85	81	65	57	148	16
(% out of CMD selection)	7	23	21	19	21	16	15
(% out of 148 new candidate YSO sample)	22	57	55	44	39	100	11
# previously identified NM (all)	47	51	33	38	30	98	10
(% out of CMD selection)	10	14	8	11	11	11	9
(% out of 821 previously identified NM sample)	6	6	4	5	4	12	1
# new NM (all)	270	92	147	121	72	487	12
(% out of CMD selection)	60	25	38	36	27	55	11
(% out of 489 new NM sample)	55	19	30	25	15	100	2
# SWIRE (all; for comparison)	57	29	20	42	7	109	1
(% out of entire SWIRE sample)	3	1	0.9	2	0.3	5	0.04
Just the faint sample							
# previously identified YSOs (faint)	0	3	15	5	...	19 ^b	2 ^b
(% out of CMD selection)	0	0.8	3	1	...	2 ^b	1 ^b
(% out of 215 previously identified YSO sample)	0	1	7	2	...	9 ^b	1 ^b
# new candidate YSOs (faint)	6	9	21	32	...	56 ^b	4 ^b
(% out of CMD selection)	4	3	6	10	...	8 ^b	5 ^b
(% out of 148 new candidate YSO sample)	4	6	14	22	...	38 ^b	3 ^b
# previously identified NM (faint)	8	16	6	32	...	49 ^b	8 ^b
(% out of CMD selection)	1	4	1	9	...	5 ^b	7 ^b
(% out of 821 previously identified NM sample)	1	2	0.7	4	...	5 ^b	1 ^b
# new NM (faint)	156	43	110	111	...	371 ^b	11 ^b
(% out of CMD selection)	34	12	28	33	...	42 ^b	10 ^b
(% out of 489 new NM sample)	32	9	22	23	...	76 ^b	2 ^b
# SWIRE (all; for comparison)	40	15	13	24	...	107	1
(% out of entire SWIRE sample)	2	0.7	0.6	1	...	5 ^b	0.04 ^b

^aAs an example for how to read this table, in the case of the 24/70 CMD, 447 objects are selected by our color cuts in this diagram. Of these, 19% are previously identified YSOs, 7% are new candidate YSOs, 10% are previously identified non-members, and 60% are new non-members. And, out of the 215 stars that compose our previously identified Taurus member sample, 41% are recovered in the 24/70 diagram, of the 148 objects in our candidate YSO sample, 22% are found here, of the 821 previously identified non-members, 6% are found in this diagram, and of the 489 new non-members, 55% are found here.

^bObjects listed here were picked in *any* diagram as being faint.

Table 3. Sample properties II.

property	prev. ident. YSOs ^a total (fraction) ^b	prev. ident. YSOs, bright ^c total (fraction)	new candidate YSOs total (fraction)	new candidate YSOs, bright total (fraction)
total sample size	215 (1.00)	196 (1.00)	148 (1.00)	92 (1.00)
having IRAC 3.6 μm	193 (0.90)	174 (0.89)	142 (0.96)	86 (0.93)
having IRAC 4.5 μm	189 (0.88)	170 (0.87)	145 (0.98)	90 (0.98)
having IRAC 5.8 μm	212 (0.99)	193 (0.98)	147 (0.99)	91 (0.99)
having IRAC 8.0 μm	206 (0.96)	187 (0.95)	147 (0.99)	92 (1.00)
having MIPS 24 μm	173 (0.80)	154 (0.79)	135 (0.91)	82 (0.89)
having MIPS 70 μm	95 (0.44)	89 (0.45)	35 (0.24)	17 (0.18)
having all 4 IRAC	187 (0.87)	168 (0.86)	141 (0.95)	86 (0.93)
having all 4 IRAC+MIPS 24	154 (0.72)	135 (0.69)	128 (0.86)	76 (0.83)
having both MIPS	89 (0.41)	83 (0.42)	35 (0.24)	17 (0.18)
having K_s	209 (0.97)	194 (0.99)	140 (0.95)	92 (1.00)
having prior name	215 (1.00)	196 (1.00)	65 (0.44)	46 (0.50)

^aPreviously identified YSO Taurus members

^bNotation indicates in each case that the first number is the total number in that (sub-)sample, and the second number (in parentheses) is the sample fraction, e.g., 192 out of 215 previously identified Taurus members have 3.6 μm measurements, or 90% of the 215 star sample.

^cPreviously identified YSO Taurus members, bright sub-sample, e.g., those not flagged as red and faint; see §3.1.4. The purpose of extracting the bright sample as distinct from the entire sample is to demonstrate the properties of the brightest objects, e.g., in the case of the new candidate Taurus members, those least statistically likely to be galaxies.

3.2. Implementation of the Spitzer Selection Criteria

3.2.1. Selection via $[24]$ vs. $[24]-[70]$

The $[24]$ vs. $[24]-[70]$ diagram has been used before to find new candidate YSOs (e.g., Padgett et al. 2008b, Rebull et al. 2007). Figure 1 shows this color-magnitude diagram for the 6 samples mentioned in §3.1.5 above (left to right, top to bottom): SWIRE (expected to be essentially entirely galaxies), the entire Taurus sample, previously identified Taurus members, new candidate Taurus members, previously identified non-members (stars identified via proper motions, background giants, and galaxies identified in the literature), and new candidate non-members identified here.

By inspection of Figure 1, we find that objects with $[24]>7$ and $[24]-[70]$ between about 4 and 7 are statistically likely to be galaxies. Unadorned photospheres (e.g., old foreground stars) will be bright and have $[24]-[70]\sim 0$; an A3 ZAMS photosphere has $[24]\sim 7$ at the distance of Taurus, and for a median Taurus-age member, $[24]\sim 7$ corresponds to mid-K. Compared to the SWIRE catalog, the entire Taurus catalog contains many objects with similar colors, but also many objects that are similarly red and much brighter at $[24]$, and therefore are candidate dusty young stars.

Based on the properties of the previously identified member and non-member samples, the properties of the SWIRE sample, and discussions in the literature, the selection we impose to search for new candidate YSOs is either $[24]<7$ or $[24]-[70]>6$. Statistics on this sample are given in Table 2 (along with statistics from the SWIRE sample for comparison); in summary, this cut yields ~ 450 objects, each of which we investigated at all our available imaging bands; $\sim 20\%$ of them are previously identified Taurus members, $\sim 7\%$ of them survive the tests to be potential new YSOs, and $\sim 70\%$ are previously identified or new non-member objects. Nearly all of the previously identified Taurus members that appear in this plot have $[24]<7$. This is a likely bias in that all of the previous infrared surveys searching for Taurus members were much shallower than this Spitzer survey – the IRAS sensitivity limit was about 0.3 Jy, so we are going 7 magnitudes fainter than IRAS. However, in order to appear in this plot, the objects have to have been detected at $70\ \mu\text{m}$ as well, so the sensitivity of the $70\ \mu\text{m}$ survey is usually the limiting factor. Of the entire sample of previously identified Taurus members within our survey, 80% are detected at $24\ \mu\text{m}$ (see Table 3), and just 45% are detected at $70\ \mu\text{m}$; $\sim 5\%$ of the previously identified Taurus members are saturated in MIPS-24 and $\sim 3\%$ are saturated in MIPS-70.

In this diagram, the set of previously-identified Taurus objects is generally distinguished from the distribution of faint objects found in the SWIRE sample. Fainter Taurus objects ($[24]>7$) could exist, but objects that faint are statistically likely to be galaxies; their properties at other bands could suggest otherwise. Objects surviving the imaging test (and other qualitative criteria – see §3.1.4) but with $[24]>7$ are therefore further identified as “faint.” About 17% of the ~ 35 potential new YSOs in this parameter space are faint. Many of the other faint objects selected by our color/magnitude cut indeed resolve into galaxies when examined using the CFHT or SDSS imaging – $\sim 60\%$ of all of the objects selected in this space are new galaxy candidates. About 100 of the brighter objects selected by this color cut resolve into galaxies, so faintness alone is insufficient for locating and identifying galaxies. As can be seen in Figure 1, most of the previously-identified non-members and new candidate non-members resemble the colors of objects found in SWIRE. Figure 1 and the statistics in Table 3 also demonstrate that our sample of candidate new YSOs is on average redder and fainter than the sample of previously identified YSOs.

As discussed above (§2.3), we have obtained Palomar and/or Keck spectroscopy of many of our candidate objects. Because this color selection uses bandpasses far from optical, these objects are often very faint indeed

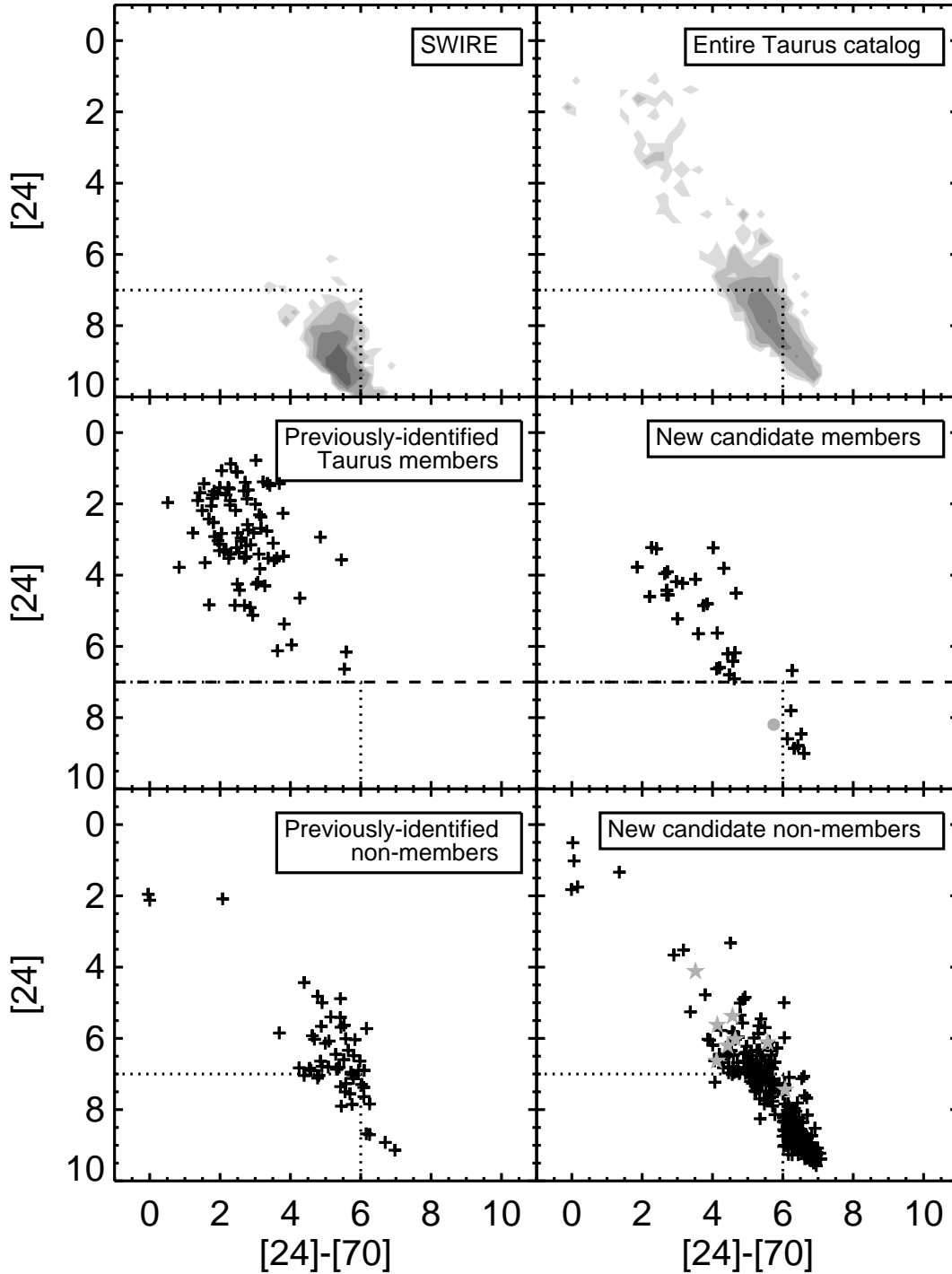


Fig. 1.— $[24]$ vs. $[24]-[70]$ for (TOP) the SWIRE sample (essentially all galaxies; contours at 1,2,4,8,16 objects), the entire Taurus sample (YSOs+contaminants; contours at 1,2,5,15,35; dotted line indicates region considered for YSO candidacy), (MIDDLE) the sample of previously-identified Taurus members, and the sample of all new candidate members (+ = objects selected in this color-magnitude space; grey dots=objects selected based on other color-magnitude spaces; dotted line indicates region considered for YSO candidacy; dashed line indicates cutoff for “faint” flag), and (BOTTOM) the sample of previously-identified non-members (stars and galaxies) and the sample of new candidate non-members(stars and galaxies) (+ = objects selected in this color-magnitude space; grey stars=objects selected as YSOs but spectroscopically confirmed to be non-members; dotted line indicates region considered for YSO candidacy).

at optical or NIR bands. We have spectroscopy for about 70% of the 34 new candidate YSOs selected in this color space. So far, almost 90% of those are stellar (e.g., YSOs or stars that could still be shown to be foreground stars or background giants), and just 4 are confirmed to be extragalactic objects.

3.2.2. Selection via K_s vs. $K_s-[24]$

As for $[24]$ vs. $[24]-[70]$, the K_s vs. $K_s-[24]$ diagram has been used previously to find new candidate YSOs (e.g., Padgett et al. 2008b, Rebull et al. 2007). Figure 2 shows this color-magnitude diagram for the same samples as Fig. 1 (see §3.1). The SWIRE sample clearly (more obviously than the previous diagram) consists of both galaxies ($K_s \gtrsim 14$ and $K_s-[24]$ between about 4 and 8) and stars ($K_s \lesssim 10$ and $K_s-[24] \sim 0$). As before, the entire Taurus catalog has many objects with colors similar to the SWIRE sample, but also many objects that have properties different than the SWIRE sample, e.g., redder than $K_s-[24] \sim 1$ and brighter than $K_s \sim 14$, as well as redder than $K_s-[24] \sim 8$. Note that the lack of sources in the lower left of each panel is an artifact of the sensitivity limits of the survey.

The sample of previously identified Taurus members, for the most part, have $K_s < 14$, which generally avoids the region populated by galaxies in the SWIRE sample, but there are legitimate YSOs mixed in with the galaxies in this parameter space. Here too, the historical bias towards brighter objects in prior surveys can be seen, and faint red objects could be legitimate YSOs. Essentially all of the previously identified YSO sample has a K_s measurement in our database, but as mentioned above, just $\sim 80\%$ are cleanly detected at $24 \mu\text{m}$ (see Table 3). As above, fainter objects are statistically likely to be galaxies.

The selection we impose on this parameter space to search for new candidate YSOs is that $K_s < 14$ and $K_s-[24] > 1$. Again, Table 2 summarizes the sample sizes; ~ 360 objects meet these criteria, including most of the (detected) previously identified Taurus members; note that there are some stars without apparent IR excess (e.g., likely WTTS) with $K_s-[24] \sim 0$, and there are YSOs that have colors resembling galaxies. Note also that late-type stars do not have $K_s-[24]=0$ (Gautier et al. 2007). Objects with $K_s > 13.5$ are further identified as “faint” and thus statistically likely to be galaxies. Previously identified Taurus members compose 135 of the objects meeting the basic color criteria; about 50 are previously identified non-member objects, most of which are 2MASS extended sources (which could be galactic or extragalactic objects). By inspection of the individual images, about 100 of the objects selected here are clearly resolved galaxies. Besides the previously identified Taurus objects, 85 objects are indistinguishable from point sources, or have morphologies consistent with YSO candidates, and meet all the other qualitative criteria (see §3.1.4) for potential new YSOs selected via this color space; a quarter of these were already found via the $24/70$ color magnitude diagram above.

In this parameter space, there is still a bias (relative to the previously identified Taurus member sample) towards finding red and faint objects, but this appears to be not nearly as strong as it was in the $24/70$ space above. Of the 85 candidate YSOs found in this space, we have already obtained Palomar and/or Keck spectroscopy (see §2.3) for 85% of them. All of them except for 1 are stellar (e.g., YSOs or stars that could still be shown to be foreground stars or background giants); just 1 is rejected outright as a galaxy.

A relatively high fraction of literature background giants appear as selected in this parameter space. Because there is a large difference in wavelength between K_s and $[24]$, this search is particularly sensitive to objects with small excesses, which could be interesting transition disk candidates. However, these objects could also be subject to reddening from the Taurus cloud that is high enough to significantly affect K_s but not $24 \mu\text{m}$, or Taurus cloud emission affecting the $24 \mu\text{m}$ but not the K_s photometry – background giants

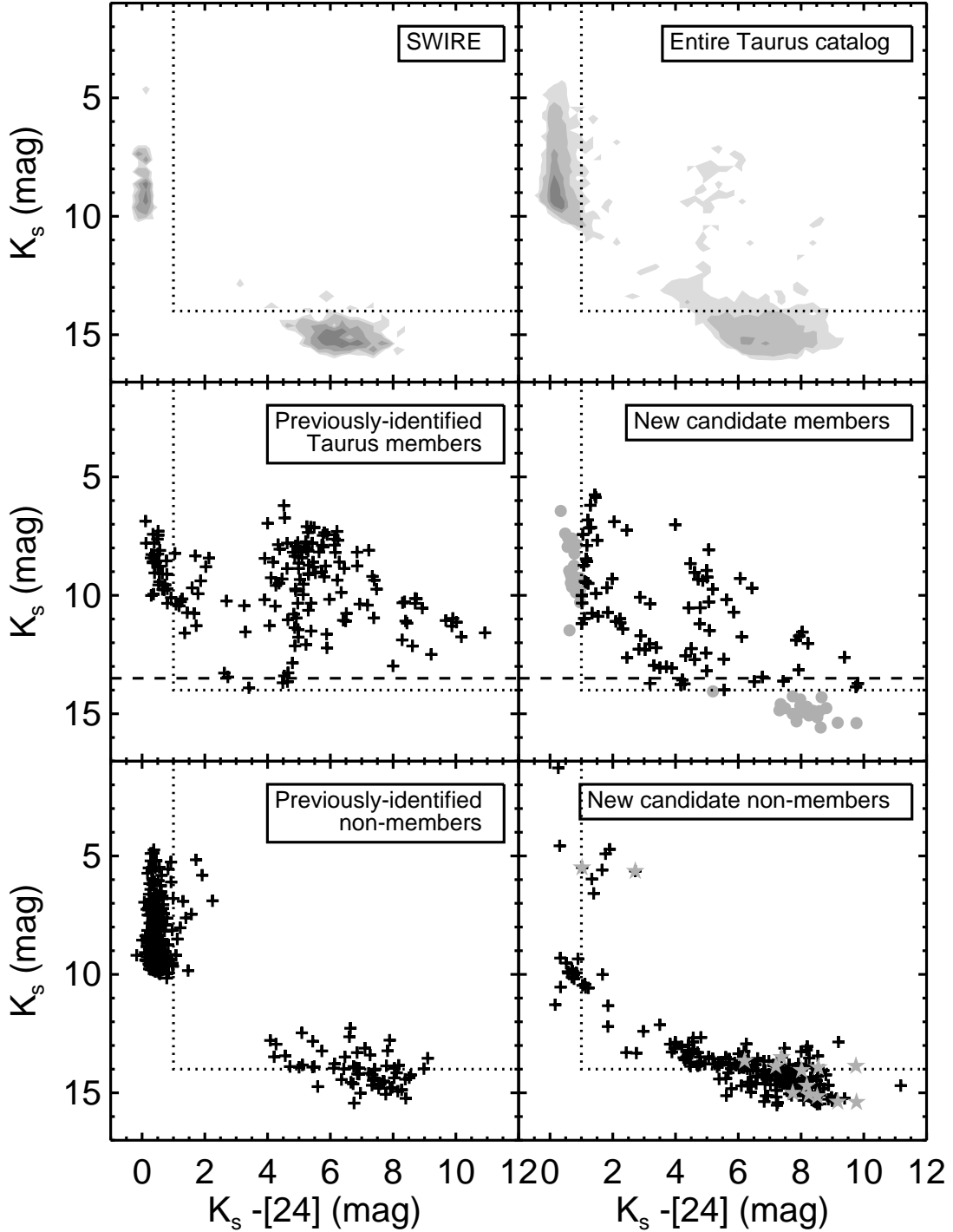


Fig. 2.— K_s vs. $K_s - [24]$ for (TOP) the SWIRE sample (galaxies & foreground stars; contours at 1,2,4,8,16 objects), the entire Taurus sample (YSOs+contaminants; contours at 1,5,50,100,200 objects; dotted line indicates region considered for YSO candidacy), (MIDDLE) the sample of previously-identified Taurus members, and the sample of all new candidate members (+ = objects selected in this color-magnitude space; grey dots=objects selected based on other color spaces; dotted line indicates region considered for YSO candidacy; dashed line indicates cutoff for “faint” flag), and (BOTTOM) the sample of previously-identified non-members (stars and galaxies) and the sample of new candidate non-members(stars and galaxies) (+ = objects selected in this color-magnitude space; grey stars=objects selected as YSOs but spectroscopically confirmed to be non-members; dotted line indicates region considered for YSO candidacy).

are therefore potentially selected in this space. Several objects presented in the literature as *candidate* background objects based on shorter-wavelength photometric observations (i.e., without confirming spectroscopy) appear here as objects with potential excesses only at the longer wavelengths. With the information we have, we are unable to distinguish currently between transition disk candidates (i.e., Taurus objects with excesses only at $24\ \mu\text{m}$) and confirmed background giants. These objects are all identified in Table 5 as candidate non-members which we have promoted to low-grade candidate YSOs. The SEDs that appear in Appendix A reveal that several of our candidate objects indeed have K_s values significantly affected by reddening and some candidate objects with clear cloud emission at 8 and/or $24\ \mu\text{m}$ are indicated in Table 7; also see §B.5 for discussion of objects with very small excesses, usually just at $24\ \mu\text{m}$. We expect that several of the objects we have identified here will turn out to be background giants. Some candidate transition disk objects will be discussed in McCabe et al. (2009).

We note here that for surveys where the IRAC and MIPS coverage is well-matched, using [3.6] or even [4.5] in place of K_s for this color-magnitude space is likely to be a better choice for searching for YSOs for two reasons: (a) minimizing the influence of reddening on K_s (3.6 or $4.5\ \mu\text{m}$ is less affected by reddening than K_s ; see Padgett et al. 2008b for more discussion on the influence of A_V), and (b) minimizing the intrinsic range of star colors – the intrinsic K_s –[24] color of M stars is not zero (Gautier et al. 2007) whereas [3.6]–[24] or [4.5]–[24] is zero for those stars. Specifically for our survey, the overall A_V towards Taurus is low, and all young stars at the distance of Taurus should be visible to 2MASS unless they are edge-on substellar objects. Moreover, using [3.6] or [4.5] in place of K_s does not reveal any YSO candidates not already selected by the color spaces used here, and finds in total only 2 more extragalactic objects. Had we used either [3.6] or [4.5] in place of K_s , however, we would have found a factor of ~ 4 fewer objects that we believe (based on inspection and our qualitative criteria) to be likely reddened background giant contaminants.

3.2.3. Selection via [8] vs. [8]–[24]

While essentially all of the previously identified YSOs have 2MASS detections at K_s , some fainter legitimate YSOs may be embedded enough that the relatively shallow 2MASS survey will not detect the objects at K_s , whereas they will be detected by our IRAC survey. Thus, we chose to investigate the [8] vs. [8]–[24] parameter space; see Figure 3.

The morphology of this space is similar to the K_s vs. K_s –[24] space, except the region occupied primarily by galaxies is now more elongated in color and has a more prominent slope towards fainter and redder objects. In order to select specifically for objects redder than most galaxies, the selection criteria we used consist of three line segments: (a) [8]–[24] > 0.5 to avoid the stars without excesses; and (b) ([8]–[24] < 4 and [8] < 10) to catch the bright stars in the middle of the plot; OR ([8]–[24] \geq 4 and [8] < $2.5 \times$ ([8]–[24])) to obtain the reddest stars. Objects with [8] > 9.5 are statistically likely to be galaxies, and thus those are further identified as “faint” in Table 5.

About 380 objects in the catalog meet these criteria, ~ 120 of which are previously identified YSOs, ~ 180 of which are non-members (previously identified or new), and ~ 80 of which survive the imaging test (and other qualitative criteria – see §3.1.4) and remain potential YSOs. Of these, ~ 25 were already found using the [24] and [70] selection criteria (§3.2.1), ~ 55 were found using K_s and [24] (§3.2.2), and ~ 20 were found in all three color-magnitude planes.

There is an apparent gap in the last panel of Figure 3 inside the “galaxy blob” at [8]–[24] > 4 and [8] > 10. This is a direct result of our selection methodology. The fainter, bluer part of the distribution are

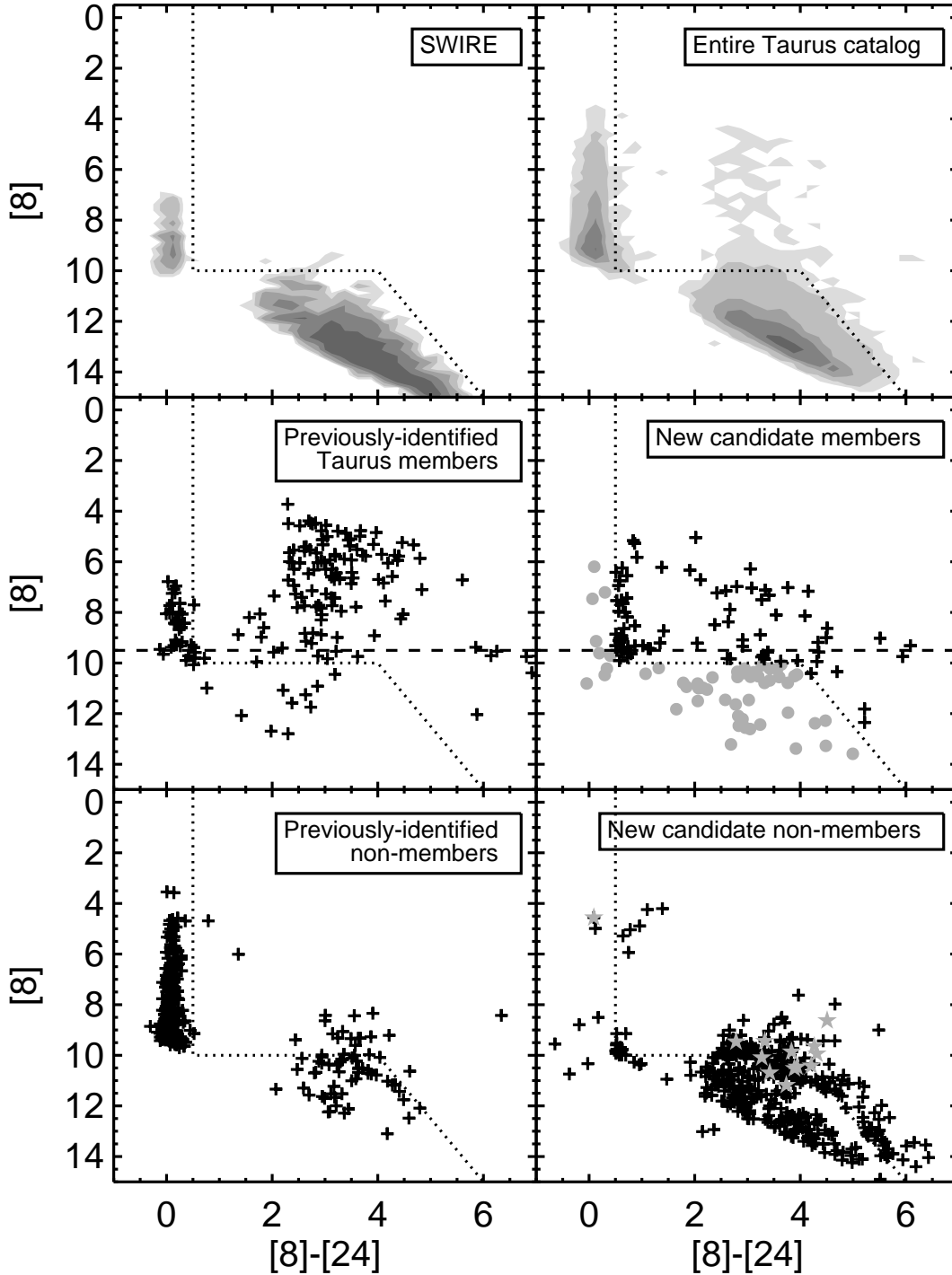


Fig. 3.— $[8]$ vs. $[8]-[24]$ for (TOP) the SWIRE sample (galaxies & foreground stars; contours at 1,2,4,8,16 objects), the entire Taurus sample (YSOs+contaminants; contours at 1,5,50,100,200 objects), (MIDDLE) the sample of previously-identified Taurus members, and the sample of all new candidate members (+ = objects selected in this color-magnitude space; grey dots=objects selected based on other color spaces; dotted line indicates region considered for YSO candidacy; dashed line indicates cutoff for “faint” flag), and (BOTTOM) the sample of previously-identified non-members (stars and galaxies) and the sample of new candidate non-members(stars and galaxies) (+ = objects selected in this color-magnitude space; grey stars=objects selected as YSOs but spectroscopically confirmed to be non-members; dotted line indicates region considered for YSO candidacy).

largely those objects that were not obviously point sources in the optical imaging, and the redder part of the distribution closely tracks the (dotted) dividing line we used for our selection criteria. This population is composed of objects we rejected as candidate YSOs based on the qualitative criteria listed in §3.1.4 above.

We have followup spectroscopy (see §2.3) for $\sim 80\%$ of the 81 new candidate YSOs selected in this color space. Nearly all (95%) of these are stellar; just 3 are rejected as galaxies.

3.2.4. Selection via $[4.5]$ vs. $[4.5]-[8]$

To this point, we have required MIPS-24 detections for YSO candidate selection, which strongly biased our sample of new potential YSOs towards the generally brighter and/or larger excess objects (by comparison to the rest of the catalog). As an example of how many YSOs we may be missing by requiring $24\ \mu\text{m}$, just $\sim 80\%$ of the previously identified YSOs are detected at $24\ \mu\text{m}$. This results from a combination of intrinsic disk properties (where disk emission makes the objects easier to detect at $24\ \mu\text{m}$) and the Spitzer sensitivity relative to low-mass photospheres at the Taurus distance (for those YSOs without disks). By loosening this restriction and not requiring MIPS-24, we extend the sample of potential objects, but also the potential contamination. We now investigate the $[4.5]$ vs. $[4.5]-[8]$ parameter space; see Figure 4. This parameter space, on its own, provides the largest possible initial sample size we have yet investigated, as 17% of the entire catalog is detected in these two IRAC bands (compared with just 2% of the entire catalog detected at MIPS-24; see P09 for additional similar statistics). To first order, the morphology of this space is similar to the other spaces we have investigated, with the photospheres clustering around $[4.5]-[8]\sim 0$ and the galaxies in a red and faint grouping. There are some new features apparent in this space, however. Saturation at $4.5\ \mu\text{m}$ occurs at 650 mJy (6.1 mags), so the locus of colorless objects is truncated at that level. In the sample of previously identified Taurus members, there is a clear distinction between the disked and non-disked population (a gap near $[4.5]-[8]=0.5$) which is not seen when considering the entire catalog.

The selection criteria we used to find candidate YSOs in this space selected the brighter and redder objects; we did this by stitching together several line segments. They are: (a) $[4.5] < 6$ AND (b) ($[4.5] \geq 6$ and $[4.5] \leq 11.5$ and $[4.5]-[8] > 0.4$) OR (c) ($[4.5] > 11.5$ and $[4.5] < 0.6944 \times ([4.5]-[8]) + 11.22$). About 335 objects meet these basic criteria, ~ 100 of which are previously identified YSOs, and ~ 160 of which are new or previously identified non-members. About 65 objects survive the imaging test (and other qualitative criteria – see §3.1.4) and are new candidate YSOs. The distribution of these objects in this color-magnitude space is very different than that for the previously identified members; these new objects are distinctly fainter and redder on the whole than the previously identified sample. Objects with $[4.5]>11$ are given the “faint” flag in Table 5.

About a third of the new candidate YSO sample selected here are also retrieved from the $24/70$ space above and about two-thirds are also retrieved from the $K_s/24$ and $8/24$ spaces above.

About 65% of these 65 candidate Taurus objects have Palomar and/or Keck spectroscopy (see §2.3), and nearly all are stellar; just 4 are dropped as galaxies.

3.2.5. Selection via IRAC color-color diagram

As our final selection mechanism, we use the IRAC color-color diagram (as seen in, e.g., Allen et al. 2004). This parameter space, on its own, provides an initial sample size comparable to the previous $4.5/8$

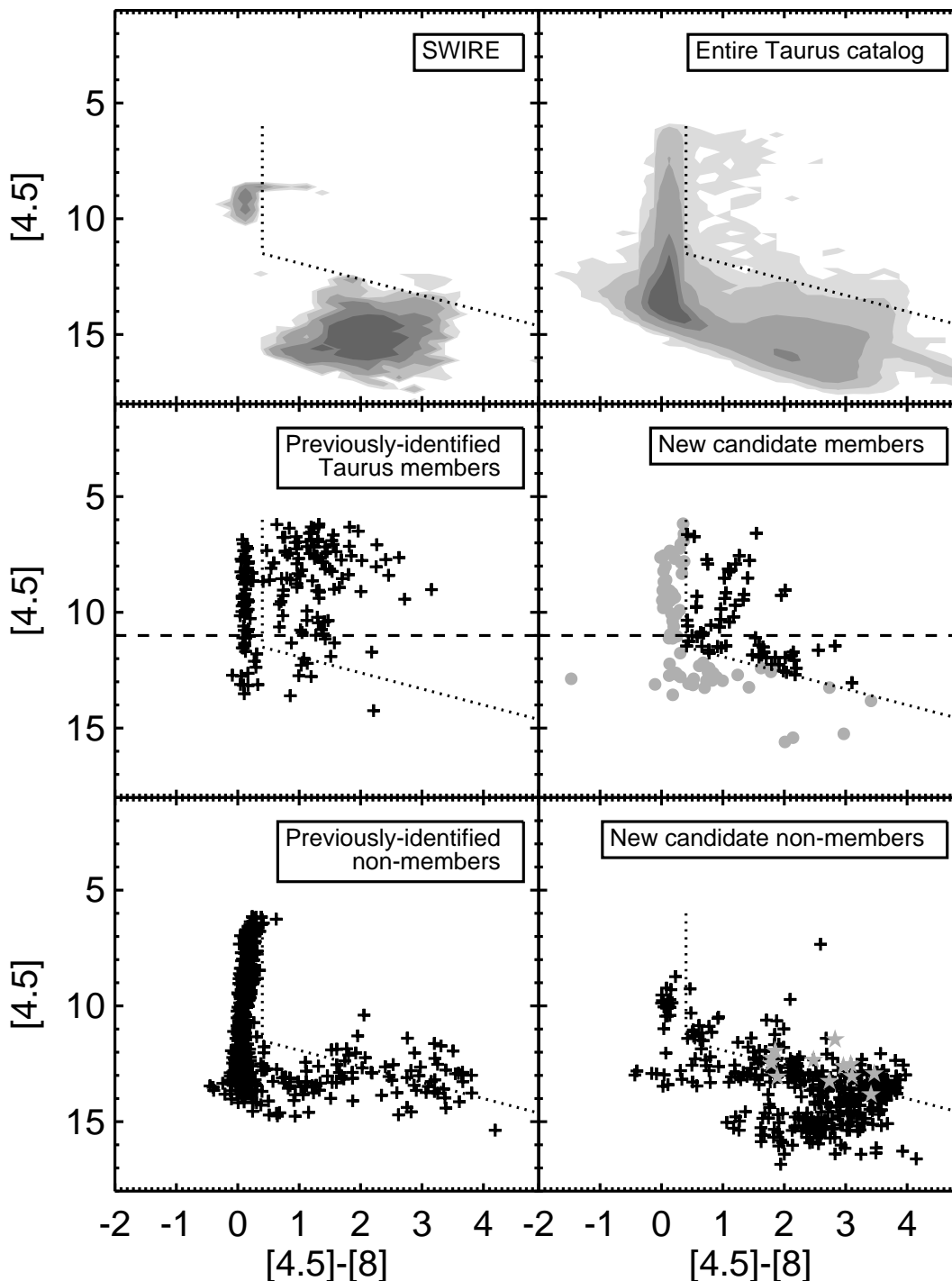


Fig. 4.— $[4.5]$ vs. $[4.5]-[8]$ for (TOP) the SWIRE sample (galaxies & foreground stars; contours at 1,2,4,8,16 objects), the entire Taurus sample (YSOs+contaminants; contours at 1,10,100,1000,2000 objects; dotted line indicates region considered for YSO candidacy), (MIDDLE) the sample of previously-identified Taurus members, and the sample of all new candidate members (+ = objects selected in this color-magnitude space; grey dots=objects selected based on other color spaces; dotted line indicates region considered for YSO candidacy; dashed line indicates cutoff for “faint” flag), and (BOTTOM) the sample of previously-identified non-members (stars and galaxies) and the sample of new candidate non-members(stars and galaxies) (+ = objects selected in this color-magnitude space; grey stars=objects selected as YSOs but spectroscopically confirmed to be non-members; dotted line indicates region considered for YSO candidacy).

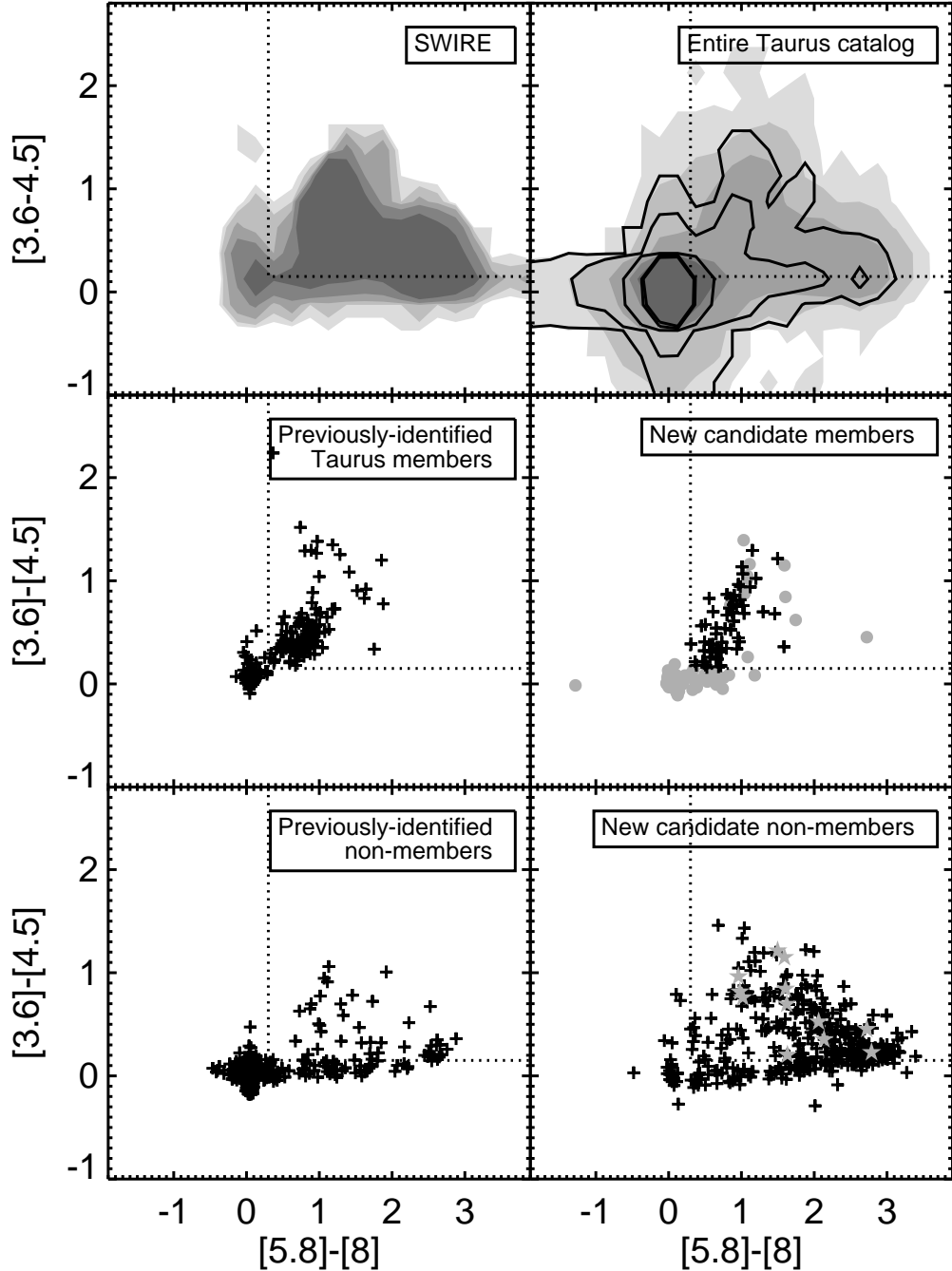


Fig. 5.— $[3.6]-[4.5]$ vs. $[5.8]-[8]$ for (TOP) the SWIRE sample (galaxies & foreground stars; contours at 1,2,4,8,16 objects), the entire Taurus sample (YSOs+contaminants; grey contours at 1,10,100,1000,2000 objects; solid line contours are for the entire Taurus sample with an additional $[3.6]<13.5$, same contour limits as the grey contours), (MIDDLE) the sample of previously-identified Taurus members, and the sample of all new candidate members (+ = objects selected in this color-color space; grey dots=objects selected based on other color spaces; dotted line indicates region considered for YSO candidacy), and (BOTTOM) the sample of previously-identified non-members (stars and galaxies) and the sample of new candidate non-members(stars and galaxies) (+ = objects selected in this color-color space; grey stars=objects selected as YSOs but spectroscopically confirmed to be non-members; dotted line indicates region considered for YSO candidacy). An additional $[3.6]$ brightness cut was also imposed on the YSO selection in this color space; see text.

color selection, as 13% of the entire catalog is detected in all 4 IRAC bands (to be compared with just 2% of the entire catalog being detected at MIPS-24, and 17% detected at 4.5 and 8 microns; see P09 for additional similar catalog statistics). However, by using the IRAC color-color diagram on its own, we are blind to any luminosity information about the sources. This information was present previously because we were using color-magnitude, not color-color, diagrams. Given the surface density of galaxies, as well as the fact that the galaxy/YSO separation is not as vivid in this parameter space, the luminosity information is crucial. We imposed a *requirement* of $[3.6] < 13.5$, and the cut we used on the IRAC color-color space was (based on literature discussions) $[3.6] - [4.5] > 0.15$ and $[5.8] - [8] > 0.3$. This approach is different than in our consideration of the above parameter spaces, where we specifically called out YSO candidates fainter than a specific level.

Using these criteria, ~ 265 objects are selected, ~ 100 of which are previously identified Taurus members, ~ 100 of which are non-members (previously identified or new), and ~ 65 of which are new candidate YSOs. Of those, $\sim 35\%$ were also found using 24/70, $\sim 60\%$ were found using $K_s/24$ or $8/24$, and $\sim 80\%$ were found using 4.5/8. (More on objects selected using all CMDs in §4.1 below.)

As can be seen in Figure 5, the previously identified Taurus members roughly fall into two groups – those with little or no IRAC excess, and those with substantial excesses. Among our new candidate members, we have some objects with little or no IRAC excess (selected from other parameter spaces), as well as objects with more substantial excesses, but the division is not as clean, suggesting contaminants in our YSO candidate list. We have also selected some objects that are very red in $[5.8] - [8]$ but nearly colorless in $[3.6] - [4.5]$. These could be disks with large inner holes, or galaxies.

A little more than half of these 57 candidate objects have spectroscopy (see §2.3) from Palomar and/or Keck; just 4 are galaxies.

3.3. Tables of objects

Now that we have used the Spitzer properties of the previously-identified Taurus member sample to select a new candidate YSO sample, we present the data tables with observed and derived properties of both sets of objects. In this section, we review the contents of Tables 4–8. The contents of Tables 4 and 5 are similar but not identical, as are the contents of Tables 6 and 7. Table 8 summarizes the new members, sorted by confidence level.

Tables 4 and 5 present, for each of the previously identified Taurus members and the new candidate Taurus members identified here, respectively, SST Tau names (note, as IAU-compliant names, the Right Ascension and Declination as given in the name are truncated, not rounded), a common name from previous studies (if applicable), and measurements in the Spitzer bands. For most of these objects, this is the first time that MIPS flux densities have appeared in the literature. Since many of the previously identified and new candidate Taurus members appear as having YSO-like colors in more than one of the color-magnitude and color-color diagrams of Table 1 and Figures 1-5, Tables 4 and 5 also present the color criteria that are met by each object individually, for each of the color spaces we use here to identify YSO candidates. Objects appearing faint and red (see §3.1.4 above) are indicated as such. SEDs for each of the previously identified members and new candidates appear in Appendix A; the SED properties of the sample as whole will be discussed in §4.5 below. Table 5 additionally contains notes about individual objects. These tables are sorted by SST Tau name, effectively sorted by RA and then Dec.

Additional information about each of the previously identified Taurus members and the new candidate Taurus members identified here appears in Tables 6 and 7, respectively. Both of these tables start by repeating the SST Tau name, and a previous common name (if applicable). Table 7 then lists the grade ranking (see §3.1.4 above) that we assigned each of the candidate objects. Note that these tables are still sorted by position; Table 8 later presents the candidate Taurus members in order of confidence.

We compare our search method to others in the literature in §4.7 below; in preparation for that, Tables 6 and 7 indicate, for each of the previously identified Taurus members, how (or if) the c2d (Harvey et al. 2007) or Gutermuth et al. (2008) criteria for YSOs identified the object. (NB: whether or not our search recovered each previously identified object can be found in Table 4.)

Tables 6 and 7 contain a YSO classification. The near- to mid-IR slope of each SED, α , is what we used for determining a YSO classification for these objects. For each of the previously identified and new candidate objects in our survey, we performed a simple ordinary least squares linear fit to all available photometry (just detections, not including upper or lower limits) between 2 and 24 μm , inclusive. Note that errors on all of the infrared points are so small as to not affect the fitted SED slope, and that a forthcoming paper will investigate the (small) effects of fitting a line to all available points within a different wavelength range, e.g., 3.6 to 24 μm . In the spirit of Wilking et al. (2001), we define $\alpha = d \log \lambda F_\lambda / d \log \lambda$, where $\alpha > 0.3$ for a Class I, 0.3 to -0.3 for a flat-spectrum source, -0.3 to -1.6 for a Class II, and < -1.6 for a Class III. We realize that the precise definition of α can vary, resulting in different classifications for certain objects; detailed discussion of this issue is beyond the scope of this paper. Classification via this method is provided for all previously identified and new candidate objects specifically to enable comparison within this paper via internally consistent means.

Adopted spectral types appear in Tables 6 and 7. This spectral type comes from the literature (see §3.1.1) or from our spectra (§2.3); if the latter, it is indicated as such in the “notes” column. If we obtained a spectrum for the object, and if $\text{H}\alpha$ was measurable, we report the equivalent width in these Tables (see §2.3 for analysis details). If the Ca infrared triplet was in emission at the time of our observation, it is noted in the “notes” column.

Tables 6 and 7 include an estimate of the star’s luminosity (L_*) and an estimate of the ratio of the infrared excess luminosity to the star’s total (photospheric+infrared) luminosity ($L_{\text{IR}}/L_{\text{total}}$, where $L_{\text{total}} = L_* + L_{\text{IR}}$). We describe briefly our procedure to determine the infrared luminosity. Many faint sources were undetected at the longest wavelengths; we extrapolated missing data points for wavelengths longer than 8.0 μm . We used the longest wavelength available data point as a reference and assumed that its flux density corresponded to blackbody emission peaking at that wavelength. We then used this blackbody function to estimate the missing fluxes at the longer wavelengths. We compared the measured $J - H$ colors and the expected photospheric $(J - H)_0$ colors (as tabulated in Chapter 7 of Allen’s *Astrophysical Quantities*; Cox 2001), attributing any difference to extinction, A_V , and we corrected the photometric fluxes for it. We obtained a spline curve through the corrected fluxes in $\log F_\lambda$, $\log \lambda$ space on a wavelength grid from 0.1 \AA to 1000 \AA with a $\Delta\lambda = 0.02 \text{\AA}$. To determine the infrared excess, we determined the underlying stellar photospheric emission using PHOENIX stellar atmosphere models for $T_{\text{eff}} \leq 10,000 \text{ K}$ and Kurucz models for $T_{\text{eff}} > 10,000 \text{ K}$ and matched the stellar atmosphere model to the corrected J -band fluxes. The infrared luminosity was calculated by measuring the difference between the spline curve and the stellar atmosphere model. We emphasize that care was taken to ensure that we included only adequate excess luminosity contributions at each wavelength of the grid (e.g., if the stellar atmosphere model showed a drop in flux between the K_s and 3.6 μm fluxes, and the spline curve was above but there was no obvious sign of infrared excess at those wavelengths, the contribution to the infrared luminosity was not included). We also only included

contributions if the spline curve was at least 1.5 times larger than the stellar atmosphere contribution. Finally, we determined if the calculated infrared luminosity was an upper limit by checking that at least one of the corrected photometric fluxes beyond $3.6 \mu\text{m}$ were real and not extrapolated. If the latter, the infrared luminosity was indicated as an upper limit. Note that this method is subject to several caveats: (a) objects that do not have spectral types (particularly common in the list of new candidate objects) do not have a calculated A_V , and therefore no L_* or $L_{\text{IR}}/L_{\text{total}}$; (b) this method of dereddening using $J - H$ ignores the potential for near-IR excess (as well as veiling and the H-opacity minimum at $1.6 \mu\text{m}$) and therefore this method can overestimate L_* ; (c) YSOs intrinsically vary at essentially all the wavelengths used here, and the photometry across the SED for each object was not obtained contemporaneously. Our values for $L_{\text{IR}}/L_{\text{total}}$ are probably good to a factor of 2, and are sufficient to determine if a source has an envelope, is an optically thick disk only, a highly flattened / thinning disk, or a debris-like system. (See §4.6 for more discussion.) This approach is demonstrably inaccurate in comparison to more complex methods, such as those employing bolometric corrections to reddening-corrected flux densities in well-calibrated passbands. However, more detailed modeling is beyond the scope of this paper.

For the 148 new candidate Taurus members, Table 7 also contains an adopted membership classification indicating whether or not we regard the object as a Taurus member. This classification combines information from all of the available photometric and optical spectroscopic data (see §4.1 and §3.1.4). Extragalactic objects are noted as “xgal.” Objects that we believe to be reliable new members are indicated as “new member.” Objects that we think are likely to be new members but there is still some doubt are listed as “probable new member.” Objects with the next gradation of confidence are “possible new members.” Objects for which we have spectra but cannot determine clear membership are listed as “needs additional followup” and, finally, objects with no spectroscopic data yet are “pending followup.” There are 34 new members, 3 probable new members, 10 possible new members, 7 extragalactic objects, 2 other objects, 60 stars needing additional follow-up observations, and 33 pending any follow-up observations. Note that while all the “new members” are also grade A objects, not all grade A objects are “new members”, because of the need for additional data in many cases.

A final data table, Table 8, lists the new members in order of quality, sorted by their category (new member, probable new member, possible new member, needs additional followup, or pending followup), and then by our rank (and then by catalog number), such that the objects we grade as most likely to be new members appear at the top of the list. Table 8 also contains the projected angular separation from to the nearest previously-identified Taurus object.

Table 4—Continued

SST Tau name	common name	[3.6] (mag)	[4.5] (mag)	[5.8] (mag)	[8] (mag)	[24] (mag)	[70] (mag)	[160] (mag)	ident. in 24/70 CMD	ident. in $K_s/24$ CMD	ident. in 8/24 CMD	ident. in 4.5/8 CMD	ident. in IRAC CCD	notes
043638.9+225811	CFHT-3	11.79± 0.05	11.69± 0.05	11.59± 0.06	11.57± 0.06	> 8.55	> 1.12	no	no	...
043649.1+241258	HD 283759	8.32± 0.05	8.25± 0.05	8.30± 0.05	8.20± 0.05	6.64± 0.05	1.10± 0.22	> 0.51	yes	yes	yes	no	no	...
043800.8+255857	ITG 2	9.60± 0.05	9.47± 0.05	9.37± 0.05	9.31± 0.05	9.17± 0.19	> 0.96	> -2.05	...	no	no	no	no	...
043814.8+261139	J04381486+2611399	10.80± 0.05	10.21± 0.05	9.64± 0.05	8.92± 0.05	4.98± 0.04	> 0.80	> -1.11	...	yes	yes	yes	yes	...
043815.6+230227	RXJ0438.2+2302	9.69± 0.05	9.69± 0.05	9.64± 0.05	9.60± 0.05	> 9.35	> 1.08	no	no	...
043821.3+260913	GM Tau	9.27± 0.05	8.77± 0.05	8.43± 0.05	7.81± 0.05	5.33± 0.04	> 0.97	> -1.31	...	yes	yes	yes	yes	...
043828.5+261049	DO Tau	< 6.62	< 6.10	5.26± 0.05	4.77± 0.05	1.09± 0.04	-1.37± 0.22	-3.92± 0.34	yes	yes	yes
043835.2+261038	HV Tau AB	7.65± 0.05	7.59± 0.05	7.49± 0.05	7.46± 0.05	...	> 0.72	> -3.65	no	no	...
043835.4+261041	HV Tau C	11.33± 0.14	10.74± 0.05	10.22± 0.05	9.38± 0.04	3.52± 0.04	-0.09± 0.22	...	yes	no	yes	yes	yes	e
043858.5+233635	J0438586+2336352	10.51± 0.05	...	9.84± 0.05	...	6.39± 0.05	> 0.85	yes
043901.6+233602	J0439016+2336030	9.76± 0.05	...	9.18± 0.05	...	6.28± 0.05	> 2.30	yes
043903.9+254426	CFHT-6	10.75± 0.05	10.45± 0.05	10.02± 0.06	9.14± 0.05	6.51± 0.05	> 0.47	> -0.54	...	yes	yes	yes	yes	c
043906.3+233417	J0439064+2334179	10.73± 0.05	...	10.62± 0.06	...	> 9.32
043913.8+255320	IRAS04361+2547 AB	8.00± 0.05	7.08± 0.05	6.46± 0.05	4.82± 0.05	< 0.45	< -2.30	< -4.73	yes	yes	...
043917.7+222103	LkCa 15	7.61± 0.05	7.41± 0.05	7.23± 0.05	6.64± 0.05	3.11± 0.04	-0.40± 0.22	-2.47± 0.22	yes	yes	yes	yes	yes	...
043920.9+254502	GN Tau B	6.99± 0.05	6.58± 0.05	6.21± 0.05	5.42± 0.05	2.82± 0.04	1.59± 0.22	> -2.43	yes	yes	yes	yes	yes	...
043935.1+254144	IRAS04365+2535	7.22± 0.05	< 6.10	4.87± 0.05	4.16± 0.05	< 0.45	-2.17± 0.22	> -3.82	yes	c
043947.4+260140	CFHT-4	9.54± 0.05	9.07± 0.05	8.60± 0.05	7.78± 0.05	4.95± 0.04	> 0.91	> -4.76	...	yes	yes	yes	yes	...
043953.9+260309	IRAS 04368+2557	13.39± 0.11	11.15± 0.08	10.09± 0.07	9.73± 0.08	2.69± 0.04	< -2.30	> -4.40	yes-faint	yes-faint	yes	c d
043955.7+254502	IC2087 IRS	< 6.62	< 6.10	< 3.49	< 3.52	< 0.45	-2.17± 0.22	> -5.41	c
044001.7+255629	CFHT-17 AB	10.15± 0.05	9.96± 0.05	9.87± 0.05	9.82± 0.06	9.10± 0.18	> 0.74	> -2.26	...	yes	yes-faint	no	no	...
044008.0+260525	IRAS 04370+2559	7.96± 0.05	7.38± 0.05	6.93± 0.05	5.93± 0.05	2.43± 0.04	0.75± 0.22	> -1.78	yes	yes	yes	yes	yes	...
044039.7+251906	J04403979+2519061 AB	9.84± 0.05	9.68± 0.06	9.62± 0.05	9.57± 0.05	7.55± 0.05	> 1.00	> -2.43	...	yes	yes-faint	no	no	...
044049.5+255119	JH223	8.90± 0.05	8.60± 0.05	8.24± 0.05	7.74± 0.05	5.13± 0.04	2.20± 0.22	> 0.93	yes	yes	yes	yes	yes	...
044104.2+255756	Haro 6-32	9.66± 0.05	9.56± 0.06	9.49± 0.05	9.46± 0.06	9.59± 0.33	> 0.70	> -0.83	...	no	no	no	no	...
044104.7+245106	IW Tau AB	8.13± 0.05	8.15± 0.05	8.08± 0.05	8.03± 0.05	7.97± 0.07	> 1.08	no	no	no	no	...
044108.2+255607	ITG 33 A	9.68± 0.05	9.05± 0.05	8.49± 0.05	7.73± 0.05	4.60± 0.04	> 0.67	> 0.73	...	yes	yes	yes	yes	...
044110.7+255511	ITG 34	10.78± 0.05	10.35± 0.05	9.92± 0.06	9.22± 0.05	6.48± 0.05	> 0.74	> -1.25	...	yes	yes	yes	yes	...
044112.6+254635	IRAS04381+2540	9.15± 0.05	7.76± 0.05	6.72± 0.05	5.75± 0.05	1.43± 0.04	-1.92± 0.22	-4.33± 0.34	yes	yes	yes	yes	yes	...
044138.8+255626	IRAS04385+2550	8.24± 0.05	7.74± 0.05	7.13± 0.05	6.05± 0.05	1.86± 0.04	-0.90± 0.22	-2.73± 0.22	yes	yes	yes	yes	yes	...
044148.2+253430	J04414825+2534304	11.43± 0.05	10.93± 0.05	10.50± 0.06	9.54± 0.05	6.33± 0.05	> 1.02	> -4.57	...	yes	yes-faint	yes	yes	...
044205.4+252256	LkHa332/G2 AB	7.99± 0.05	7.87± 0.05	7.74± 0.05	7.70± 0.05	7.18± 0.05	...	> -4.69	...	yes	yes	no	no	b
044207.3+252303	LkHa332/G1 AB	7.65± 0.05	7.62± 0.05	7.53± 0.05	7.51± 0.06	...	> 0.51	> -2.34	no	no	b
044207.7+252311	V955 Tau Ab	6.99± 0.05	6.58± 0.05	6.15± 0.05	5.40± 0.05	2.76± 0.04	-0.56± 0.22	> -2.07	yes	yes	yes	yes	yes	b
044221.0+252034	CIDA-7	9.51± 0.05	9.11± 0.05	8.65± 0.05	7.79± 0.05	4.20± 0.04	1.13± 0.22	> -1.18	yes	yes	yes	yes	yes	...
044237.6+251537	DP Tau	7.57± 0.05	6.90± 0.05	6.34± 0.05	5.37± 0.05	1.90± 0.04	0.54± 0.22	> -1.70	yes	yes	yes	yes	yes	...
044303.0+252018	GO Tau	8.90± 0.05	8.64± 0.05	8.21± 0.05	7.42± 0.05	4.30± 0.04	1.03± 0.22	> 0.53	yes	yes	yes	yes	yes	...
044427.1+251216	IRAS04414+2506	9.56± 0.05	9.00± 0.05	8.36± 0.05	7.43± 0.05	4.25± 0.04	1.76± 0.22	> 0.05	yes	yes	yes	yes	yes	...
044642.6+245903	RXJ04467+2459	10.05± 0.05	9.97± 0.05	9.87± 0.06	9.90± 0.05	9.53± 0.26	> 0.96	no	no	no	no	...

^aTable will be presented both in the print and in the electronic version. To convert between magnitudes and flux densities, we use $M = 2.5 \log(F_{\text{zeropt}}/F)$ where the zero-point flux densities for the seven Spitzer bands are 280.9, 179.7, 115.0, and 64.13 Jy for IRAC and 7.14, 0.775, and 0.159 Jy for MIPS. IRAC effective wavelengths are 3.6, 4.5, 5.8, and 8.0 μm ; MIPS effective wavelengths are 24, 70, and 160 μm .

^bMIPS-160 flux density for this object is subject to confusion with a nearby source or sources.

^cMIPS-160 flux density for this object is compromised by missing and/or saturated data.

^dMIPS-160 flux density for this object is hard saturated.

^eIRAC flux densities for 043835.4+261041=HV Tau C do not appear in our automatically-extracted catalog. Flux densities here are those from Hartmann et al. (2005); since their observations have more redundancy at IRAC bands, they are able to obtain reliable flux densities for this object at IRAC bands. MIPS flux densities are determined from our data.

^fThe image morphology around 041426.2+280603 is complex; careful PSF subtraction and modeling will be required to apportion flux densities among the three local maxima seen in close proximity in the IRAC images, which may or may not be three physically distinct sources.

Table 5—Continued

SST Tau name	common name	[3.6] (mag)	[4.5] (mag)	[5.8] (mag)	[8] (mag)	[24] (mag)	[70] (mag)	[160] (mag)	ident. in 24/70 CMD	ident. in $K_s/24$ CMD	ident. in 8/24 CMD	ident. in 4.5/8 CMD	ident. in IRAC CCD	notes
043944.8+260152	ITG 15	8.47± 0.05	8.13± 0.05	7.69± 0.05	7.04± 0.05	3.96± 0.04	1.32± 0.22	> -2.26	yes	yes	yes	yes	yes	e g
044000.6+235821	J04400067+2358211	10.89± 0.05	10.64± 0.05	10.35± 0.06	9.70± 0.06	6.40± 0.05	> 0.78	> 1.15	...	yes	yes-faint	yes	yes	g
044022.8+243307	...	13.06± 0.06	12.25± 0.06	11.43± 0.06	10.46± 0.06	6.52± 0.05	> 0.83	> -0.91	...	no	no	yes-faint	yes	...
044023.0+255702	...	10.68± 0.05	10.63± 0.05	10.57± 0.06	10.43± 0.06	9.36± 0.22	> 0.92	> -1.37	...	yes	no	no	no	...
044048.4+233941	...	13.52± 0.06	...	13.55± 0.08	...	9.35± 0.20	> 1.12	> -0.74	...	yes-faint
044124.6+254353	ITG 40	10.43± 0.05	9.85± 0.05	9.39± 0.05	8.88± 0.05	5.64± 0.04	> 0.95	> -2.01	...	yes	yes	yes	yes	e g
044125.7+254349	...	13.80± 0.06	12.41± 0.06	11.25± 0.06	10.22± 0.06	6.80± 0.05	2.32± 0.22	> -2.26	yes	...	no	yes-faint	no	...
044200.4+235813	...	14.19± 0.06	13.04± 0.06	11.53± 0.06	9.94± 0.05	5.62± 0.04	1.49± 0.22	> -0.12	yes	no	yes-faint	yes-faint	no	...
044241.1+244117	CCDM J04427+2441AB	7.61± 0.05	7.55± 0.05	7.54± 0.05	7.52± 0.05	6.90± 0.05	> 1.06	> -1.45	...	no	yes	no	no	...
044253.9+253709	...	12.84± 0.06	12.79± 0.06	12.61± 0.07	12.48± 0.08	9.64± 0.24	> 1.01	> 0.95	...	yes	no	no	no	...
044315.8+235358	...	12.94± 0.06	11.87± 0.05	10.78± 0.06	9.76± 0.06	6.49± 0.05	> 0.95	> -0.89	...	no	yes-faint	yes-faint	yes	...
044325.1+255706	...	9.35± 0.05	9.33± 0.05	9.20± 0.05	9.17± 0.05	8.59± 0.12	> 0.87	> -0.81	...	no	yes	no	no	...
044345.3+243908	TYC 1834-591-1	9.49± 0.05	9.46± 0.05	9.42± 0.05	9.43± 0.05	8.31± 0.09	> 1.04	> 0.07	...	yes	yes	no	no	...
044358.3+235103	...	6.85± 0.05	6.73± 0.05	6.23± 0.05	6.19± 0.05	6.10± 0.04	> 0.81	> 0.05	...	no	no	yes	no	...
044518.2+242436	HD 30067	7.99± 0.05	8.02± 0.05	7.96± 0.06	7.95± 0.05	7.39± 0.06	> 0.60	> -0.65	...	no	yes	no	no	...
044539.8+251704	...	8.28± 0.05	8.33± 0.05	8.08± 0.05	8.00± 0.05	7.31± 0.05	> 1.02	> -0.35	...	yes	yes	no	no	f
044550.7+254448	...	12.91± 0.06	11.94± 0.05	11.05± 0.06	10.09± 0.06	6.82± 0.05	> 1.06	> -1.01	...	no	no	yes-faint	yes	...
044555.7+261858	...	10.99± 0.05	11.04± 0.05	10.91± 0.06	10.79± 0.06	9.00± 0.16	2.40± 0.22	> -0.43	yes-faint	yes	no	no	no	...
044557.0+244042	...	13.12± 0.06	12.94± 0.06	12.62± 0.07	12.12± 0.07	> 10.06	> 0.82	> -0.13	no	yes	...
044609.6+245237	...	12.78± 0.06	12.69± 0.06	12.53± 0.07	12.43± 0.07	9.19± 0.21	> 0.87	> -1.49	...	yes	no	no	no	...
044639.8+242526	...	< 6.62	< 6.10	5.44± 0.05	5.27± 0.05	4.41± 0.04	> 1.10	> 0.12	...	yes	yes	f
044644.4+262306	...	< 6.62	6.17± 0.05	5.98± 0.05	5.82± 0.05	4.91± 0.04	> 1.01	> -3.17	...	yes	yes	no
044650.3+243815	...	13.50± 0.06	13.11± 0.22	13.52± 0.09	13.22± 0.11	10.53± 0.25	> 0.88	> 0.29	...	yes-faint	no	no	yes	...
044802.3+253359	...	10.05± 0.05	10.06± 0.05	9.92± 0.06	9.90± 0.06	9.33± 0.21	> 1.03	> -1.34	...	no	yes-faint	no	no	...
044832.3+234746	...	12.89± 0.06	11.95± 0.05	11.05± 0.06	9.93± 0.06	6.30± 0.05	> 0.92	> -1.88	...	no	yes-faint	yes-faint	yes	...
044857.4+255853	2MASX 04485745+2558527	13.30± 0.06	13.26± 0.06	12.94± 0.08	12.56± 0.07	9.60± 0.25	> 1.00	> -1.03	...	yes-faint	no	no	no	...
044900.1+241346	...	14.28± 0.06	13.82± 0.06	13.14± 0.08	10.41± 0.06	6.21± 0.05	1.78± 0.22	> -0.85	yes	no	yes-faint	no	no	...
044913.7+252549	...	13.49± 0.06	12.81± 0.18	13.37± 0.09	11.91± 0.06	> 9.24	> 0.83	> -1.04	no	yes	...
044916.3+243827	CCDM J04493+2438A	8.92± 0.05	8.93± 0.05	8.87± 0.05	8.86± 0.05	8.35± 0.09	> 0.88	> -0.57	...	no	yes	no	no	...
044941.5+254010	...	12.80± 0.06	12.73± 0.06	12.59± 0.07	12.61± 0.09	9.56± 0.26	> 0.76	yes	no	no	no	...

^aTable will be presented both in the print and in the electronic version. To convert between magnitudes and flux densities, we use $M = 2.5 \log(F_{\text{zeropt}}/F)$ where the zero-point flux densities for the seven Spitzer bands are 280.9, 179.7, 115.0, and 64.13 Jy for IRAC and 7.14, 0.775, and 0.159 Jy for MIPS. IRAC effective wavelengths are 3.6, 4.5, 5.8, and 8.0 μm ; MIPS effective wavelengths are 24, 70, and 160 μm .

^bMIPS-160 flux density for this object is subject to confusion with a nearby source or sources.

^cMIPS-160 flux density for this object is compromised by missing and/or saturated data.

^dMIPS-160 flux density for this object is hard saturated.

^eObject previously identified in the literature as a potential YSO.

^fObject previously identified in the literature as a potential non-member.

^gObject identified as a Taurus member by other authors using portions of this Spitzer Legacy data set.

Table 6. Derived properties of previously identified Taurus members^a

SST Tau name	common name	c2d category	Gutermuth category	our class	spectral type	our H α EQW (Å)	A_V (mags)	log L_* (L_\odot)	L_{IR}/L_{total}	notes
041314.1+281910	LkCa 1	ysc	star	III	M4	...	1.3	-0.3	< 2.0e-05	...
041327.2+281624	Anon 1	ysc	star	III	M0	...	3.2	0.4	< 3.8e-05	...
041353.2+281123	IRAS04108+2803 A	ysc	class II	flat	d
041354.7+281132	IRAS04108+2803 B	ysc	embedded	I	d
041357.3+291819	IRAS04108+2910	ysc	class II	II	K5e	-201.4	4.8	-0.4	0.37	b c
041411.8+281153	J04141188+2811535	ysc	class II	II	M6.25	...	1.7	-1.6	0.25	...
041412.2+280837	IRAS04111+2800G	ysc	embedded	I	d
041412.9+281212	V773 Tau ABC	II	K3	...	2.8	0.9	0.047	...
041413.5+281249	FM Tau	ysc	class II	II	M0	-99.1	2.4	-0.3	0.18	b
041414.5+282758	FN Tau	ysc	class II	II	M5	...	1.6	-0.2	0.22	...
041417.0+281057	CW Tau	II	K3	-137.9	6.9	0.6	0.22	b
041417.6+280609	CIDA-1	ysc	class II	II	M5.5	...	4.6	-0.7	0.32	...
041426.2+280603	IRAS04113+2758 A	I	M2.5	...	17.1	0.3	0.50	...
041430.5+280514	MHO-3	...	embedded	flat	K7	...	11.3	0.3	0.17	...
041447.3+264626	FP Tau	ysc	class II	II	M4	...	0.8	-0.4	0.083	...
041447.8+264811	CX Tau	ysc	class II	II	M2.5	...	1.4	-0.3	0.11	...
041447.9+275234	LkCa 3 AB	ysc	star	III	M1	...	0.7	0.3	< 4.3e-05	...
041449.2+281230	FO Tau AB	ysc	class II	II	M2	...	3.7	0.0	0.094	...
041505.1+280846	CIDA-2	ysc	star	III	M4.5	...	0.6	-0.5	< 8.2e-05	...
041514.7+280009	KPNO-1	...	star	III	M8.5	...	1.7	-2.4	0.013	...
041524.0+291043	J04152409+2910434	...	star	III	M7	...	1.3	-1.9	< 0.0046	...
041612.1+275638	J04161210+2756385	ysc	class II	II	M4.75	...	4.6	-0.9	0.15	...
041618.8+275215	J04161885+2752155	...	star	III	M6.25	...	1.1	-1.5	< 0.0020	...
041628.1+280735	LkCa 4	ysc	star	III	K7	...	0.8	-0.0	< 5.7e-05	...
041639.1+285849	J04163911+2858491	ysc	class II	II	M5.5	...	2.3	-1.4	0.082	...
041733.7+282046	CY Tau	ysc	class II	II	M1	...	1.7	-0.2	0.076	...
041738.9+283300	LkCa 5	III	M2	...	0.2	-0.5	< 5.7e-05	...
041749.5+281331	KPNO-10	ysc	class II	II	M5	...	1.1	-1.2	0.12	...
041749.6+282936	V410 X-ray 1	ysc	class II	II	M2	...	5.5	-0.3	0.12	...
041807.9+282603	V410 X-ray 3	ysc	star	III	M6	...	0.8	-1.1	< 0.00025	...
041817.1+282841	V410 Anon 13	ysc	class II	II	M5	...	5.9	-1.1	0.068	...
041822.3+282437	V410 Anon 24	ysc	star	II	G1	...	22.5	0.1	< 5.8e-06	...
041829.0+282619	V410 Anon 25	ysc	star	II	M1	...	22.9	0.0	< 1.2e-05	...
041830.3+274320	KPNO-11	...	star	III	M5.5	...	0.0	-1.3	< 0.0018	...
041831.1+282716	V410 Tau ABC	ysc	star	III	K3	...	1.1	0.4	< 6.5e-05	...
041831.1+281629	DD Tau AB	II	M1	...	4.3	0.1	0.30	...
041831.5+281658	CZ Tau AB	ysc	embedded	II	M1.5	...	0.7	-0.6	0.53	...
041832.0+283115	IRAS04154+2823	ysc	class II	I	M2.5	...	19.0	-0.6	0.63	...
041834.4+283030	V410 X-ray 2	ysc	class II	flat	M0	...	21.0	0.3	0.024	...
041840.2+282424	V410 X-ray 4	ysc	star	II	M4	...	18.0	-0.1	< 6.3e-06	...
041840.6+281915	V892 Tau	flat	A6	-12.7	14.3	2.0	0.089	...
041841.3+282725	LR1	ysc	class II	flat	K4.5	...	24.0	-0.3	0.12	...
041842.5+281849	V410 X-ray 7	ysc	class II	II	M1	...	10.3	-0.1	0.0092	...
041845.0+282052	V410 Anon 20	...	star	flat	K3	...	21.6	-0.6	< 0.00022	...
041847.0+282007	Hubble 4	ysc	star	III	K7	...	2.5	0.4	< 6.0e-05	...
041851.1+281433	KPNO-2	...	star	III	M7.5	...	0.3	-2.1	0.0096	...
041851.4+282026	CoKu Tau/1	ysc	embedded	I	K7	...	6.5	-0.9	0.72	...
041858.1+281223	IRAS04158+2805	ysc	class II	flat	M6	...	7.0	-1.3	0.76	...
041901.1+281942	V410 X-ray 6	ysc	star	II	M4.5	...	2.7	-0.5	0.082	...
041901.2+280248	KPNO-12	...	class II	II	M9	...	1.4	-2.9	0.12	...
041901.9+282233	V410 Tau X-ray 5a	ysc	star	III	M5	...	5.1	-0.8	< 0.00015	...
041912.8+282933	FQ Tau AB	ysc	class II	II	M2	...	1.1	-0.6	0.086	...
041915.8+290626	BP Tau	ysc	class II	II	K7	...	2.1	0.2	0.094	...
041926.2+282614	V819 Tau	ysc	star	III	K7	...	1.9	0.0	0.0018	...
041935.4+282721	FR Tau	ysc	class II	II	M5e	-58.9	1.0	-0.9	0.17	c g
041941.2+274948	LkCa 7 AB	ysc	star	III	K7	...	1.0	0.0	< 6.1e-05	...
041942.5+271336	IRAS04166+2706	ysc	embedded	I
041958.4+270957	IRAS04169+2702	ysc	embedded	I	d
042025.5+270035	J04202555+2700355	ysc	class II	II	M5.25	...	2.1	-1.5	0.14	...
042039.1+271731	2MASS J04203918+2717317	ysc	star	III	g

Table 6—Continued

SST Tau name	common name	c2d category	Gutermuth category	our class	spectral type	our H α EQW (Å)	A_V (mags)	log L_* (L_\odot)	L_{IR}/L_{total}	notes
042107.9+270220	CFHT-19	ys	class II	I	M5.25	...	10.3	-1.0	0.83	...
042110.3+270137	IRAS04181+2654B	ys	class II	I	d
042111.4+270109	IRAS04181+2654A	ys	embedded	I	d
042134.5+270138	J04213459+2701388	ys	class II	II	M5.5	...	2.7	-1.0	0.029	...
042146.3+265929	CFHT-10	ys	class II	II	M6.25	...	4.0	-1.7	0.056	...
042154.5+265231	J04215450+2652315	not ys	star	II	M8.5	...	3.3	-2.4	0.012	...
042155.6+275506	DE Tau	ys	class II	II	M2	...	2.2	0.1	0.13	...
042157.4+282635	RY Tau	II	K1	-16.8	4.8	1.3	0.10	b
042158.8+281806	HD283572	star	star	III	G5	...	0.4	0.8	< 3.0e-05	...
042200.6+265732	FS Tau B	ys	embedded	I	d
042202.1+265730	FS Tau Aab	ys	class II	flat	M0e	-46.8	6.9	0.0	0.36	b c
042203.1+282538	LkCa 21	star	star	III	M3	...	1.3	-0.2	< 2.9e-05	...
042216.4+254911	CFHT-14	...	star	III	M7.75	...	0.4	-1.8	< 0.0030	...
042216.7+265457	CFHT-21	ys	class II	II	M1.25	...	7.7	-0.3	0.23	...
042224.0+264625	2MASS J04222404+2646258	ys	star	III	g
042307.7+280557	IRAS04200+2759	ys	class II	flat	M2	...	8.1	-0.9	0.53	d
042339.1+245614	FT Tau	ys	class II	II	M3e	-254.3	3.8	-0.2	0.13	b c
042426.4+264950	CFHT-9	ys	class II	II	M6.25	...	0.5	-1.7	0.11	...
042444.5+261014	IRAS04216+2603	ys	class II	II	M1	...	3.4	-0.4	0.29	...
042445.0+270144	J1-4423	...	star	II	M5	...	0.1	-1.1	< 0.00095	...
042449.0+264310	RXJ0424.8	ys	star	III	K1	...	1.2	0.4	< 6.1e-05	...
042457.0+271156	IP Tau	ys	class II	II	M0	...	1.9	-0.2	0.10	...
042517.6+261750	J1-4872 AB	ys	star	III	K7	...	3.7	0.2	< 2.6e-05	...
042629.3+262413	KPNO-3	ys	class II	II	M6	...	1.6	-1.7	0.13	...
042630.5+244355	J04263055+2443558	ys	class II	II	M8.75	...	0.6	-2.4	0.16	...
042653.5+260654	FV Tau AB	II	K5	...	8.7	0.6	0.13	...
042654.4+260651	FV Tau/c AB	ys	class II	II	M3.5	...	5.9	-0.2	0.096	...
042656.2+244335	IRAS04239+2436	...	embedded	I	d
042657.3+260628	KPNO-13	ys	class II	II	M5	...	4.3	-0.6	0.078	...
042702.6+260530	DG Tau B	I
042702.8+254222	DF Tau AB	II	M3	...	2.4	0.5	0.11	...
042704.6+260616	DG Tau A	II	K5e	-90.7	3.2	0.5	0.20	b c
042727.9+261205	KPNO-4	not ys	star	II	M9.5	...	2.8	-2.3	0.037	...
042745.3+235724	CFHT-15	...	star	III	M8.25	...	0.3	-2.5	< 0.0043	...
042757.3+261918	IRAS04248+2612 AB	ys	embedded	flat	M5.5	...	5.8	-0.6	0.55	...
042838.9+265135	LDN 1521F-IRS	ys	contam.	I
042842.6+271403	J04284263+2714039 AB	ys	class II	II	M5.25	...	3.7	-1.0	0.050	...
042900.6+275503	J04290068+2755033	ys	class II	II	M8.25	...	0.3	-2.1	0.11	...
042904.9+264907	IRAS04260+2642	ys	class II	I	K6	...	9.1	-1.3	0.57	...
042920.7+263340	J1-507	ys	star	III	M4	...	0.9	-0.4	< 4.3e-05	...
042921.6+270125	IRAS04263+2654	ys	class II	II	M6.0	...	5.9	-0.3	0.094	...
042923.7+243300	GV Tau AB	I	mid-K +emiss	-296.0	11.9	0.3	< 0.92	b c
042929.7+261653	FW Tau ABC	ys	star	III	M4	...	0.3	-0.6	0.0019	...
042930.0+243955	IRAS04264+2433	ys	embedded	I	M1	...	9.5	-0.9	0.75	...
042941.5+263258	DH Tau AB	ys	star	II	M1	...	2.5	-0.1	0.086	...
042942.4+263249	DI Tau AB	...	star	III	M0	...	0.5	-0.1	< 0.0011	...
042945.6+263046	KPNO-5	...	star	III	M7.5	...	0.6	-1.6	< 0.0025	...
042951.5+260644	IQ Tau	ys	class II	II	M0.5	...	2.9	0.1	0.19	...
042959.5+243307	CFHT-20	ys	class II	II	M5.5	...	4.6	-0.7	0.10	...
043007.2+260820	KPNO-6	not ys	class II	II	M8.5	...	1.2	-2.4	0.10	...
043023.6+235912	CFHT-16	...	star	III	M8.5	...	0.5	-2.5	< 0.0038	...
043029.6+242645	FX Tau AB	ys	class II	II	M1	...	2.9	0.1	0.081	...
043044.2+260124	DK Tau AB	II	K7	...	2.9	0.4	0.13	...
043050.2+230008	IRAS04278+2253	II	F1	...	13.6	1.8	0.075	...
043051.3+244222	ZZ Tau AB	ys	class II	II	M5	-9.7	1.6	-0.2	0.029	c
043051.7+244147	ZZ Tau IRS	ys	class II	flat	M4.5	...	6.9	-0.9	0.76	...
043057.1+255639	KPNO-7	not ys	class II	II	M8.25	...	0.3	-2.3	0.13	...
043114.4+271017	JH56	ys	star	III	M0.5	...	0.0	-0.3	0.0025	...
043119.0+233504	J04311907+2335047	...	star	III	M7.75	...	1.2	-1.8	< 0.0032	...
043123.8+241052	V927 Tau AB	ys	star	III	M5.5	...	0.4	-0.4	< 5.5e-05	...

Table 6—Continued

SST Tau name	common name	c2d category	Gutermuth category	our class	spectral type	our H α EQW (Å)	A_V (mags)	log L_* (L_\odot)	L_{IR}/L_{total}	notes
043126.6+270318	CFHT-13	yso	star	III	M7.25	...	1.8	-2.3	0.0062	...
043150.5+242418	HK Tau AB	yso	class II	II	M0.5	...	4.7	-0.2	0.22	...
043158.4+254329	J1-665	yso	star	III	M5	...	1.2	-0.6	< 3.1e-05	...
043203.2+252807	J04320329+2528078	...	star	III	M6.25	...	0.0	-1.2	< 0.0025	...
043215.4+242859	Haro6-13	flat	M0	...	11.0	0.2	0.32	...
043217.8+242214	CFHT-7 AB	yso	star	III	M6.5	...	0.9	-1.1	< 0.00021	...
043218.8+242227	V928 Tau AB	yso	star	III	M0.5	...	3.9	0.1	< 2.9e-05	...
043223.2+240301	J04322329+2403013	...	star	III	M7.75	...	0.0	-1.5	< 0.0026	...
043230.5+241957	FY Tau	yso	class II	II	K7	...	5.9	0.2	0.061	...
043231.7+242002	FZ Tau	II	M0	...	7.2	0.4	0.17	...
043232.0+225726	IRAS04295+2251	yso	embedded	I	d
043243.0+255231	UZ Tau Aab	II	M1	-80.3	0.0	-0.0	0.41	b
043249.1+225302	JH112	yso	class II	II	K6	...	5.5	0.1	0.11	...
043250.2+242211	CFHT-5	yso	star	III	M7.5	...	9.5	-1.1	< 0.00015	...
043301.9+242100	MHO-8	yso	star	III	M5.5	...	0.9	-0.8	< 0.00012	...
043306.2+240933	GH Tau AB	yso	class II	II	M2	...	1.9	0.1	0.093	...
043306.6+240954	V807 Tau AB	II	K7	...	1.3	0.5	0.050	...
043307.8+261606	KPNO-14	yso	star	III	M6	...	4.1	-0.9	< 0.00012	...
043309.4+224648	CFHT-12	yso	class II	II	M6.5	...	3.2	-1.5	0.036	...
043310.0+243343	V830 Tau	yso	star	III	K7	...	0.7	-0.1	< 4.5e-05	...
043314.3+261423	IRAS04301+2608	yso	contam.	flat	M0	...	6.5	-1.6	0.62	d
043316.5+225320	IRAS04302+2247	yso	star	I	d
043319.0+224634	IRAS04303+2240	II	M0.5	...	10.8	0.2	0.45	...
043334.0+242117	GI Tau	yso	class II	II	K6	...	2.7	0.2	0.19	...
043334.5+242105	GK Tau	II	K7	...	2.7	0.3	0.16	...
043336.7+260949	IS Tau AB	yso	class II	II	K7	...	3.5	-0.2	0.15	...
043339.0+252038	DL Tau	yso	class II	II	K7	...	2.8	0.0	0.26	...
043342.9+252647	J04334291+2526470	...	star	III	M8.75	...	1.2	-2.3	< 0.0042	...
043352.0+225030	CI Tau	yso	class II	II	K7	...	3.6	0.2	0.14	...
043352.5+225626	2MASS J04335252+2256269	yso	star	III	g
043354.7+261327	IT Tau AB	yso	class II	II	K2	...	13.4	0.9	0.0082	...
043410.9+225144	JH108	yso	star	III	M1	...	1.7	-0.5	< 6.8e-05	...
043415.2+225030	CFHT-1	...	star	II
043439.2+250101	Wa Tau 1	star	star	III	K0	...	0.3	0.3	< 3.4e-05	...
043455.4+242853	AA Tau	yso	class II	II	K7	...	2.2	0.1	0.15	...
043508.5+231139	CFHT-11	not yso	star	III	M6.75	...	0.0	-1.6	0.00051	...
043520.2+223214	HO Tau	yso	class II	II	M0.5	...	2.6	-0.7	0.11	...
043520.8+225424	FF Tau AB	yso	star	III	K7	0.0	1.9	-0.1	< 6.3e-05	...
043527.3+241458	DN Tau	yso	class II	II	M0	...	1.1	0.0	0.095	...
043535.3+240819	IRAS04325+2402 A	yso	class II	I	d
043540.9+241108	CoKu Tau/3 AB	yso	class II	II	M1	...	7.7	0.1	0.11	...
043541.8+223411	KPNO-8	...	star	III	M5.75	...	0.0	-1.7	< 0.0020	...
043545.2+273713	J04354526+2737130	...	star	III	M9.25	...	1.0	-2.5	< 0.0021	...
043547.3+225021	HQ Tau	II	K2	-1.2	3.8	0.6	0.098	c d g
043551.0+225240	KPNO-15	star	star	III	M1.5	...	2.7	-0.7	< 2.2e-05	...
043551.4+224911	KPNO-9	...	star	III	M8.5	...	1.4	-2.6	< 0.0040	...
043552.0+225503	2MASS J04355209+2255039	...	star	III	g
043552.7+225423	HP Tau AB	II	K3	-11.2	4.8	0.3	0.24	e
043552.8+225058	2MASS J04355286+2250585	yso	star	III	g
043553.4+225408	HP Tau/G3 AB	...	star	III	K7	...	2.2	-0.2	< 0.0011	...
043554.1+225413	HP Tau/G2	...	star	III	G0	...	2.6	0.8	< 0.00059	...
043556.8+225436	Haro 6-28 AB	yso	class II	II	M5	...	4.1	-0.6	0.11	...
043558.9+223835	2MASS J04355892+2238353	...	star	III	g
043610.3+215936	J04361030+2159364	not yso	class II	II	M8.5	...	0.8	-2.4	0.096	...
043610.3+225956	CFHT-2	...	star	III	M7.5	...	3.0	-1.8	< 0.0024	...
043619.0+254258	LkCa 14	yso	star	III	M0	...	0.0	-0.2	< 4.5e-05	...
043638.9+225811	CFHT-3	...	star	III	M7.75	...	1.8	-1.9	< 0.0025	...
043649.1+241258	HD 283759	yso	star	II	F2	5.5	0.4	0.4	0.0037	c
043800.8+255857	ITG 2	yso	star	III	M7.25	...	2.3	-0.9	< 8.9e-05	...
043814.8+261139	J04381486+2611399	yso	class II	I	M7.25	...	3.5	-2.3	0.75	...

Table 6—Continued

SST Tau name	common name	c2d category	Gutermuth category	our class	spectral type	our H α EQW (Å)	A_V (mags)	$\log L_*$ (L_\odot)	L_{IR}/L_{total}	notes
043815.6+230227	RXJ0438.2+2302	...	star	III	M1	...	0.3	-0.7	< 0.00078	...
043821.3+260913	GM Tau	ys0	class II	II	d
043828.5+261049	DO Tau	II	M0	...	4.9	0.3	0.28	...
043835.2+261038	HV Tau AB	...	star	III	M1	...	2.5	0.1	< 0.0012	...
043835.4+261041	HV Tau C	ys0	class II	flat	M4e	-10.0	1.9	-1.7	0.71	c
043858.5+233635	J0438586+2336352	II	M4.25	...	0.0	-1.3	0.085	...
043901.6+233602	J0439016+2336030	II	M6	-3.3	0.9	-1.0	0.044	...
043903.9+254426	CFHT-6	ys0	class II	II	M7.25	...	1.3	-1.5	0.12	...
043906.3+233417	J0439064+2334179	III	M7.5	...	0.0	-1.4	< 0.0	...
043913.8+255320	IRAS04361+2547 AB	...	class II	I	d
043917.7+222103	LkCa 15	ys0	class II	II	K5	...	1.9	0.0	0.10	...
043920.9+254502	GN Tau B	ys0	class II	II	M2.5	...	5.7	0.0	0.20	...
043935.1+254144	IRAS04365+2535	I	d
043947.4+260140	CFHT-4	ys0	class II	II	M7	...	4.4	-1.0	0.14	...
043953.9+260309	IRAS 04368+2557	ys0	embedded	I
043955.7+254502	IC2087 IRS	flat	K4	...	18.0	1.3	0.41	...
044001.7+255629	CFHT-17 AB	ys0	star	III	M5.75	...	8.4	-0.9	< 0.00023	...
044008.0+260525	IRAS 04370+2559	ys0	class II	II	<M0	...	13.1	-0.0	0.15	...
044039.7+251906	J04403979+2519061 AB	ys0	star	III	M5.25	...	3.6	-0.9	0.0042	...
044049.5+255119	JH223	ys0	class II	II	M2	...	1.5	-0.6	0.080	...
044104.2+255756	Haro 6-32	star	star	III	M5	...	0.6	-0.9	< 2.9e-05	...
044104.7+245106	IW Tau AB	star	star	III	K7	...	1.1	0.0	< 4.0e-05	...
044108.2+255607	ITG 33 A	ys0	class II	flat	M3	...	8.3	-1.1	0.33	...
044110.7+255511	ITG 34	ys0	class II	II	M5.5	...	4.0	-1.4	0.10	...
044112.6+254635	IRAS04381+2540	ys0	embedded	I	d
044138.8+255626	IRAS04385+2550	ys0	class II	flat	M0	...	9.3	-0.2	0.30	...
044148.2+253430	J04414825+2534304	ys0	class II	II	M7.75	...	2.4	-1.8	0.21	...
044205.4+252256	LkHa332/G2 AB	ys0	star	III	K7	...	4.3	0.1	0.00016	...
044207.3+252303	LkHa332/G1 AB	...	star	III	M1	...	4.6	0.2	< 0.00065	...
044207.7+252311	V955 Tau Ab	ys0	class II	II	K7	...	5.0	0.2	0.14	...
044221.0+252034	CIDA-7	ys0	class II	II	M3	...	1.6	-0.9	0.20	...
044237.6+251537	DP Tau	ys0	class II	II	M0.5	...	5.6	-0.3	0.37	...
044303.0+252018	GO Tau	ys0	class II	II	M0	...	2.3	-0.5	0.096	...
044427.1+251216	IRAS04414+2506	ys0	class II	II	M7.25	...	1.6	-1.3	0.44	...
044642.6+245903	RXJ04467+2459	ys0	star	III	M4	...	0.0	-1.0	< 0.00015	...

^aTable will be presented both in the print and in the electronic version.

^bCa IR triplet in emission in our spectrum.

^cNew spectral type, reported here.

^dUnreduced IR spectrum in-hand, to be discussed in a later paper.

^e043552.7+225423=HP Tau AB was observed twice in the same night (3 Dec 2008), and within 7 hrs the H α equivalent width changed from 1.95 Å in absorption to 11.24 Å in emission.

Table 7. Derived properties of new potential Taurus members^a

SST Tau name	common name	our rank	c2d category	Gutermuth category	our class	spectral type	our H α EQW (Å)	A_V (mags)	$\log L_*$ (L_\odot)	L_{IR}/L_{total}	adopted memb. classification	notes
041159.7+294236	...	C	III	G8-K1	0.9	2.8	-0.8	0.0020	needs add'l followup	c
041332.3+291726	...	A	not yso	star	II	pending followup	d
041339.4+292114	...	B-	ys	embedded	flat	pending followup	k
041427.3+255130	...	B+	not yso	star	III	G5	2.5	0.4	-1.7	0.0095	possible new member	c o
041535.6+284741	...	A-	ys	embedded	I	pending followup	d
041539.1+281858	...	A+	ys	class II	II	M5	-7.2	2.8	-0.5	0.075	new member	c g m
041542.7+290959	...	A+	ys	star	II	M0 w/ Av	-1.9	2.5	-0.5	0.099	new member	c g
041557.9+274617	...	A+	ys	class II	II	M6	-32.2	1.1	-1.1	0.12	new member	c g m
041604.8+261801	...	C-	ys	embedded	flat	pending followup	...
041605.8+281426	...	C	not yso	contam.	I	pending followup	...
041624.5+290858	HD 281820	B	ys	star	III	A2	11.5	0.8	0.3	0.00017	needs add'l followup	c o
041706.2+264413	...	B+	not yso	star	III	K3	1.5	0.9	-1.0	0.0020	needs add'l followup	c
041801.1+283526	...	B+	not yso	star	III	K0-K2:	1.1	6.2	-0.9	0.0013	possible new member	c p
041803.3+244009	...	B	ys	star	III	A9	7.9	0.3	-0.3	0.0022	needs add'l followup	c f o
041810.5+284447	...	C	ys	class II	I	pending followup	...
041810.7+251957	[GBM90] L1506 1	A+	ys	class II	II	K8-M0	-4.3	4.3	-0.3	0.11	new member	b c f g p
041823.2+251928	2MASX 04182321+2519281	B+	ys	class II	flat	G	1.9	7.7	-1.8	0.34	needs add'l followup	c f m o
041831.2+282617	...	B+	ys	class II	I	pending followup	d
041858.0+235031	...	B	ys	embedded	flat	pending followup	d
041859.0+255740	...	B-	ys	embedded	I	pending followup	...
041936.2+265256	...	B	not yso	star	III	G3	2.7	0.8	-1.3	0.0032	needs add'l followup	c o
041940.4+270100	...	B-	ys	embedded	I	pending followup	h m
041941.4+271607	HH390 star	A	ys	class II	I	<M0	...	5.5	-1.7	0.87	probable new member	d m
041946.5+271255	...	B	ys	embedded	I	pending followup	d g
042016.1+282132	...	A+	ys	class II	II	M6e	-133.1	0.2	-2.1	0.13	new member	c d g l
042021.4+281349	...	A+	ys	class II	flat	M0e	-489.1	3.5	-2.4	0.44	new member	b c d g m
042025.8+281923	...	A+	ys	class II	flat	M4e	-102.2	11.2	-1.5	0.71	new member	c d g l m
042025.8+281641	...	B	ys	star	III	G2:	3.1	1.0	-0.2	0.00016	needs add'l followup	c
042026.0+280408	...	A+	ys	class II	II	M2	-5.3	0.0	-0.7	0.26	new member	c d g l m
042109.3+275036	...	A+	ys	class II	III	M3-4e	-17.6	0.0	-1.0	0.020	new member	c d g l m
042110.9+255259	V412 Tau	B	III	A1	9.2	8.3	2.1	7.1e-05	needs add'l followup	c m
042135.6+253835	...	B	not yso	star	III	F6-G0	3.1	1.2	-1.2	0.0043	possible new member	c o
042146.3+242505	...	B+	ys	star	III	M3	0.0	2.9	0.1	< 0.00023	needs add'l followup	c l
042151.3+265720	...	B	...	star	II	pending followup	d
042200.9+235430	...	B+	ys	star	III	M3	0.0	3.7	0.2	< 4.6e-05	needs add'l followup	c l m
042212.9+254659	...	B-	ys	class II	flat	pending followup	f m
042215.6+265706	2MASS J04221568+2657060	A+	ys	class II	I	K8-M0	-7.8	4.5	-1.5	0.65	new member	c d g h i j m
042220.9+264248	...	A	ys	embedded	I	pending followup	...
042247.8+264553	IRAS04196+2638	A+	ys	class II	II	M1	...	6.9	-0.4	0.24	new member	e g m
042254.6+282354	NSV 1577	A	ys	star	II	A0	10.0	1.5	1.4	0.00060	probable new member	c n
042306.0+280119	J04230607+2801194	A+	ys	class II	II	M6	...	0.0	-1.5	0.10	new member	g m
042318.2+264115	J04231822+2641156	A+	ys	class II	II	M3.5	...	8.7	-0.6	0.081	new member	g
042325.9+250354	...	C-	ys	star	II	pending followup	d
042335.3+250302	FU Tau	A+	ys	class II	II	M5e	-88.4	1.9	-0.7	0.18	new member	c g g l m
042339.0+251855	...	C	not yso	contam.	I	pending followup	...
042350.1+264006	FS 116	C	...	star	III	G6-K2 w/Av	1.6	8.2	-0.6	< 0.0011	needs add'l followup	c p
042356.0+242705	HD 283663	B	ys	star	III	A1	6.0	1.6	0.3	0.00012	needs add'l followup	c o
042358.6+244742	...	B-	...	star	III	K2	2.5	0.0	-1.0	0.0052	needs add'l followup	c
042420.9+263051	J04242090+2630511	A+	ys	class II	II	M6.5	...	0.3	-1.9	0.12	new member	g m
042423.2+265008	...	A	ys	star	III	M3	-4.7	1.3	-0.7	0.0019	possible new member	c l m
042515.5+282927	...	A+	ys	star	III	M6e	-23.5	0.0	-1.1	< 0.00019	new member	c l m
042518.6+255535	...	B	III	M5	0.0	3.7	0.5	< 0.00013	needs add'l followup	c f l
042519.1+234716	HD 27923	B-	ys	star	III	B9	8.6	0.1	1.2	4.0e-05	needs add'l followup	c n o
042558.8+273701	HD 283637	B-	ys	star	III	B9	7.0	2.1	0.6	3.5e-05	needs add'l followup	c o
042653.3+255858	...	C	not yso	contam.	I	pending followup	...
042721.0+240829	...	C-	...	star	III	G6	2.8	0.2	-1.8	0.0042	needs add'l followup	c k o
042728.1+262323	...	C+	not yso	star	III	K1 w/ Av	1.3	0.0	-1.6	0.0070	needs add'l followup	c o
042730.2+244123	2MASX 04273023+2441232	B-	...	star	I	pending followup	d
042810.4+243553	...	C	not yso	embedded	flat	pending followup	...
042857.4+243607	...	A	ys	star	III	pending followup	d

Table 7—Continued

SST Tau name	common name	our rank	c2d category	Gutermuth category	our class	spectral type	our H α EQW (Å)	A_V (mags)	log L_* (L_\odot)	L_{IR}/L_{total}	adopted memb. classification	notes
042902.9+243140	...	C-	ysp	star	III	pending followup	d
042905.2+261535	2MASX 04290517+2615358	B-	...	star	II	pending followup	...
042916.2+285627	HD 283629	B+	ysp	star	III	G6	2.5	0.5	-0.1	0.00015	needs add'l followup	c
042920.8+274207	IRAS 04262+2735	A	ysp	class II	II	M6	0.0	4.0	0.4	0.040	possible new member	c d e f l p
042932.0+243059	...	A	ysp	embedded	I	pending followup	d g
042936.0+243555	J04293606+2435556	A+	ysp	class II	II	M3	...	6.6	-0.1	0.048	new member	g h i m
042949.9+284253	...	C-	not ysp	class II	flat	pending followup	...
043004.7+283306	...	B+	ysp	star	III	K2	1.6	1.3	-0.4	0.00036	needs add'l followup	c
043024.1+281916	...	B	ysp	star	III	M5	0.0	5.1	0.5	< 9.6e-05	needs add'l followup	c f l
043034.2+252427	...	B+	not ysp	star	II	G5-G6 w/ Av	2.7	2.3	-1.9	0.0085	needs add'l followup	c o
043042.8+274329	...	B+	ysp	star	III	M6	0.0	3.6	0.1	< 0.00032	needs add'l followup	c f l
043044.7+263308	...	B+	ysp	star	III	K3	1.1	2.2	0.5	0.00089	needs add'l followup	c m
043131.4+230025	...	B-	...	star	III	K2	1.5	1.7	-0.7	0.0027	needs add'l followup	c
043133.1+292856	...	B-	ysp	star	III	B9 w/ Av	10.7	2.6	0.5	3.3e-05	needs add'l followup	c o
043141.2+293922	...	C-	...	star	III	K2	1.2	1.4	-1.7	0.011	needs add'l followup	c k o
043145.0+285908	...	B	not ysp	star	III	F0	1.1	1.3	-0.6	0.0010	needs add'l followup	c o
043213.6+251746	GSC 01833-00754	C+	ysp	star	III	A9	6.4	1.3	-0.0	8.2e-05	needs add'l followup	c o
043214.6+223742	...	C	not ysp	embedded	flat	pending followup	...
043224.1+225108	...	A+	ysp	class II	II	M5e	-14.4	1.5	-1.0	0.064	new member	c d g l
043225.1+264732	...	B-	not ysp	star	III	K1 w/ Av	1.3	3.1	-0.9	0.0017	needs add'l followup	c
043228.1+271122	...	B	ysp	star	III	M6	0.0	7.0	0.5	< 4.0e-05	needs add'l followup	c f l
043244.2+230224	not ysp	embedded	I	xgal	d
043249.3+225308	...	A+	...	class II	II	early K	-25.9	7.1	-0.0	0.030	new member	b c g k p
043256.4+222342	HD 284481	B-	ysp	star	III	A8	6.5	1.0	0.3	6.4e-05	needs add'l followup	c o
043304.2+292149	HD 282276	A	ysp	star	II	B8V	5.7	needs add'l followup	d n
043312.6+291250	HD 282277	B	ysp	star	III	A7V	6.9	needs add'l followup	...
043316.6+262724	...	B+	ysp	class II	flat	pending followup	...
043326.2+224529	2MASS J04332621+2245293	A	ysp	star	II	M4	-6.8	5.9	-0.6	0.015	probable new member	c d g h l
043339.0+222720	...	A+	ysp	class II	II	M1e	-23.7	7.9	-0.9	0.12	new member	c d g l
043341.8+223836	...	B-	...	star	III	K2 w/ Av	0.7	4.9	-0.9	< 0.0021	needs add'l followup	c
043344.6+261500	...	A+	ysp	class II	II	M6e	-82.2	5.4	-0.6	0.13	new member	c d f g l m
043349.5+291528	IRAS 04306+2909	...	ysp	embedded	I	xgal	-1.9	9.5	0.2	0.021	xgal	c e
043352.4+261254	J04335245+2612548	A+	ysp	class II	II	M8.5	...	4.9	-2.4	0.13	new member	g
043359.2+293636	...	B+	ysp	star	III	M3 w/Av	0.0	5.5	0.4	< 8.0e-05	needs add'l followup	c l
043419.5+265210	...	A	not ysp	star	III	pending followup	d
043419.8+232649	HD 284530	B-	ysp	star	III	B8	7.7	1.9	1.2	3.8e-05	needs add'l followup	c n o
043435.4+264406	...	B-	III	M3	1.4	5.8	0.6	0.0010	needs add'l followup	c f l
043452.5+240244	...	B+	not ysp	star	III	K2 w/ Av	1.6	4.4	-1.1	0.0038	needs add'l followup	c
043456.9+225835	2MASS J04345693+2258358	A+	ysp	star	III	M0	-4.5	1.8	-0.5	0.00023	new member	c g h j
043521.3+255510	ysp	embedded	flat	xgal	d
043542.0+225222	2MASS J04354203+2252226	A+	ysp	star	III	M5e	-18.6	2.1	-0.8	< 0.00014	new member	c g h j l
043557.6+225357	J04355760+2253574	A+	ysp	star	II	M5:e	-30.4	3.4	-2.3	0.15	new member	c d l
043559.4+223829	...	A+	ysp	class II	flat	K7-M0	-1.7	2.0	-2.0	0.53	new member	c
043621.4+271912	...	A-	ysp	star	II	K2e	0.8	2.6	-1.5	0.012	possible new member	c o p
043621.5+235116	J04362151+2351165	A+	ysp	class II	II	M5.25	...	0.1	-1.8	0.065	new member	d g
043636.1+265910	...	B	...	star	III	K2	1.0	1.1	-1.4	0.0078	needs add'l followup	c
043642.0+265339	...	B	ysp	embedded	I	pending followup	...
043720.8+250019	...	B+	ysp	star	III	G0	3.5	0.8	-0.3	0.00035	needs add'l followup	c
043724.8+270919	SV* SVS 1085	B	ysp	class II	III	B8e	-20.4	2.3	0.7	0.00056	background Be	c d
043756.7+254622	ITG 1	A+	ysp	class II	II	new member	d e g
043801.9+251926	...	A+	not ysp	star	II	K8	-1.9	3.3	-1.6	0.015	new member	c d
043803.6+221223	...	C-	not ysp	star	III	G0	3.2	0.3	-1.0	0.0020	needs add'l followup	c o
043816.5+261450	...	C-	ysp	star	III	pending followup	d
043826.7+265501	...	B+	ysp	star	III	G6-K2	1.8	1.0	-0.4	0.00019	needs add'l followup	c
043905.2+233745	J04390525+2337450	A+	ysp	class II	flat	K5e	-28.2	4.1	-1.3	0.39	new member	c d g
043933.6+235921	J04393364+2359212	A+	ysp	class II	II	M5	...	1.3	-1.0	0.15	new member	g
043939.9+252034	JH 225	B-	ysp	star	III	B9 w/ Av	10.5	4.1	0.9	5.0e-05	needs add'l followup	c f o
043943.8+271956	...	C	...	star	III	K0-K2	1.2	2.5	-0.9	< 0.0014	needs add'l followup	c
043944.8+260152	ITG 15	A+	ysp	class II	II	M5	...	4.4	-0.3	0.072	new member	e g m
044000.6+235821	J04400067+2358211	A+	ysp	class II	II	M6	...	0.0	-1.5	0.096	new member	g

Table 7—Continued

SST Tau name	common name	our rank	e2d category	Gutermuth category	our class	spectral type	our H α EQW (Å)	A_V (mags)	$\log L_*$ (L_\odot)	L_{IR}/L_{total}	adopted memb. classification	notes
044022.8+243307	ys0	embedded	I	xgal	d
044023.0+255702	ys0	star	III	G0	1.0	7.4	-0.5	0.00022	needs add'l followup	m
044048.4+233941	...	A-	II	K0	0.8	2.1	-1.9	0.012	possible new member	c o
044124.6+254353	ITG 40	A+	ys0	class II	flat	M3.5	...	22.2	-0.8	0.060	new member	e g
044125.7+254349	...	B	not ys0	embedded	I	pending followup	f h
044200.4+235813	ys0	embedded	I	xgal	d
044241.1+244117	CCDM J04427+2441AB	B+	ys0	star	III	A0	9.8	needs add'l followup	m
044253.9+253709	...	B	not ys0	star	III	F5	3.3	2.2	-1.5	0.0043	needs add'l followup	o
044315.8+235358	...	C-	ys0	embedded	I	pending followup	...
044325.1+255706	...	B+	ys0	star	III	K7-M0	0.5	0.2	-0.5	0.00020	needs add'l followup	c m
044345.3+243908	TYC 1834-591-1	B	ys0	star	III	pending followup	d n
044358.3+235103	...	C-	ys0	star	III	M3	1.4	3.7	0.8	< 9.5e-06	needs add'l followup	c l
044518.2+242436	HD 30067	B+	ys0	star	III	A4V	10.6	needs add'l followup	m n
044539.8+251704	...	B	ys0	star	III	M5	0.0	4.9	-0.1	< 7.3e-05	needs add'l followup	c d f l m
044550.7+254448	ys0	embedded	flat	xgal	d
044555.7+261858	...	A	not ys0	star	II	K4	1.3	2.4	-1.0	0.021	possible new member	c d
044557.0+244042	...	B-	...	class II	III	K2	1.5	1.8	-1.9	0.015	needs add'l followup	c f o
044609.6+245237	...	A-	not ys0	star	II	early G	2.4	5.4	-1.4	0.0043	possible new member	c d o
044639.8+242526	...	C-	III	M5	0.0	4.5	1.0	< 0.00018	needs add'l followup	c f l m
044644.4+262306	...	B+	III	M4	0.0	3.7	0.8	< 0.00018	needs add'l followup	c l m
044650.3+243815	...	B-	not ys0	star	III	K0-K1 w/ Av	2.1	1.8	-2.0	0.0079	needs add'l followup	c o
044802.3+253359	...	B	ys0	star	III	K0-K1 w/ Av	0.0	5.9	-0.4	8.0e-05	needs add'l followup	c m
044832.3+234746	...	C	ys0	embedded	I	pending followup	...
044857.4+255853	2MASX 04485745+2558527	B+	not ys0	class II	II	K	0.0	5.0	-1.9	0.015	possible new member	c d o
044900.1+241346	ys0	contam.	I	xgal	d
044913.7+252549	...	C-	...	contam.	III	F6	2.6	4.5	-1.6	0.011	needs add'l followup	c o
044916.3+243827	CCDM J04493+2438A	C	ys0	star	III	K2 w/ Av	1.6	0.5	-0.2	0.00018	needs add'l followup	c k
044941.5+254010	...	B+	not ys0	star	III	M3	0.0	1.5	-2.0	0.011	needs add'l followup	c d l

^aTable will be presented both in the print and in the electronic version.

^bCa IR triplet in emission in our spectrum.

^cNew spectral type, reported here.

^dUnreduced IR spectrum in-hand, to be discussed in a later paper.

^eObject previously identified in the literature as a potential Taurus member.

^fObject previously identified in the literature as a potential non-member.

^gObject identified as a Taurus member by other authors using portions of this Spitzer Legacy data set.

^hX-ray source in the XEST survey.

ⁱUltraviolet source in the XEST survey (optical monitor data).

^jObject found via X-rays in Scelsi et al. (2007) and confirmed as new member in Scelsi et al. (2008); object also independently rediscovered via IR excesses here.

^kHigh spatial-resolution optical images suggest IR flux density may be subject to confusion with a nearby object.

^lGravity analysis (see text) suggests intermediate gravity object and therefore likely member.

^mUV excess source in SDSS data.

ⁿExtended emission seen in image at 8 μ m or longer, which may be affecting the long-wavelength photometry.

^oObject appears lower in the HR diagram than most Taurus members; object may suffer from additional (unmodelled) extinction such as may be found in edge-on disks, but may also be background giant.

^pNotes on specific objects: 041810.7+251957 = [GBM90] L1506 1 was observed in Jan and Dec 2008, and the object went from 4.31 Å in emission to 0.983 Å in absorption at H α .

043621.4+271912: many emission lines in the blue spectrum, but not in the red.

042350.1+264006=FS 116: appears in Hawarden et al. (2001) as a UKIRT *JHK* standard.

042215.6+265706=2MASS J04221568+2657060: has detected nebulosity in Sloan images, which may be contributing to the measured flux density at the longest Spitzer bands.

043249.3+225308 : within 6 arcsec of a known object (043249.1+225302).

041801.1+283526 : may be double source in CFHT image.

042920.8+274207 : shares many characteristics of young stars, but also those of some post-main-sequence objects.

Table 8. List of new confirmed, probable, possible, and pending Taurus members

SST Tau name	common name	RA (J2000)	Dec (J2000)	our rank	distance ^a (arcmin)
new members					
041539.1+281858	...	63.913178	28.316282	A+	12.66
041542.7+290959	...	63.928283	29.166586	A+	4.14
041557.9+274617	...	63.991642	27.771547	A+	7.54
041810.7+251957	[GBM90] L1506 1	64.544954	25.332630	A+	62.64
042016.1+282132	...	65.067129	28.359041	A+	10.67
042021.4+281349	...	65.089345	28.230326	A+	16.91
042025.8+281923	...	65.107642	28.323265	A+	13.65
042026.0+280408	...	65.108609	28.069153	A+	17.42
042109.3+275036	...	65.288930	27.843567	A+	11.17
042215.6+265706	2MASS J04221568+2657060	65.565341	26.951694	A+	2.16
042247.8+264553	IRAS04196+2638	65.699455	26.764736	A+	5.35
042306.0+280119	J04230607+2801194	65.775303	28.022081	A+	4.65
042318.2+264115	J04231822+2641156	65.825957	26.687672	A+	13.16
042335.3+250302	FU Tau	65.897483	25.050739	A+	6.86
042420.9+263051	J04242090+2630511	66.087089	26.514210	A+	13.83
042515.5+282927	...	66.314616	28.490980	A+	36.65
042936.0+243555	J04293606+2435556	67.400276	24.598793	A+	4.05
043224.1+225108	...	68.100646	22.852333	A+	6.06
043249.3+225308	...	68.205751	22.885616	A+	0.11
043339.0+222720	...	68.412730	22.455774	A+	19.77
043344.6+261500	...	68.436051	26.250147	A+	2.74
043352.4+261254	J04335245+2612548	68.468574	26.215237	A+	0.74
043456.9+225835	2MASS J04345693+2258358	68.737218	22.976627	A+	6.93
043542.0+225222	2MASS J04354203+2252226	68.925159	22.872963	A+	2.11
043557.6+225357	J04355760+2253574	68.990035	22.899303	A+	0.67
043559.4+223829	...	68.997913	22.641430	A+	0.17
043621.5+235116	J04362151+2351165	69.089655	23.854609	A+	20.04
043756.7+254622	ITG 1	69.486267	25.773035	A+	12.61
043801.9+251926	...	69.507964	25.324060	A+	28.65
043905.2+233745	J04390525+2337450	69.771877	23.629189	A+	1.89
043933.6+235921	J04393364+2359212	69.890187	23.989231	A+	24.14
043944.8+260152	ITG 15	69.937014	26.031330	A+	0.62
044000.6+235821	J04400067+2358211	70.002817	23.972546	A+	25.99
044124.6+254353	ITG 40	70.352685	25.731396	A+	3.82
probable new members					
041941.4+271607	HH390 star	64.922838	27.268616	A	2.52
042254.6+282354	NSV 1577	65.727597	28.398354	A	11.46
043326.2+224529	2MASS J04332621+2245293	68.359223	22.758150	A	1.97
possible new members					
042423.2+265008	...	66.096734	26.835686	A	0.78
042920.8+274207	IRAS 04262+2735	67.336817	27.702072	A	13.68

Table 8—Continued

SST Tau name	common name	RA (J2000)	Dec (J2000)	our rank	distance ^a (arcmin)
044555.7+261858	...	71.482339	26.316357	A	61.92
043621.4+271912	...	69.089458	27.320208	A-	19.72
044048.4+233941	...	70.202020	23.661591	A-	24.00
044609.6+245237	...	71.540265	24.877144	A-	9.85
041427.3+255130	...	63.613782	25.858398	B+	55.12
041801.1+283526	...	64.504653	28.590672	B+	5.44
044857.4+255853	2MASX 04485745+2558527	72.239482	25.981394	B+	67.12
042135.6+253835	...	65.398398	25.643232	B	14.03
needs additional followup (beyond the spectra we have)					
043304.2+292149	HD 282276	68.267613	29.363867	A	101.91
041706.2+264413	...	64.276248	26.737167	B+	31.11
041823.2+251928	2MASX 04182321+2519281	64.596722	25.324471	B+	60.42
042146.3+242505	...	65.442927	24.418116	B+	40.35
042200.9+235430	...	65.503948	23.908342	B+	65.66
042916.2+285627	HD 283629	67.317694	28.940914	B+	61.49
043004.7+283306	...	67.519643	28.551838	B+	40.58
043034.2+252427	...	67.642795	25.407726	B+	20.43
043042.8+274329	...	67.678529	27.724981	B+	25.37
043044.7+263308	...	67.686434	26.552361	B+	13.42
043359.2+293636	...	68.497083	29.610262	B+	120.82
043452.5+240244	...	68.718796	24.045792	B+	11.26
043720.8+250019	...	69.336752	25.005396	B+	36.60
043826.7+265501	...	69.611576	26.917101	B+	43.44
044241.1+244117	CCDM J04427+2441AB	70.671643	24.688299	B+	24.00
044325.1+255706	...	70.854940	25.951765	B+	23.92
044518.2+242436	HD 30067	71.325984	24.410131	B+	39.42
044644.4+262306	...	71.685220	26.385118	B+	73.58
044941.5+254010	...	72.423263	25.669575	B+	57.67
041624.5+290858	HD 281820	64.102356	29.149654	B	10.65
041803.3+244009	...	64.514100	24.669361	B	77.88
041936.2+265256	...	64.900850	26.882286	B	13.40
042025.8+281641	...	65.107869	28.278227	B	15.39
042110.9+255259	V412 Tau	65.295779	25.883303	B	15.21
042356.0+242705	HD 283663	65.983654	24.451431	B	29.40
042518.6+255535	...	66.327763	25.926657	B	16.52
043024.1+281916	...	67.600602	28.321260	B	30.42
043145.0+285908	...	67.937661	28.985607	B	73.56
043228.1+271122	...	68.117315	27.189692	B	15.88
043312.6+291250	HD 282277	68.302720	29.214066	B	95.45
043636.1+265910	...	69.150616	26.986322	B	39.68
044253.9+253709	...	70.724809	25.619368	B	15.05
044539.8+251704	...	71.416097	25.284595	B	17.13
044802.3+253359	...	72.009726	25.566454	B	39.31
042358.6+244742	...	65.994199	24.795076	B-	9.60
042519.1+234716	HD 27923	66.329856	23.788006	B-	34.93
042558.8+273701	HD 283637	66.495259	27.617020	B-	28.58

Table 8—Continued

SST Tau name	common name	RA (J2000)	Dec (J2000)	our rank	distance ^a (arcmin)
043131.4+230025	...	67.880924	23.007208	B-	9.47
043133.1+292856	...	67.888044	29.482388	B-	99.66
043225.1+264732	...	68.104744	26.792301	B-	20.46
043256.4+222342	HD 284481	68.235238	22.395138	B-	23.30
043341.8+223836	...	68.424276	22.643473	B-	9.54
043419.8+232649	HD 284530	68.582806	23.447161	B-	18.83
043435.4+264406	...	68.647885	26.735069	B-	31.98
043939.9+252034	JH 225	69.916487	25.342842	B-	13.60
044023.0+255702	...	70.095875	25.950682	B-	4.81
044557.0+244042	...	71.487694	24.678431	B-	21.06
044650.3+243815	...	71.709980	24.637739	B-	20.87
042728.1+262323	...	66.867199	26.389803	C+	7.71
043213.6+251746	GSC 01833-00754	68.056868	25.296129	C+	10.62
041159.7+294236	...	62.998870	29.710224	C	35.29
042350.1+264006	FS 116	65.958819	26.668579	C	12.67
043943.8+271956	...	69.932822	27.332352	C	55.67
044916.3+243827	CCDM J04493+2438A	72.318089	24.640902	C	40.52
042721.0+240829	...	66.837538	24.141438	C-	12.40
043141.2+293922	...	67.921919	29.656178	C-	110.09
043803.6+221223	...	69.515227	22.206503	C-	19.22
044358.3+235103	...	70.992959	23.850939	C-	68.89
044639.8+242526	...	71.666086	24.423908	C-	33.63
044913.7+252549	...	72.307325	25.430412	C-	43.42
pending (spectroscopic) followup					
041332.3+291726	...	63.384823	29.290760	A	5.52
042220.9+264248	...	65.587113	26.713463	A	3.69
042857.4+243607	...	67.239295	24.602066	A	6.74
042932.0+243059	...	67.383731	24.516598	A	2.77
043419.5+265210	...	68.581613	26.869499	A	39.11
041535.6+284741	...	63.898611	28.794920	A-	17.79
041831.2+282617	...	64.630173	28.438248	B+	0.47
043316.6+262724	...	68.319252	26.456673	B+	11.46
041858.0+235031	...	64.741993	23.841991	B	91.73
041946.5+271255	...	64.944061	27.215336	B	1.13
042151.3+265720	...	65.463854	26.955629	B	2.10
043642.0+265339	...	69.175240	26.894352	B	45.35
044125.7+254349	...	70.357346	25.730341	B	4.04
044345.3+243908	TYC 1834-591-1	70.938928	24.652491	B	34.45
041339.4+292114	...	63.414342	29.353973	B-	4.88
041401.7+280857	...	63.507256	28.149384	B-	2.35
041859.0+255740	...	64.745898	25.961126	B-	45.20
041940.4+270100	...	64.918731	27.016882	B-	9.79
042212.9+254659	...	65.553995	25.783281	B-	2.34
042730.2+244123	2MASX 04273023+2441232	66.876130	24.689869	B-	8.02
042905.2+261535	2MASX 04290517+2615358	67.271721	26.259964	B-	5.64
043523.7+240450	...	68.848785	24.080612	B-	4.39

Table 8—Continued

SST Tau name	common name	RA (J2000)	Dec (J2000)	our rank	distance ^a (arcmin)
041331.6+280613	...	63.381946	28.103617	C	7.03
041605.8+281426	...	64.024513	28.240591	C	8.41
041810.5+284447	...	64.544147	28.746483	C	13.68
042339.0+251855	...	65.912544	25.315405	C	22.69
042653.3+255858	...	66.722092	25.982811	C	6.87
042810.4+243553	...	67.043381	24.598303	C	16.92
043214.6+223742	...	68.060855	22.628393	C	15.59
044832.3+234746	...	72.134884	23.796349	C	75.53
041604.8+261801	...	64.020153	26.300299	C-	33.29
042325.9+250354	...	65.858228	25.065123	C-	8.24
042902.9+243140	...	67.262433	24.527840	C-	4.90
042949.9+284253	...	67.458318	28.714808	C-	49.05
043816.5+261450	...	69.569150	26.247238	C-	3.19
044315.8+235358	...	70.816129	23.899599	C-	60.39

^aAngular distance to nearest previously-identified Taurus member.

4. Discussion

4.1. Overall Sample Properties

4.1.1. The sample as a whole

There are 215 previously identified Taurus members and 148 candidate new Taurus members discussed here. Table 2 summarizes the samples selected from each color-magnitude or color-color space, along with relevant numbers from the SWIRE sample for comparison. Table 3 summarizes the fraction of the previously identified and new candidate sources detected at each Spitzer band.

Table 2 captures the fraction of objects found in each CMD or CCD that fall into the categories of previously identified YSOs, new candidate YSOs, previously identified non-members, and new non-members, and also the fraction of each of these categories that is found in each of the CMDs or CCD. For example, in the case of the 24/70 CMD, 447 objects are selected by our color cuts in this diagram. Of these, 19% are previously identified YSOs, 7% are new candidate YSOs, 10% are previously identified non-members, and 60% are new non-members. And, out of the 215 stars that compose our previously identified Taurus member sample, 41% are recovered in the 24/70 diagram, of the 148 objects in our candidate YSO sample, 22% are found here, of the 821 previously identified non-members, 6% are found in this diagram, and of the 489 new non-members, 55% are found here. This table reveals that the $K_s/24$ diagram recovers the highest fraction of previously identified objects and of new candidate objects. The 24/70 CMD finds the highest fraction of new non-members (by fraction of objects found in this diagram as well as by fraction of the entire new non-member list); this is not particularly surprising, as the objects that are detected at $70\ \mu\text{m}$ tend to be either YSOs or extragalactic objects. This table also shows that the $\sim 6^\circ$ ELAIS N1 SWIRE sample is largely found outside of our color selection criteria; few galaxies of the sort found in this SWIRE sample are likely to be selected by our criteria.

Table 3 shows, of the entire sample of previously-identified Taurus members, essentially all are seen in at least one band of IRAC, most ($\sim 80\%$) are detected in MIPS-24, and just $\sim 45\%$ are seen at MIPS-70. However, $\sim 10\%$ of these famous, bright objects are saturated in at least one Spitzer band, and many objects do not have infrared excesses (or have excesses too weak to be measured at, e.g., $70\ \mu\text{m}$). Those that are missing flux densities (e.g., without even limits) in Table 4 (or Table 5) are missing because they are off the edge of the covered area, or there is a cosmic ray cluster near the location of the source, corrupting the photometry.

As can be seen in Table 2, out of the 215 previously identified Taurus members, 144 (67%) are selected in at least one of our color spaces as having a Spitzer infrared excess. This is roughly consistent with the 2/3rds disk fraction in Taurus. Just 65 (30%) are selected in all of our color spaces simultaneously. Out of our 148 new candidate Taurus members, 17 (16%) are selected in all of our color spaces simultaneously (two of which are likely galaxies, 043349.5+291528 and 044554.8+240843, based on spectroscopy). Interestingly, there are a comparable number of non-members (new or previously identified), 21 objects, that are selected in all of our color spaces together.

For the new candidate members, we have an obvious bias in that we cannot find stars without Spitzer IR excesses; note that the sample of previously identified Taurus members includes Taurus members without IR excesses. We also have a bias in that three of these color selections use $24\ \mu\text{m}$ in some fashion (either as overall brightness or as part of the color). This selection mechanism biases our sample of YSO candidates towards a high fraction with $24\ \mu\text{m}$ detections; see Table 3. Just $\sim 9\%$ of these objects are not seen at

24 μm . Moreover, because previous surveys on the whole were using less sensitive instruments, the new potential objects that we have discovered here are on average fainter in the optical and NIR than the sample of previously identified Taurus members (see Table 3).

Many objects newly identified here have large IR excesses, but several of them have small excesses at 8 μm and either a low excess or no detection at all at longer wavelengths. These objects are the unselected objects (grey dots) in the K_s vs. $K_s-[24]$ diagram (Fig. 2) that have $K_s-[24]$ near 0. These objects are included in our list of new candidate Taurus members only if they have more than 4σ excess (see §3.1.4); we have dropped objects whose apparent 8 μm excess is completely inconsistent based on Planck function considerations with a photospheric 24 μm measurement (or limit). These 4σ 8 μm points seem to be real, in that the distribution of, e.g., [3.6]–[8] colors are near zero for the overwhelming majority of stars in the catalog, and these objects are clearly redder than average. However, without detailed modeling beyond the scope of this paper, it is puzzling how objects could have legitimate, real 4σ excesses at 8 μm and small 24 μm excesses. These objects have low grades of confidence in Table 7, and generally will require additional observations to resolve.

4.1.2. Additional information from the spectroscopy

Of the 83 stars with optical spectroscopy, not all of them are securely identified members of Taurus. Additional information, such as emission lines which are typical of 1-5 Myr T Tauri stars, can help inform our membership assessment. Twenty-six have $\text{H}\alpha$ in emission at any level. M stars that are not members of Taurus but possess typical levels of stellar activity can also have $\text{H}\alpha$ in emission. Figure 6 shows the $\text{H}\alpha$ equivalent width as a function of spectral type for all stars reported in this work (including those stars listed solely in the Appendix which we dropped as non-members). The lines shown are from Slesnick et al. (2008) and Barrado y Navascués & Martín (2003), dividing accretion from “normal” activity levels of $\text{H}\alpha$ at the late M types. Stars for which we have detected a strong IR excess plus an $\text{H}\alpha$ equivalent width in emission larger than the cutoff as a function of spectral type are objects we have placed in the secure “new member” bin – see §3.3 and the data tables – except for the Be star which cannot be a member of Taurus (see §B.3). We also list objects that have a more moderate $\text{H}\alpha$ emission but still a very strong IR excess (not Class III but Class I, II, or flat) as secure new members. Objects with moderate or no $\text{H}\alpha$ emission and small IR excess (Class III) need additional indications of membership, such as lithium, radial velocities, proper motions, or high-spectral-resolution observations of gravity-sensitive lines.

One way to identify intermediate-gravity objects, e.g., neither giants nor dwarfs but YSO-like gravities, is found in Slesnick et al. (2008) and applies to stars of type M1 and later. It uses the TiO 8465 Å index and Na 8190 Å index; this analysis for our qualifying stars is presented in Figure 7. All of our new members except one have gravities in the region of this diagram occupied by previously identified Taurus members; all of the rest of our candidate members shown here are also roughly consistent with YSO gravities, given the scatter in this measurement. These objects are indicated in the notes column of Table 7. The one new member that may have more giant-like gravity is SST Tau 042920.8+274207, which may appear in that location in the diagram due to reddening; reddening will push points up and to the left in this figure. This object is particularly perplexing, in that it has many characteristics of youth and also those of the post-main sequence. Our calculation of A_V (§3.3) suggests that $A_V \sim 4$. Additional modeling (beyond the scope of this paper) is needed to further investigate this object. We note here that several of the objects discarded as giants (based on visual examination; see §B.4) would appear in this diagram as having gravities consistent with giant gravities, if they were included in this Figure.

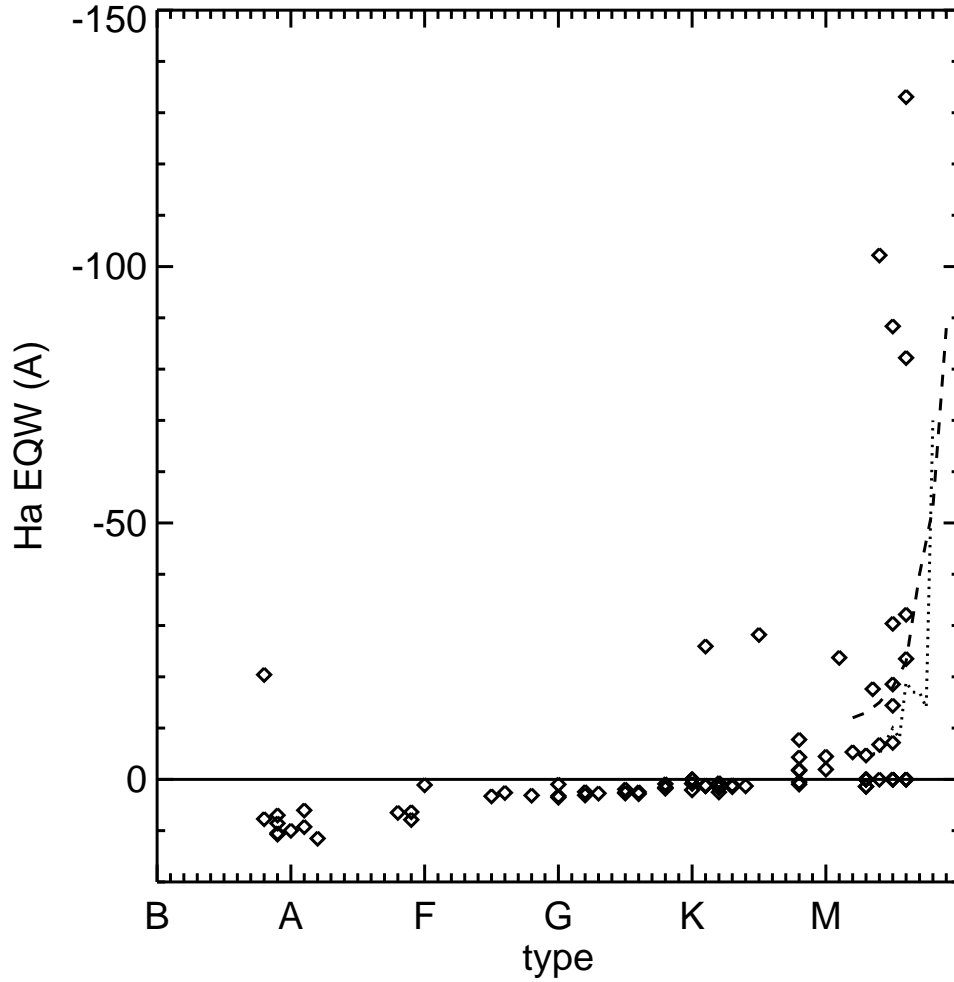


Fig. 6.— $H\alpha$ equivalent widths (where values <0 indicate emission) as a function of spectral type, for all objects with spectral types reported here (including stars listed solely in the Appendix and dropped as non-members). Note that there is an additional M0 star, not shown, with an $H\alpha$ equivalent width of -498\AA . The dotted and dashed lines are, respectively, lines from Slesnick et al. (2008) and Barrado y Navascués & Martín (2003), and indicate the expected quiescent $H\alpha$ emission from normal stellar activity. We take stars with emission beyond these levels as clear YSOs.

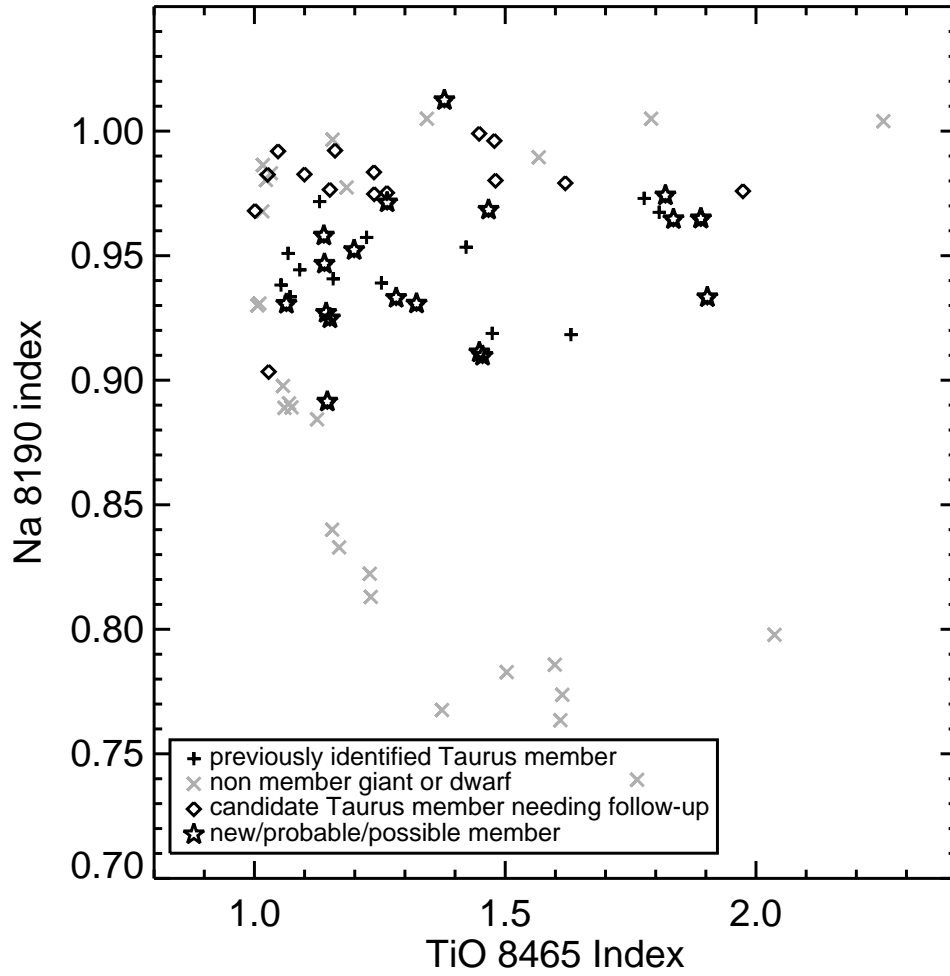


Fig. 7.— Na 8190 and TiO 8465 indices for the M1 and later stars in our optical spectroscopic sample. Grey \times symbols are objects from Slesnick et al. (2008) that are known giants (large Na 8190 indices) or dwarfs (the remaining points, with smaller Na 8190 indices). The + signs are previously-identified Taurus members. The star symbols are new members, probable new members, and possible new members. The diamonds are remaining objects with spectra from the 148-object list of new candidate YSOs, e.g., those objects needing more follow-up. All but one of our new members have gravity measurements consistent with YSO gravities, and even that one may be YSO-like (see text).

4.1.3. Summary of properties of all the new members

Out of the 148 candidate new Taurus members, according to the letter grades we assigned (§3.1.4), there are 50 with letter “A+”, “A”, or “A-” (most believable), 66 with grade “B+”, “B”, or “B-”, and 25 with grade “C+”, “C”, or “C-” (least believable). These grades incorporate all the available photometric and spectroscopic information for each object; the remaining 7 do not have grades because they are galaxies based on the follow-up spectroscopy. We have spectroscopy for 114 of the 148 objects, 90 of which are optical spectra that have been analyzed. We can report stellar spectral types for 83 (~90%) of those (again, the remaining 7 are galaxies). Although we have biased our spectroscopic followup towards the brighter objects, such a low rate of finding galaxies gives us confidence that our YSO selection process is reasonably successful in that it finds many more stars than galaxies. Note that, while all the “new members” are also grade A objects, not all grade A objects are “new members” because of the need for additional data in many cases. The 83 stellar objects include newly confirmed YSOs and objects that will most likely turn out to be background giants when more data are acquired.

There are 34 new members, 3 probable new members, 10 possible new members, 7 extragalactic objects, 1 other object (Be star), 60 stars needing additional follow-up observations, and 33 pending any follow-up observations. All of the individual SEDs appear in Appendix A. Combining the 34 new members of Taurus, 3 probable new members, and 10 possible new members yields a total of 47 new objects of various shades of confidence. This represents an increase of ~20% (by number) over the previously-identified members covered by our map.

Of the remaining 148 objects less the 47 new Taurus members (new, probable new, and possible new), 60 more objects have optical spectra resembling stars, but we need additional data to distinguish these potentially interesting (often transition disk-type SED) objects from background giants or foreground objects (using, e.g., lithium abundances, radial velocities, proper motions, etc.; these are in the “needs additional followup” category). If they turn out to be non-members, the IR excess we observe needs to be explained. Finally, 33 await additional data beyond the Spitzer photometry to confirm or refute their new Taurus membership status (“pending followup”). Thus, more new objects could still be in this data set. For completeness, the remaining 148-47 objects are also listed in Table 8, sorted by their category, such that the objects we grade as most likely to be new members appear at the top of the list.

4.2. Detection at other bands

Since we have a wealth of data at other wavelengths, it is possible that we can find some additional evidence for youth for our potential new Taurus members among them. For example, young stars are known to be bright in X-rays and ultraviolet. We did in fact include the information below in our ultimate ranking of the objects (see §3.1.4).

The XEST fields were optimized to cover the previously identified YSO population, and do not cover our entire Spitzer field. Out of the previously identified YSOs, 107 of 215 are detected in X-rays, and 50 are detected by the XMM-Newton OM (in ultraviolet). Out of the entire 148 star list of potential new Taurus members, 7 are detected in X-rays (041940.4+270100=XEST-16-024, 042215.6+265706=XEST-11-078, 042936.0+243555=XEST-13-010, 043326.2+224529=XEST-17-036, 043456.9+225835=XEST-08-003, 043542.0+225222=XEST-08-033, and 044125.7+254349=XEST-07-032), and 2 are also detected by the XMM-Newton OM (042215.6+265706=XEST-11-078=XEST-11-OM-122 and 042936.0+243555=XEST-13-010=XEST-13-OM-002). These objects are noted in Table 7. The two objects detected in both X-rays

and the XMM-Newton OM are already confirmed new members. Of the remaining objects detected in X-rays, there are three more confirmed new members, one probable, one possible, and two pending additional follow-up; five of them appear in Scelsi et al. (2007) as potential members (see Table 7).

The SDSS stripes do not cover our entire field either, but they provide u -band observations for those regions they do cover; however, extinction strongly affects the numbers of objects detected. Out of the 215 previously identified Taurus members, 109 are detected at SDSS u ; out of the 148 stars we list as potential new members, 63 are detected at SDSS u (18 of which are confirmed new members). Out of those objects, 33 have apparent UV excesses above the locus formed by *all* of the objects in our catalog with Sloan $uriz$ photometry (17 of these 33 are confirmed, probable, or possible new members). These objects are noted in Table 7.

4.3. Locations of New Candidate Taurus Members

As can be seen in Table 8, many of the new objects are quite close to previously-identified Taurus objects. Figure 8 shows the projected location of the sample of previously identified YSOs, the new YSO candidates we have selected, and those new YSO candidates with the results of the spectroscopy folded in. Because one of the goals of this project is to look for widely distributed Taurus members, we did not restrict our search for new objects to the regions already occupied by Taurus members. While proximity to previously identified YSOs was a component in our ranking scheme, it was only one of many criteria (§3.1.4). As can be seen in Figure 8, the new candidate objects are generally more isotropically distributed than the previously identified members. However, most of the new Taurus members tend to be found near the previously identified Taurus members. There is a new loose grouping of YSOs found near $(\alpha, \delta)=(70,24)$. Further spectroscopic results are needed to complete our search for an extended population of YSOs in Taurus.

4.4. Spectral types and YSO classes

Figure 9 shows a histogram of the spectral types of the previously-identified Taurus members plus the 34 confirmed new objects; most of the new objects are M spectral types – one is “early K”, one is a K5e, four are K7-M0, and the rest are M stars. Of the probable new members, there are 1 M star, one A star, and 1 “<M0”; of the possible new members, there are 2 M stars, and the rest are K4 or earlier (1 late F, 2 G stars, 5 K stars). These earlier types are less secure new members because they have small IR excesses and/or weak $H\alpha$.

Most of the 47 new objects (32 of them) are YSO class II. Figure 9 shows a histogram of the types of the previously-identified objects plus the 32 confirmed new objects. There are five “flat” YSOs in the 32 new objects, one class I, and 4 class IIIs; the rest are class II.

4.5. Ensemble SED Properties of Currently Identified Taurus Members

Having established the location and spectral type distribution of the new members relative to the established members, we now investigate the SED properties of the ensemble. Figure 10 shows representations of the SEDs for all of the 215 previously identified Taurus members with K_s detections (on the left), and

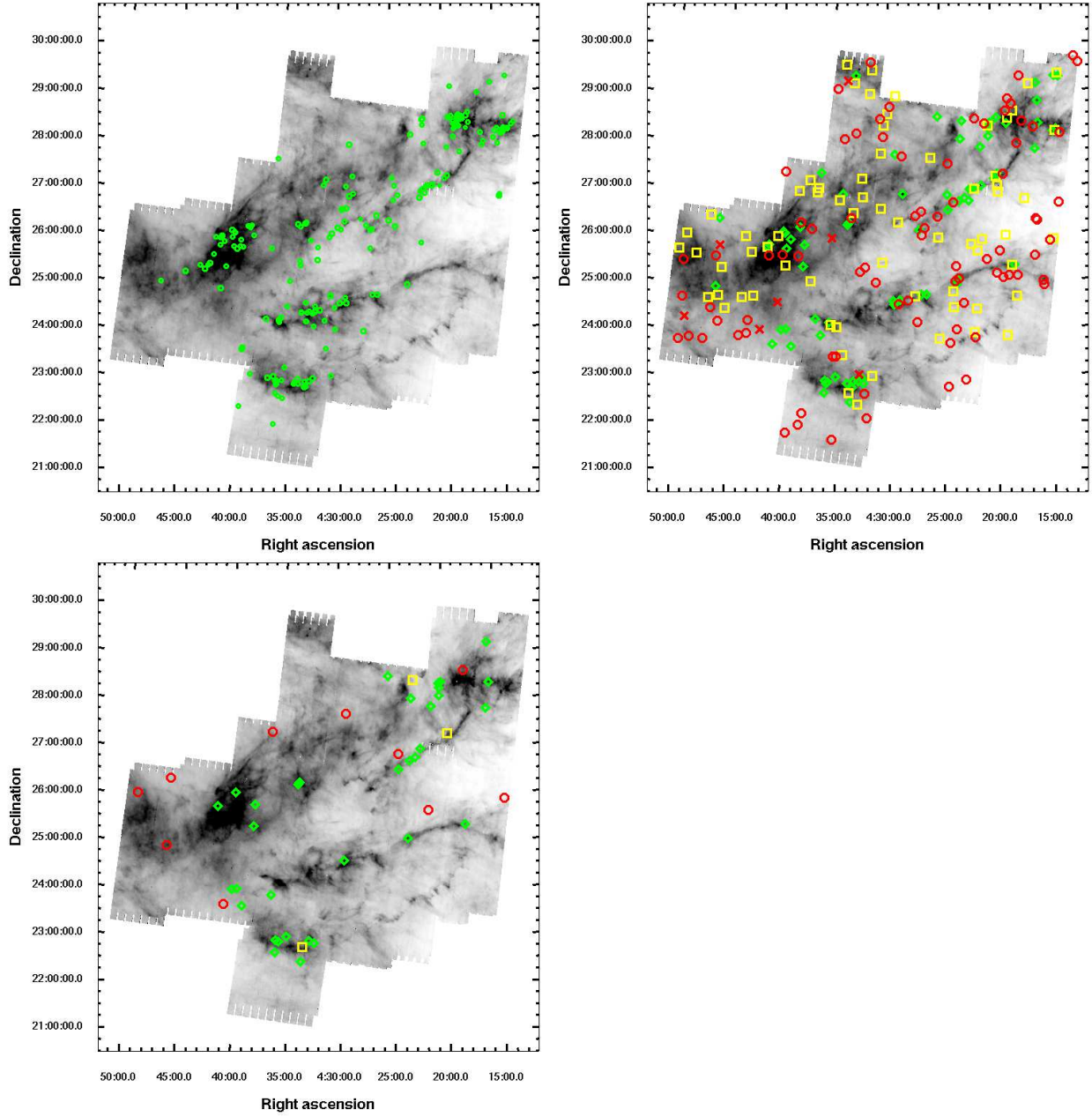


Fig. 8.— Physical location of various samples of Taurus objects on the 160 μm image (reverse greyscale): (*top left*) previously identified Taurus members (green circles), which tend to follow 160 μm emission; (*top right*) all new candidate objects: green diamonds = grade A, yellow boxes = grade B, red circles = grade C, \times = extragalactic; (*bottom left*) the 47 new Taurus objects: green diamonds = new members, yellow boxes = probable new members, red circles = possible new members. The confirmed new Taurus members thus far tend to be found near the previously identified Taurus objects.

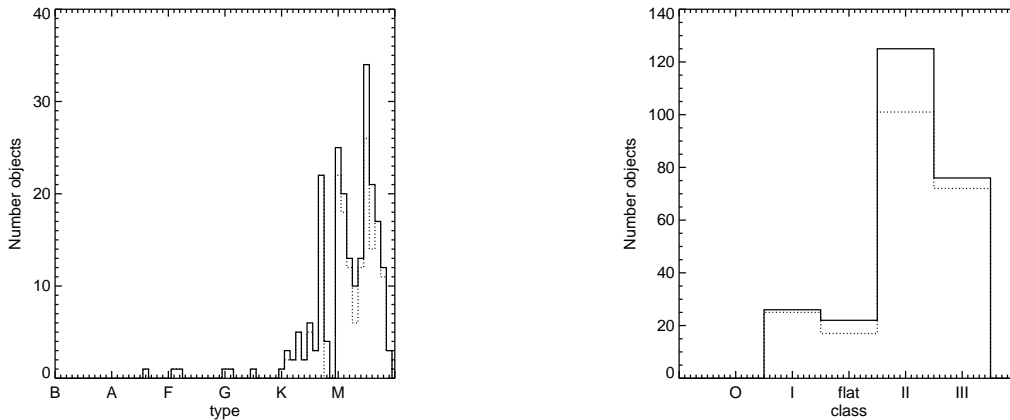


Fig. 9.— LEFT: Histogram of types for all previously-identified members with spectral types plus new confident members (solid line) and just the previously-identified members(dotted line). RIGHT: Histogram of all the previously-identified members plus new confident members (solid line) and just the previously-identified members(dotted line)

the 34 confirmed members discovered using the Spitzer data (on the right). Note that (a) these SEDs are normalized to K_s (objects missing K_s due to saturation are not included, so a total of 211 previously-identified Taurus members are shown), and (b) the SEDs appear individually in the Appendix below, see §A. We have normalized to K_s because we wished to investigate the variation of the shapes of the SEDs, not their relative intrinsic brightness and/or extinction; K_s provides a value available for most objects (see Table 3) and is an admittedly imperfect compromise between disk and photosphere emission. For each wavelength, there are very broad, non-Gaussian distributions of points. In the optical in particular, but also at wavelengths at least as long as $24 \mu\text{m}$ (see, e.g., Bary et al. 2007), the intrinsic variability of the objects can contribute significantly to the scatter.

The Figure uses box plots; these box plots have been used in other papers (e.g., Rebull et al. 2006; Flaccomio et al. 2003) as a mechanism for interpreting scatter plots. For each of the wavelength points, the boxes capture the median and the first and third quartiles of the distribution in λF_λ (including measurements only, not limits). The lines extend to the most extreme values that are not more than 1.5 times the interquartile range, and the circles are those points outside 1.5 times the interquartile range. For cases like those found in, e.g., Rebull et al. (2006), there are upper limits in the distribution, and the Kaplan-Meier (K-M) estimator for censored data can be used to take into account the upper limits present in the data. However, in this present case, for each of the Spitzer points, we have both upper and lower limits in the distribution, so the K-M estimator fails. The offset grey boxes in Figure 10 use all of the upper and lower limits as real detections at the location of the limit. The influence of the large number of limits can particularly be seen at MIPS bands, where the lower edges of the box are substantially lower with the limits included as real detections than without. There are no detections at $160 \mu\text{m}$ among the 34 new member stars, so only limits can be used.

The solid line near the medians is the “median Taurus SED” from D’Alessio et al. (1999). It is clear that we have not compensated for reddening in the optical bands, as the D’Alessio SED is significantly above our medians at blue wavelengths (shorter than $1 \mu\text{m}$). (D’Alessio et al. individually dereddened the SEDs before combining them to get the median; we would need to apply a reddening of about $A_J=0.8$ to

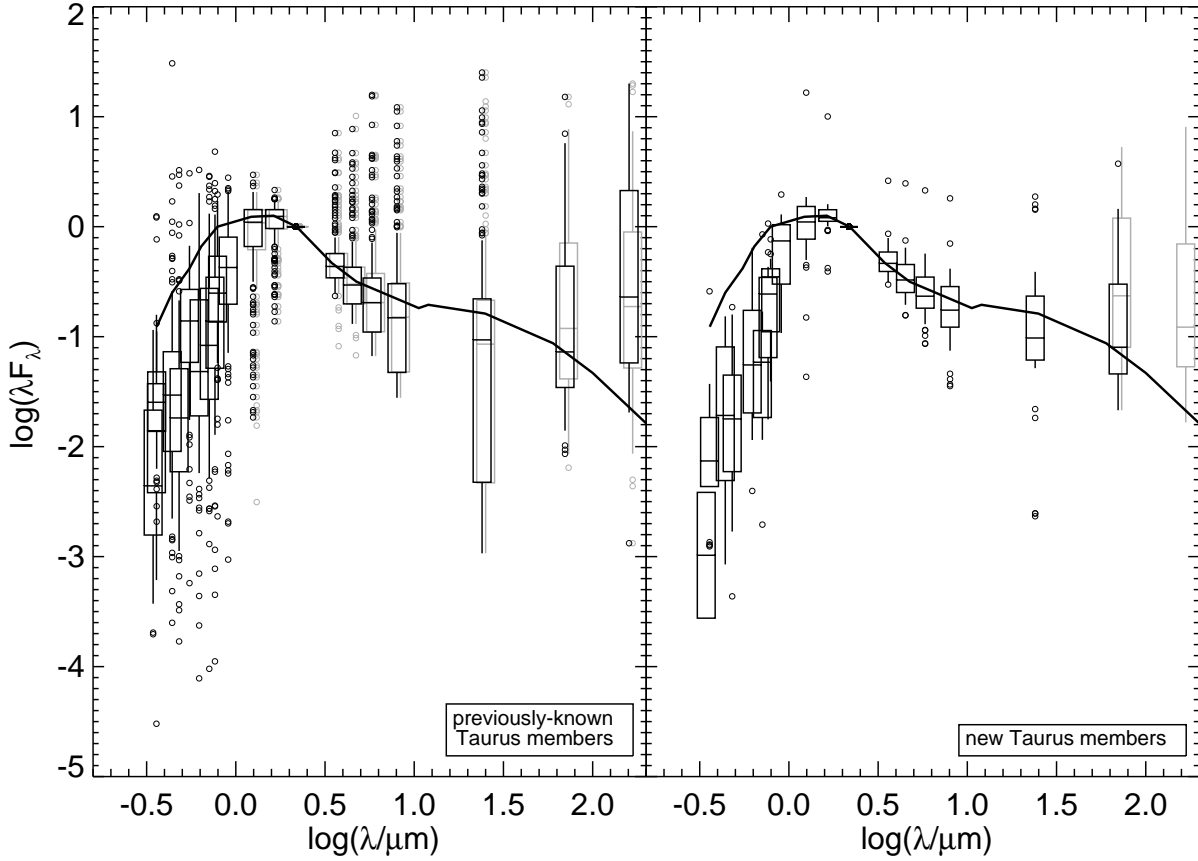


Fig. 10.— Box plot (see text) of all SEDs, normalized to K_s , for (LEFT) the 211 (out of 215 possible) previously identified Taurus members having a K_s measurement, and (RIGHT) the 34 (confirmed) new members discovered using the Spitzer data. The central line in each box denotes the median; the ends of each box are the first and third quartile of the distribution; the lines extend to the most extreme values that are not more than 1.5 times the interquartile range; and the circles are those points outside 1.5 times the interquartile range. The grey, slightly-offset boxes are the same representation, but treating all of the upper and lower limits as real detections at that limit point; see text for more discussion. (Note that none of the new members have a detection at $160 \mu\text{m}$, so that wavelength has only a grey box.) The solid line near the medians is the “median Taurus SED” from D’Alessio et al. (1999).

the D’Alessio median SED to make it match our median SED.) The D’Alessio SED tracks the rest of our medians reasonably closely, although it must be noted that our medians include all of the Taurus members, not just the K5-M2s, and not just the stars with infrared excesses. Our medians are slightly below the D’Alessio SED at 4.5-8 μm , more below the D’Alessio SED at 24 μm , then on the D’Alessio SED at 70 μm , then above it at 160 μm ; in all cases, the medians match within the box, e.g., between the first and third quartiles. Since there are more lower than upper limits at 24 μm , the “true” median is likely to be lower still, as can be seen by the location of the grey median line. Similarly, the “true” median at 70 and 160 μm is likely to be lower than our calculated value. At 160 μm in particular, we are likely seeing the effects of sensitivity; even our upper limits are reasonably shallow, and the location of the grey median line is closer to the D’Alessio SED. The medians at each band of the 34 new members are not much different than the medians of the previously-identified members, although they are slightly brighter. We are unable to find stars without IR excesses using Spitzer selection criteria, so we expect our new objects to have larger excesses on average than the entire ensemble of Taurus objects. At 70 μm , the new objects are as a whole much brighter than the previously identified sample. At 24 μm , the median is reasonably comparable but the lower boundary to the box (e.g., location of first quartile) is much brighter for the new objects than for the previously identified sample. Both of these effects are undoubtedly a result of our slight MIPS bias in source selection (see §4.1).

4.6. Ensemble $L_{\text{IR}}/L_{\text{total}}$ Properties of Currently Identified Taurus Members

We calculated $L_{\text{IR}}/L_{\text{total}}$ for the previously identified and new candidate Taurus members; see §3.3 and Tables 6 and 7. Since L_* is a by-product of this calculation, we present a Hertzsprung-Russell (HR) diagram in Figure 11. The T_{eff} values appear quantized because the T_{eff} value for each star was assumed based on its spectral type. The new members, probable new members, and possible new members are indicated separately on this diagram, along with the previously identified and pending samples. Most of the highest confidence new members have positions in this diagram quite consistent with the positions of previously-identified Taurus members. All three of the probable new members and just two of the possible new members also have consistent positions. Both the previously identified and new groups have some apparently sub-luminous members, with additional such objects among the sample awaiting more data. These objects could be sub-luminous due to being, e.g., edge-on disks, or they might not be members. Further investigation is warranted. Many of the candidates awaiting additional data and/or analysis fall in the pre-main-sequence regime of this diagram, but many do not; these are likely to turn out to be background dusty giants. There seems to be a loose clump of new objects near $\log T_{\text{eff}} \sim 3.75$, $\log L_*/L_{\odot} \sim -1.8$, and many of the earlier-type objects still awaiting additional data are also considerably too faint. These objects are probably unlikely to be Taurus members – they could be background debris disk candidates – and are indicated individually in the data tables. We included the position of the object in the HR diagram in our individual assessment and grading of each object (§3.1.4).

Figure 11 also shows the $L_{\text{IR}}/L_{\text{total}}$ vs. $\log L_*/L_{\odot}$ for the sample. Due to Spitzer’s superior sensitivity, resolution, and wavelength coverage vs. IRAS, the $L_{\text{IR}}/L_{\text{total}}$ values here are likely to be more reliable than those values presented in, e.g., Cohen, Emerson, & Beichman (1989). Systems with $L_{\text{IR}}/L_{\text{total}} > 0.2$ (e.g., GV Tau AB) are expected to be disk systems with circumstellar envelopes, and indeed most of the systems in this range show rising or flat spectral energy distributions. Systems with $L_{\text{IR}}/L_{\text{total}}$ of 0.05–0.2 (e.g., DL Tau, CY Tau) are expected to be optically thick disks lacking envelopes, with large values indicating more flared disks. Most of the known T Tauri stars in the cloud fall in this range. Systems with $L_{\text{IR}}/L_{\text{total}}$ near

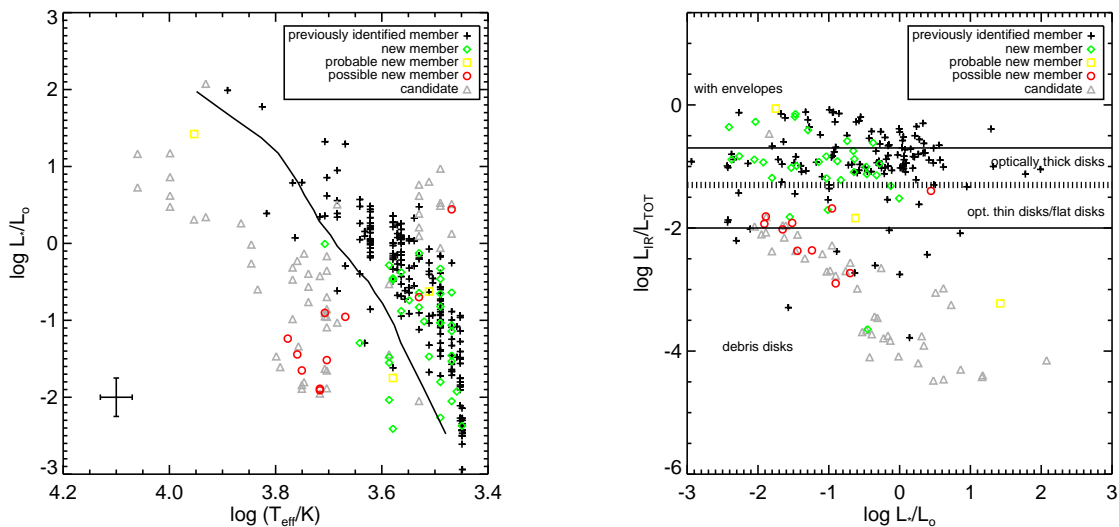


Fig. 11.— LEFT: Hertzsprung-Russell (HR) diagram for the previously-identified members (+), the new members (green diamonds), the probable new members (yellow squares), the possible new members (red circles) and the rest of the candidate members (grey triangles), using the L_* values calculated (and T_{eff} values assumed) in the process of calculating $L_{\text{IR}}/L_{\text{total}}$; see text for caveats. Typical error bars are indicated in the lower left; the error in temperature will be larger for earlier types. The ZAMS from Siess et al. (2000) for the Taurus distance is overplotted as a solid line for reference. Most of the highest confidence new members have positions in this diagram quite consistent with the positions of previously-identified Taurus members. All three of the probable new members and just two of the possible new members also have consistent positions. The remaining possible new members are apparently under-luminous; see text. Many of the candidates awaiting further data also have positions consistent with Taurus members, but many are also apparently sub-luminous. RIGHT: Plot of $L_{\text{IR}}/L_{\text{total}}$ against L_*/L_{\odot} , with the same notation as the left figure. Approximate dividing lines for the interpretation of $L_{\text{IR}}/L_{\text{total}}$ are indicated. The dividing line between optically thick disks and disks that are either optically thin or flat is hatched to indicate that it is a “fuzzy” dividing line.

0.01 (e.g., V410 Anon 24) are either optically thick disks highly flattened by dust settling, or systems just becoming optically thin as they transition to debris disks. Finally, systems with $L_{\text{IR}}/L_{\text{total}} < 0.01$ (e.g., V819 Tau) are similar to classical debris disks. Approximately 15 of these are found in the survey, among the previously-identified members combined with the new members. Most of the previously known and new objects have substantial disks or envelopes. Most of the least confident members (and most of those awaiting more data) appear to have very tenuous disks. Certainly some legitimate members appear at low $L_{\text{IR}}/L_{\text{total}}$ as well, so some of these candidates may be legitimate.

4.7. Comparison to Other Selection Methods

Thus far, our spectroscopic follow-up suggests very few galaxies are among our YSO candidates. While we have not obtained spectra of every candidate, and our spectroscopic follow-up has generally been of the brighter candidates, it is still important to note that our screening does seem to successfully weed out galaxies.

As mentioned above, there are many discussions in the literature also seeking to identify YSOs using Spitzer color selections (e.g., Allen et al. 2004, Padgett et al. 2008b, Rebull et al. 2007, Harvey et al. 2007, Gutermuth et al. 2008). In this section, we compare our color selection to two other popular color selection mechanisms. Harvey et al. (2007) describes the c2d/Gould’s Belt method, which works with large-scale maps of star-forming regions similar to that for Taurus. With the mitigation of extragalactic contamination as a primary goal, Harvey et al. (2007) apply several color cuts and use shape/fitting information from the c2d pipeline, combined with manual examination of the Spitzer images. The Gutermuth et al. (2008) criteria are being used by several different groups, including the IRAC GTO team, and is designed to find YSOs despite a wide variation of extinction values and nebulosity found in star-forming clusters within 1 kpc. We note that this method has been recently updated in Gutermuth et al. (2009), though the changes to the method are considered relatively small by the authors, and are not implemented here.

In this section, we have the goal of determining whether we can directly compare, say, the “yield” of this survey with those from other star-forming regions studied by other groups. We conclude that it is not at all straightforward, and direct comparison may not actually be possible because the selection methods are so different. Tables 9 and 10 make an attempt to compare the various methods as we have implemented them, with all the caveats discussed below, but just as it is not easy to compare the “yield,” it is not necessarily easy even to compare the methods on a precisely even footing. Note that in order to understand the assumptions that have gone into the numbers in these tables (or into the classes reported in Tables 6 and 7), reading the text below is critical.

One of the most significant differences between our *data* and those used to develop both of the other two methods is the depth of the IRAC Spitzer data that is used as input. With only two 12-sec IRAC frames per position, our data is at least a factor of two shorter integration time (at least square root of 2 less sensitive) than the other surveys that were used to construct these other selection methods. On the other hand, Taurus is also much closer than *most* of the other associations considered by the other projects. Sensitivity to legitimate YSO cluster members is at least comparable, but more faint contaminating sources will affect deeper surveys.

An important difference between our *selection mechanism* and both of the other two methods is the use not just of different color spaces but also of multiple color spaces in serial (the star is a YSO in this one AND that one AND this other one) vs. in parallel (the star is a YSO in this one OR that one OR this other

one). Table 10 explicitly lists the color parameter spaces used by each method, but the combination of them is complex and the original paper(s) for each should be consulted.

To reiterate, our method uses a combination of color cuts in a series of color spaces (which can be easily applied to other Spitzer data sets), followed by manual inspection of a variety of properties, including notably high-spatial-resolution optical imaging (which may not be easily applied to other Spitzer data sets). We used color spaces in parallel (this OR that) and manually examined those sources that met the YSO color criteria in *any* space; there are many thousands of objects that were never inspected manually but are still very likely to be stars and similarly many thousands more that are likely to be galaxies based on their colors. Table 9 indicates that we started with 122616 objects, of which 98476 had stellar-like colors in at least one of the spaces we investigated. The overwhelming majority of those, 99%, have colors consistent with stars in *all* the spaces we investigated and were never subject to the scrutiny of the YSO candidates; 513 of these were also selected as possible YSOs in at least one of the color spaces we investigated, and most have been discarded. Similarly, there are 80995 objects that are classified as galaxies in any of the spaces we investigated, and 99% of those look like galaxies in *ALL* the spaces we investigated; there are 681 that were also selected as possible YSOs in at least one of the color spaces we investigated, and most have been discarded. Note too that the numbers of stars/galaxies reported later in this table for the samples of previously-identified YSOs and new YSO candidates are again the sample of objects selected in *any* diagram; discussion of the sample selected in *all* diagrams appeared above.

We now compare the other two specific methods with our method in more detail.

4.7.1. Harvey et al. (2007; c2d) Criteria

Harvey et al. (2007) describe the criteria used by the c2d team and subsequently the Gould’s Belt team. Especially since these results are incorporated into Evans et al. (2009), which uses statistics of the Spitzer-selected sample to determine relative lifetimes of the Class 0/I/flat/II stages, it would be nice to understand how our sample selection compares so that our data on Taurus can be compared to the regions studied by these other programs.

To reiterate, we used the following parameter spaces to find candidate YSOs: (1) $[24]$ vs. $[24]–[70]$, **or** (2) K_s vs. $K_s–[24]$, **or** (3) $[8]$ vs. $[8]–[24]$, **or** (4) $[4.5]$ vs. $[4.5]–[8]$, **or** (5) $[3.6]–[4.5]$ vs. $[5.8]–[8]$ with an additional $[3.6]$ brightness cutoff, **combined with** (6) optical (SDSS/CFHT) imaging plus the additional qualitative criteria mentioned in Section 3.1.4 above. The c2d analysis described in Harvey et al. (2007) used the following parameter spaces to find candidates, assigning a quantitative probability that the object is a galaxy or YSO candidate: (1) $[4.5]$ vs. $[4.5]–[8]$, **and** (2) $[24]$ vs. $[8]–[24]$, **and** (3) $[24]$ vs. $[4.5]–[8]$, **and** (4) (if there was a 2MASS match) $H – K_s$ vs. $K_s–[4.5]$, **and** (5) fitting (and removal) of stars/reddened stars by the c2d pipeline, **and** (6) shape information gleaned from the c2d pipeline, **and** (7) manual inspection of the 2MASS+IRAC+MIPS images, **and** (8) manual addition of previously-identified YSOs to the list of YSOs. Differences between the studies include the following: (1) only one CMD is the same between the two teams; (2) the c2d team is using the intersection of all their CMDs, and we are using selection in any one color space; (3) the c2d team is using information obtainable only from their pipeline (shape, star fitting); (4) the c2d team does not have optical imaging (though we both examine the Spitzer imaging); (5) the c2d criteria *require* detection in all four IRAC bands, and MIPS-24 (they use the 2MASS information if it exists); (6) the c2d pipeline performs PSF-fitting photometry in IRAC and MIPS, and our pipeline does aperture photometry on IRAC data and PRF-fitting photometry on MIPS data. In order to attempt a comparison

Table 9. Comparison of Selection Methods I.

property	This Work	Harvey et al. (2007) criteria	Gutermuth et al. (2008) criteria
Of entire catalog...			
Part that can be considered	122616 (18%)	7119 (1%)	\gtrsim 89003 (13%) ^b
Number of stars	98476 ^a	965	74254
Number of galaxies or other contaminants	80995 ^a	4644	14176
Number of YSOs	870 ^c	1510	573
Of previously-identified members...			
Part that can be considered	206 (96%)	154 (72%)	\gtrsim 187 (87%)
Number of stars	172 ^a	6	82
Number of galaxies or other contaminants	88 ^a	7	2
Number of YSOs	144	141	103
Of sample newly-identified here...			
Part that can be considered	148 (100%)	128 (86%)	\gtrsim 141 (95%)
Number of stars	87 ^a	0	76
Number of galaxies or other contaminants	116 ^a	28	5
Number of YSOs	148	100	60

^aThis number of objects meets the star or galaxy criteria in *any* of the color-color or color-magnitude spaces used. Thus, total number of objects is not equal to number stars+number galaxies+number YSOs. See text.

^bThis method starts with a sample detected at all 4 IRAC bands (89003 objects) and semi-manually adds in additional objects (see text). The largest sample of those potential additional objects are those seen at $JHK_s[3.6][4.5]$, which in this Taurus dataset is 76522 more objects, so $\gtrsim 165525=89003+76522$ might be reported here instead to indicate this semi-manual addition of objects. However, there is no easy method to take those additional objects and break them into stars and galaxies, so the rest of this section of the table is taken out of 89003 objects.

^cThis number objects meets the YSO criteria in *any* of the color spaces investigated. After the imaging, etc. tests, this 870 number is reduced to 148 new candidate YSOs + 144 previously identified YSOs = 292.

Table 10. Comparison of Selection Methods II.

parameter space	Used by us	Used by Harvey et al. (2007)	Used by Gutermuth et al. (2008)
[24]/[24] – [70]	yes
K_s/K_s –[24]	yes
[8]/[8] – [24]	yes
[4.5]/[4.5] – [8]	yes	yes	yes
[3.6] – [4.5]/[5.8] – [8]	yes	...	yes
[24]/[8] – [24]	...	yes	...
[24]/[4.5] – [8]	...	yes	...
$H-K_s/K_s$ –[4.5]	...	yes	...
[4.5] – [5.8]/[5.8] – [8]	yes
[3.6] – [5.8]/[4.5] – [8]	yes
[3.6] – [4.5]/[4.5] – [5.8]	yes
K_s –[3.6]/[3.6] – [4.5]	yes
$J-H/H-K_s$	yes
[4.5] – [5.8]/[5.8] – [24]	yes

using the best possible criteria, we can of course impose the same color cuts. We can't obtain the shape information because we reduced our photometry differently. We can approximate the star fitting by dropping the objects with very small colors in all bands.

Out of the entire $\sim 700,000$ object catalog, these criteria can only be applied to 1% of the objects (see Table 9) because of the multiband detection requirement. Out of this 1% of the catalog, which is ~ 7100 objects, 21% are identified as YSO candidates (note that we did not manually examine the images of each of these objects in Spitzer or any other bands, whereas the c2d team would have done so), 65% are identified as galaxies, and 14% are identified as stars. Note that this does *not* mean that a c2d-selected YSO candidate sample has 65% contamination, but rather that out of the objects in the catalog to which the c2d criteria can be applied, 65% of these objects are immediately categorized as galaxies. Among our set of previously-identified Taurus members, 154 can be classified, but 61 of them (29%) cannot be classified in this scheme because of missing bands. Seven of them (3%) are identified as galaxies or other contaminants. Six of them (3%) are classified as stars (the likely WTTS out of the sample), and 141 (92%) are identified as YSOs. As intended, this selection mechanism (even as we have implemented it) is strongly biased towards YSOs. This sample of previously known YSOs cannot tell us about the contamination rate, but it can tell us about the fraction of objects that might be missed; a c2d-based YSO selection operating on this sample would miss $\sim 5\%$ of the YSOs with detections in all the requisite bands and infrared excesses. The c2d classifications for these previously identified members are listed in Table 6; the same information for the new candidate members is in Table 7. Among our new candidate objects, perhaps unsurprisingly, there is a higher fraction of contaminants. The multi-band detection requirement means that 14% (20 objects) cannot be classified. Among the remainder of the sample, there are 28 (19%) likely galaxies (or other contaminants), no stars (which makes sense because we are only selecting objects with IR excesses), and 100 (68%) likely YSOs in this attempt to use the c2d criteria on our sample. Happily, the YSO candidates compose the largest fraction of our sample.

The c2d criteria require selection in each of the Spitzer-based CMDs or CCDs; our selection requires selection in just one of the CMDs or CCDs. We have noted above in §4.1 the effects of instead requiring selection in each of our CMDs or CCDs. We note again here that, aside from the previously identified members, the number of new potential members is comparable to the contaminant hit rate. The c2d criteria require a $24\ \mu\text{m}$ detection and we are strongly biased towards objects with a $24\ \mu\text{m}$ detection, so this is perhaps not surprising.

4.7.2. *Gutermuth et al. (2008) Criteria*

Gutermuth et al. (2008), in their Section 4.1 and Appendix, describe a multi-step weeding process. They require detection in all four IRAC bands for most of the process, although they allow for semi-manual addition of objects missing some bands. The number of sources that can be considered as input for this process which appears in Table 9 attempts to represent this semi-manual addition; there are 89003 objects seen at all 4 IRAC bands, and 76522 that are seen at $\text{JHK}_s[3.6][4.5]$ but not $[5.8]$ or $[8]$, and these two components represent the bulk of the sources that can be considered. Additional provision is made in this method for bright, red objects detected at $[24]$ but not all four IRAC bands, and for stars with $24\ \mu\text{m}$ excess; since this represents addition of a few thousand sources to the 165525 sources already considered, a \gtrsim symbol is used in the Table. The Gutermuth method also works in dereddened colors for some criteria, requiring a high-spatial-resolution A_V map, which we do not have and thus cannot implement exactly in a parallel fashion. We note too that the Gutermuth et al. criteria relies mostly on the $[4.5] - [5.8]$ color to

avoid effects of reddening that may be found at $3.6 \mu\text{m}$. Since the overall median A_V towards Taurus is low ($A_V \sim 3$, which has a very small effect on $3.6 \mu\text{m}$), we did not deredden our colors, and simply applied the Gutermuth et al. criteria to our observed colors. We did not semi-manually add objects to the list following their section 4.2, and we added a few criteria to remove some blue objects found in our catalog; to their “embedded” criteria, we added an additional $[5.8] - [8] > -0.5$ and $[3.6] - [4.5] > -0.5$, and to their “Class II” criteria, we added $[3.6] - [4.5] > -0.5$. Two of the many color parameter spaces that Gutermuth et al. use are the same as ours; see Table 10.

Differences between the Gutermuth criteria and ours include the following: (1) only two CMDs are the same between the methods, (2) the Gutermuth method sometimes uses the intersection of the color spaces (like c2d) and sometimes takes selection in just one color space as sufficient (like us), (3) the Gutermuth method provides for a semi-manual addition of likely YSO objects, based on color cuts, (4) the Gutermuth method does not require intensive manual examination of multi-band images, (5) the Gutermuth method, though multi-step, can be applied to any Spitzer+2MASS catalog of a star-forming region, and is not dependent on products of pipelines or the presence of ancillary data (modulo reddening corrections), and (6) the Gutermuth method, as properly applied, needs an A_V map and needs to work in dereddened colors. In order to attempt a comparison using the best possible criteria, we have imposed the same basic color cuts, and, because of the low overall A_V towards Taurus, we have continued to work in the observed color space, and not dereddened anything. We have not semi-manually added objects to the YSO candidate list (as per Gutermuth’s Phase 2 or Phase 3).

Because of the multi-band detections necessary, these criteria cannot be applied to most of the entire $\sim 700,000$ object catalog; even with the semi-manual addition of sources allowed for in this method, between 50-75% of the catalog do not have enough detections to be included (see Table 9), but the process of semi-manual addition of sources is likely to catch most legitimate YSOs in the catalog. The sample with 4-band IRAC detections is easiest to handle automatically, and out of this sample, 83% are dropped as stars, 16% are dropped as contaminants of any of a variety of kinds, 282 (0.3%) are embedded objects (Class 0/I or flat), and 291 (0.3%) are Class II objects. Among our set of previously-identified Taurus members, 28 of them (13%) cannot be classified because of missing bands. Just 2 are dropped as contaminants and 82 (38%) are classified as stars; 15 (7%) are identified as “embedded” and 87 (41%) are identified as Class II. Again, as intended, this selection mechanism (even as we have implemented it) is strongly biased towards YSOs.

The Gutermuth et al. classifications (in more finely-grained detail) for the previously known objects are in Table 6 and those for our new candidate members are listed in Table 7. Among our new candidate objects, 95% can be considered, 76 (51%) are classified as stars, 5 (3%) are contaminants, and 60 (41%) are YSO candidates (21 objects are identified as embedded and 39 are identified as Class II). There is a slightly higher fraction of contaminants in the new sample than among the previously identified sample. We note that the overwhelming majority of objects that we dropped as a result of the review described in §3.1.4 were classified as contaminants using the Gutermuth classifications. We also note that the classification that we derive from a fit to all available points between K_s and $24 \mu\text{m}$ is in good agreement with the Gutermuth et al. SED classification except in higher-extinction situations, as expected.

4.7.3. Conclusions on Different Criteria

Comparing the different methods is clearly not at all straightforward. The differences are much more than simply different data reduction methods (aperture vs. PSF-fitting photometry) or survey depths. The

different color spaces that each study investigates, and the different assumptions that are made (e.g., ORring vs. ANDing the color selection) can be seen most clearly in the different results when considering the set of previously identified Taurus members. Since not all of the previously identified Taurus members have strong IR excesses, it is not surprising that no Spitzer-based method retrieves all of them. Interestingly, the Gutermuth et al. selection mechanism returns a higher fraction of previously identified members without infrared excesses than the c2d method.

Direct comparison of the YSOs retrieved in this paper (or over the Taurus Molecular Cloud as a whole) to any other association is not easy because the selection methods are so different. Unfortunately, numbers from this study cannot simply be dropped into tables from these other studies. Even if we were to re-reduce our data in exactly the same way as the other studies, a direct comparison would be difficult.

Even the contaminant rates are hard to compare. Since all of the follow-up data has yet to be acquired for our candidate objects, it is hard to do a final assessment of our contamination rate. Out of the 80 objects with spectra reported here, at least 45% are new members, and at least 10% are contaminants. Over 44 square degrees, including the previously identified plus the new confirmed objects, we recover at least 4.3 YSOs per square degree, and at least 0.18 contaminants per square degree. The c2d method was derived primarily using the c2d observations of Serpens (and SWIRE), and Harvey et al. (2007) estimates of order 0-1 contaminants in their 0.85 square degrees. Scaling this up to our ~ 44 square degree map, we then would expect ~ 50 contaminants in our map using the c2d method! Oliveira et al. (2009) carry out follow-up spectroscopy for the c2d Serpens sample, and find higher contamination (25%) than was originally estimated in Harvey et al. (2007). However, these contaminants are primarily AGB stars, which should not be as much of a contaminant source in the Taurus map, given the lower galactic latitude of Serpens (5°) as compared with Taurus (-15°). Gutermuth et al. (2008) estimate ~ 1 contaminant left in their $40' \times 30'$ ($=0.33 \text{ deg}^2$) map. Scaling up to 44 square degrees, then we would expect ~ 130 contaminants. However, we expect that the actual contamination is much less because this method has been tested on several maps, including larger ones. As more follow-up data are obtained for this and the other associations, a more direct comparison of the complete YSO inventories in these clouds will eventually be possible.

4.8. Stellar rotation

Rebull et al. (2006) and Cieza & Baliber (2007) found a correlation between IRAC excesses and rotation rates in Orion and NGC 2264. Taurus is one of the first associations in which rotation of young stars was studied (see, e.g., Edwards et al. 1993), but there are still only 32 stars with measured periods (see Güedel et al. 2007, and references therein, and Grankin et al. 2008) and IRAC photometry in our catalog. Figure 12 shows the rotation rate against disk excess for those stars. The relationship seen here, where the slowest rotators are much more likely than the fast rotators to have disks, is consistent with what has been found in the other associations.

5. Conclusions

We have presented here Spitzer flux densities for 215 previously-identified members of the Taurus Molecular Cloud young stellar object population. We constructed Spitzer color-color and color-magnitude diagrams, investigated where the previously identified Taurus members were located, and then used those diagrams to select additional candidate Taurus objects out of a catalog of $\sim 700,000$ objects observed with

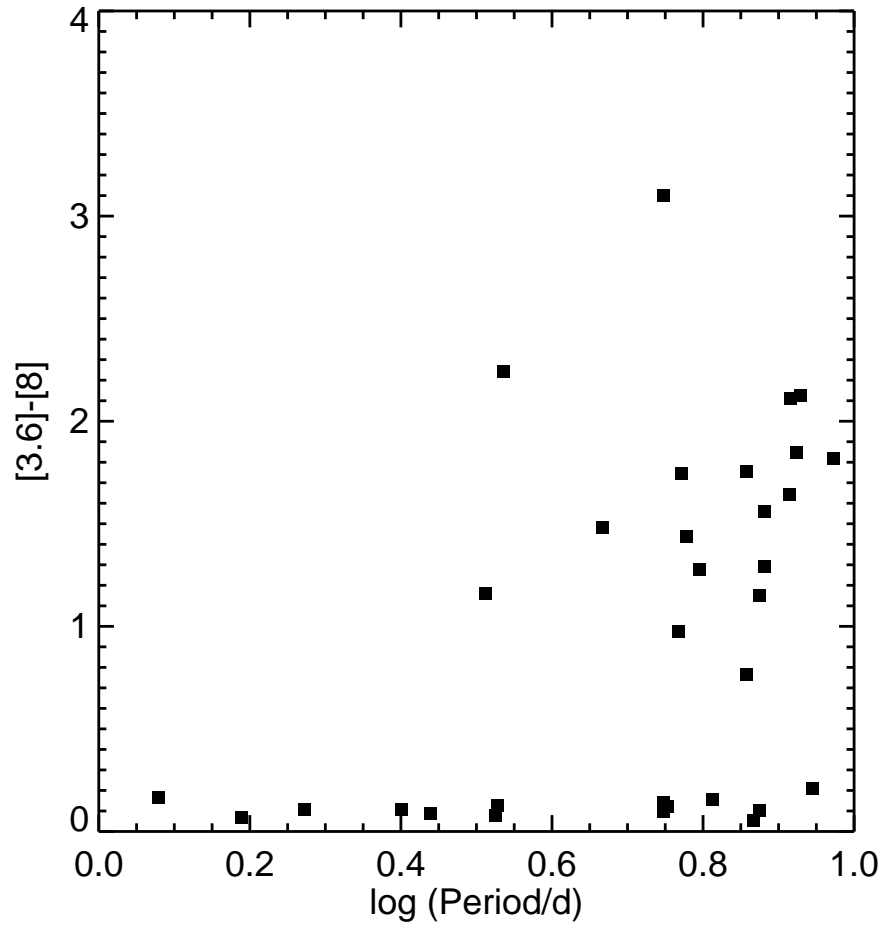


Fig. 12.— Rotation rates of Taurus stars compared to $[3.6]-[8]$ colors. The relationship seen here, where the slowest rotators are much more likely than the fast rotators to have disks, is consistent with what has been found in other young associations.

Spitzer over 44 square degrees. We used a wealth of supporting data (including ground-based optical imaging) to winnow that list down to 148 candidate new Taurus members. We obtained follow-up optical spectroscopy for about half the sample, thus far finding 34 new members, 3 probable new members, and 10 possible new members, a potential increase of 15-20% of young Taurus members. Most of the new members are located in close (projected) proximity to the previously-identified Taurus members; most of them are Class II M stars.

In addition to the new members in our sample, there are 60 stars needing additional follow-up observations, and 33 objects pending any follow-up observations at all, so more Taurus members may yet be confirmed out of our list of candidate members. We also found a background Be star, a new planetary nebula, a new carbon star, many background giants, and 100s of galaxies, just 7 of which made it into our final list of 148 YSO candidates.

As part of this project’s classification as a Spitzer Legacy Project, enhanced data products have been delivered back to the Spitzer Science Center (SSC), including the catalogs on which this present paper is based.

This study has demonstrated the unique power of Spitzer to efficiently survey large areas of the sky and provide new information on membership and YSO properties even in nearby star forming regions such as Taurus, which has been extensively studied for decades. Even after many decades of study, our knowledge of membership in Taurus is still incomplete, but definitely improving, thanks to Spitzer.

A. Spectral Energy Distributions (SEDs) for all of the Previously-Identified and New Candidate Taurus Members

For each of the previously-identified Taurus members, and each of the new candidate members, we provide an SED here in this on-line-only Appendix. Notation is as follows: triangles–XMM-Newton OM, +–literature Johnson photometry, *–Sloan photometry, ×–CFHT photometry, diamonds–2MASS, circles–IRAC, squares–MIPS. Limits for any band are indicated by arrows. The wavelength is in microns; λF_λ is in cgs units ($\text{erg s}^{-1} \text{cm}^{-2}$). Each plot has the SST Tau catalog number and, if relevant, a more common name.

For reference, the IRAS PSC all-sky completeness limits at 12, 25, 60, and 100 μm for a region outside of the Galactic plane are 0.4, 0.5, 0.6, 1.0 Jy, respectively. These limits would appear in the Figure at $\log \lambda F_\lambda = -10.00, -10.22, -10.52, \text{ and } -10.52$.

Table 11. Individual miscellaneous non-YSO objects with YSO-like colors^a

SST Tau number	Other names	Notes
Planetary nebulae		
041936.1+271731	...	New object; CFHT imaging suggests PN
043723.4+250242	PN G174.2-14.6	Well-studied PN
Carbon stars		
043748.2+254926	C* 228	well-studied carbon star
042818.5+253140	V414 Tau	well-studied carbon star
043250.3+294239	IRAS04296+2936	new (?) carbon star
Background giants from literature		
043724.8+270919	SV* SVS 1085, HD283751	new(?) Be background giant
043939.9+252034	JH 225	B9 with substantial A_V
042021.2+272102	phi Tau	literature giant
042136.8+282458	HD 283570	literature giant
043238.9+235825	IRAS 04296+2352	literature giant
043858.2+263108	Eliia 3-14	literature giant
043926.9+255259	Eliia 3-15	literature giant
043938.8+261126	Eliia 3-16	literature giant
044057.4+255413	[TNS87] 8	literature giant
042907.6+244350	Elias 3-6	background giant; name incorrectly associated with IRAS 04260+2437 and HH 414
Background giants based on brightness		
041324.4+290722	HDS 537	bright, assumed to be giant; our type is M5
041443.5+281708	[WSB2007] J041443.5+281708	bright, assumed to be giant
041943.4+272056	...	bright, assumed to be giant; our type is M3
042115.2+272101	HD 27482	bright, assumed to be giant
042344.1+225753	V1142 Tau	bright, assumed to be giant; our type is M2
042344.1+225757	...	bright, assumed to be giant
042345.3+234503	IRAS 04207+2338	bright, assumed to be giant
042517.3+280440	IRAS 04221+2757	bright, assumed to be giant; our type is M5
042519.3+261701	IRAS 04222+2610	bright, assumed to be giant; our type is M4
042630.0+255344	IRAS 04234+2547	bright, assumed to be giant; our type is M6
042731.3+270958	IRAS 04244+2703	bright, assumed to be giant; our type is M9
042805.4+284433	...	bright, assumed to be giant; our type is K6
042955.3+225857	IRAS 04269+2252 = 2MASS 04295531+2258579	bright, assumed to be giant (also Shenoy et al. object); our type is M8
043121.1+265842	...	bright, assumed to be giant (also Shenoy et al. object); our type is M8
043248.0+223952	GSC 01829-01009 = 2MASS J04324806+2239523	bright, assumed to be giant; our type is M9
043453.4+270534	2MASS J04345345+2705346	bright, assumed to be giant; our type is K7 with substantial A_V
043706.6+214241	...	bright, assumed to be giant; our type is K2-3
043856.3+271642	HD 283753	bright, assumed to be giant; literature type is F6III
044118.4+240157	...	bright, assumed to be giant (also Shenoy et al. object); our type is M5
044401.6+252014	DO 10700	bright, assumed to be giant; our type is M5
044435.0+250108	...	bright, assumed to be giant (also Shenoy et al. object); our type is M9
044510.7+244156	IRC +20091	bright, assumed to be giant; our type is M8
044659.2+253657	IRC +30094 = 2MASS J04465929+2536575	bright, assumed to be giant
Insignificant IR excess		
041501.1+250432	...	our type is G8-K0
041539.2+235344	...	(unobserved)
041643.3+244717	NLTT 12897	(unobserved)
041702.9+242425	...	our type is K0-K2
041707.0+293104	...	our type is K3
041734.0+240153	...	our type is G6
041934.0+252302	...	our type is K2

Table 11—Continued

SST Tau number	Other names	Notes
042216.3+262635	...	our type is G3-G5
042359.7+251452	...	our type is M4
042414.2+252350	...	our type is F5
042635.1+254223	...	our type is G6
042739.6+254208	...	our type is F0
042834.4+262104	...	(unobserved)
042859.4+273625	...	our type is B9-A0 w/ substantial A_V
043040.8+235034	...	our type is F6
043203.7+241223	...	our type is F0
043223.4+230059	...	our type is K2-K3 w/ substantial A_V
043237.5+292556	...	our type is F0
043254.0+294538	...	our type is G6-K0
043304.9+253705	...	our type is K0-K2
043335.6+242800	2MASS J04333567+2428004	our type is K2 w/ substantial A_V
043348.2+274400	...	our type is F0
043354.3+285413	...	(unobserved)
043433.3+244312	IRAS 04315+2436	our type is M5
043458.8+240958	2MASS J04345881+2409587	our type is K2
043544.2+215743	...	our type is F0
043822.9+221048	...	our type is K2-K3
043853.4+251909	...	our type is F8
044018.8+243234	...	our type is G5
044146.7+253824	[THL2004] 2MASS TMR523	reported as potential Taurus member in literature
044216.7+263917	...	our type is K2
044329.3+260818	...	our type is K1
044334.9+263505	...	our type is G8-K2
044348.0+242723	...	our type is K0-K2
044415.9+255300	...	our type is F1
044453.1+261257	...	our type is A9-F0
044700.1+242745	...	our type is G8-K2
044734.9+234528	...	our type is M2
044827.1+263006	...	our type is F0-F1
044931.5+244935	...	our type is K5
8 μ m pop-ups		
041136.6+293522	...	likely galaxy
041351.6+263819	2MASX 04135166+2638195	likely galaxy
041447.7+254956	2MASX 04144776+2549564	likely galaxy
041525.4+245339	2MASX 04152538+2453388	likely galaxy
041529.1+245942	...	likely galaxy
041556.9+261559	...	likely galaxy
041613.6+253134	2MASX 04161364+2531351	likely galaxy
041711.4+282157	...	likely galaxy
041718.0+291940	...	likely galaxy
041742.5+275427	...	likely galaxy
041756.2+250622	...	likely galaxy
041829.1+285127	...	likely galaxy
041842.1+283543	...	likely galaxy
041843.7+250715	...	likely galaxy
041903.8+271552	...	likely galaxy
041916.1+250413	...	likely galaxy
041929.7+253802	...	likely galaxy
041950.1+251009	...	likely galaxy
042043.7+252715	...	likely galaxy
042047.0+282000	...	likely galaxy
042140.8+282611	2MASX 04214085+2826119	likely galaxy; spectroscopically confirmed xgal
042159.7+234810	...	likely galaxy
042252.9+225507	2MASX 04225293+2255071	likely galaxy; spectroscopically confirmed xgal
042257.6+243206	...	likely galaxy
042342.1+235903	...	likely galaxy

Table 11—Continued

SST Tau number	Other names	Notes
042343.7+245945	...	likely galaxy
042417.0+234144	...	likely galaxy
042417.9+272942	...	likely galaxy
042429.2+224613	...	likely galaxy
042521.7+262249	2MASX 04252174+2622493	likely galaxy
042634.9+260816	2MASS J04263497+2608161	likely galaxy; spectroscopically confirmed xgal
042654.0+262921	...	likely galaxy
042843.2+274001	...	likely galaxy
043028.2+280420	...	likely galaxy
043044.5+282640	...	likely galaxy
043114.1+245838	...	likely galaxy
043205.6+220627	...	likely galaxy
043241.0+251308	...	likely galaxy
043303.9+280846	...	likely galaxy
043329.4+262052	...	likely galaxy
043407.2+280154	...	likely galaxy; very noisy spectrum, could be consistent with low-z galaxy or late G/early K
043446.1+290451	2MASX 04344611+2904516	identified by both Gutermuth and c2d methods as likely YSO, but SED suggests likely galaxy; spectroscopically confirmed xgal
043456.7+232501	2MASX 04345670+2325016	likely galaxy
043513.3+232449	...	likely galaxy
043516.1+213943	...	likely galaxy
043712.3+260733	...	likely galaxy
043820.5+215748	2MASX 04382057+2157489	likely galaxy
043828.3+253223	...	likely galaxy
043931.8+214742	...	likely galaxy
043958.0+253354	...	likely galaxy
044114.8+253242	...	likely galaxy
044308.1+240957	...	likely galaxy
044554.8+240843	IRAS04428+2403	galaxy; listed by Kenyon et al. (2008) as confirmed Taurus member
044614.5+253100	...	likely galaxy
044717.7+234529	2MASX 04471766+2345296	likely galaxy
044933.6+234518	...	likely galaxy

^aThese objects were selected at various points in our selection process, but we have rejected these as YSOs. See associated text for much more information.

Table 12. Literature non-members regarded as potential new members

SST Tau number	Other names	Notes
041803.3+244009	2MASS 04180338+2440096	needs additional follow-up; our type is A9
041810.7+251957	[GBM90] L1506 1	probable new member, our type is K8-M0
041823.2+251928	2MASS 04182321+2519280	needs additional follow-up; our type is G:
042212.9+254659	2MASS 04221295+2546598	pending follow-up
042518.6+255535	2MASS 04251866+2555359	Shenoy et al. object; needs additional follow-up; our type is M5.
042920.8+274207	2MASS 04292083+2742074	possible new member; our type is M6.
043024.1+281916	2MASS 04302414+2819165	Shenoy et al. object; needs additional follow-up; our type is M5
043042.8+274329	2MASS 04304284+2743299	Shenoy et al. object; needs additional follow-up; our type is M6
043228.1+271122	2MASS 04322815+2711228	Shenoy et al. object; needs additional follow-up; our type is M6
043344.6+261500	2MASS 04334465+2615005	new member; Shenoy et al. object; our type is M6e
043435.4+264406	2MASS 04343549+2644062	Shenoy et al. object; needs additional follow-up; our type is M3
044125.7+254349	2MASS 04412575+2543492	pending follow-up
044539.8+251704	2MASS 04453986+2517045	Shenoy et al. object; needs additional follow-up; our type is M5
044557.0+244042	2MASS 04455704+2440423	needs additional follow-up; our type is K2
044639.8+242526	2MASS 04463986+2425260	Shenoy et al. object; needs additional follow-up; our type is M5

^aThese objects were noted in the literature as likely non-members, but we have promoted them to be candidate members based on our Spitzer observations. See text for more information.

B. Comments on individual miscellaneous non-YSO objects with YSO-like colors

In the process of conducting our detailed source-by-source examination, we encountered many objects with YSO-like colors that were not YSOs, such as planetary nebulae and carbon stars. In some cases, these objects are new discoveries, or our observations shed new light on the nature of the object.

B.1. Planetary nebulae

Based on imaging, we may have discovered a planetary nebula: SST Tau 041936.1+271731. It appears bright at 24 and 70 μm , but CFHT imaging reveals a circularly symmetric structure that strongly suggests a planetary nebula. We have not yet obtained follow-up spectroscopy.

PN G174.2-14.6 (=043723.4+250242) is a well-studied planetary nebula (55 references are given in SIMBAD). It appears to have YSO-like colors in [24] vs. [24]–[70], [8] vs. [8]–[24], [4.5] vs. [4.5]–[8] (although it appears as faint enough to likely be a galaxy here), and the IRAC color-color diagram. We ruled it out as a YSO candidate based on the literature early on in our weeding process.

B.2. Carbon stars

C* 228 (043748.2+254926) is a previously identified carbon star. It has YSO-like colors in [24] vs. [24]–[70] and [8] vs. [8]–[24]. We ruled it out as a YSO candidate based on the literature early on in our weeding process.

Two of the objects we selected initially as YSO candidates turned out to be carbon stars when we obtained spectra: 043250.3+294239 (=IRAS 04296+2936) and 042818.5+253140 (=V414 Tau). IRAS 04296+2936 appears to have no references in SIMBAD and may therefore be a newly discovered carbon star; V414 Tau appears in a handful of publications as a carbon star, including Alksnis et al. (2001). IRAS 04296+2936 has a significantly reddened spectrum, at least in comparison to V414 Tau.

The 2MASS NIR JHK_s photometry for these objects are 8.02, 6.59, and 5.64 for IRAS 04296+2936, 7.28, 6.11, and 5.49 for V414 Tau; C* 228 is only unsaturated at H and is 3.38 mag. These first two objects both have colors considerably redder than those for carbon giants or dwarfs as appearing in Lowrance et al. (2003), and all three are very much brighter than those in Lowrance et al. (2003). If they are carbon dwarfs, they would have to be considerably closer than Taurus, as in ~ 10 pc. However, they are so red in $J - H$ that they are most likely giants; they are so bright that they are most likely background objects, behind the Taurus molecular cloud.

Thus far, we have found 3 carbon stars with YSO-like colors in this ~ 44 square degree survey. It is possible, indeed likely, that more carbon stars are in our survey, but have not been identified as such.

B.3. Be background giant(s)

One of the stars we selected as a YSO candidate based on three of our color spaces, 043724.8+270919 (also known as SV* SVS 1085=HD 283751), has $H\alpha$ strongly in emission, and we classify it as a B8e. We do not have any optical photometry for it, but its 2MASS JHK_s are 9.79, 9.55, and 9.30 mags, respectively.

Using its K_s mag and assuming no reddening (as a worst-case but clearly incorrect scenario), and comparing the observed K_s to that expected for young stars, we calculate a distance of ~ 700 pc. It seems to be a Be star well behind the Taurus cloud.

043939.9+252034 (JH 225) is listed in the literature as likely non-member based solely on high proper motions. We find that it is a B9 with substantial A_V . Its 2MASS JHK_s are 9.48, 9.01, and 8.73 mags, respectively. As we did above, we calculate a distance of 600 pc. It is also unlikely to be truly a member of Taurus, but additional follow-up is needed. It does not have emission lines.

Since these objects were selected as YSO candidates, flux densities appear in the Tables above, and SEDs appear in Appendix A.

B.4. Other very bright objects and giants

Table 11 includes several bright objects either assumed or confirmed to be background giants.

Several giants are confirmed in the literature (via spectroscopy) as being giants, but are selected in at least one of our color spaces as being YSO candidates. We ruled these out as YSO candidates based on the literature early on in our weeding process.

Elias 3-6 (SST Tau J042907.6+244350) has often appeared in lists of Taurus cloud members. There has been confusion in the literature about its IRAS association, with a mistaken identification with IRAS 04264+2433 (the HH 414 jet source) often quoted (e.g., Motte and Andre 2001). Elias 3-6 is actually IRAS 04260+2437. At $K_s=2.85$, it is much brighter than any known Taurus member, is saturated in the Spitzer IRAC bands, and shows a $[24]-[70]$ color of 0.04 mag that is consistent with a bright photosphere. Elias et al. (1978) classify it as a field M8 III giant with 6 mag of visual extinction. The Spitzer results are fully consistent with Elias’ original result that this object is not a Taurus member. We drop it from the list as a background giant.

Several objects listed in Table 11 are very, very bright in our survey, and we have assumed primarily based on brightness (and the fact that they seem to have little legitimate IR excess as far as we can determine) that they are background giants. Several of them were selected in at least one of our color spaces as potential YSOs (given the available photometry points; in many cases later inspection of these images suggested that they were probably saturated, or at least in the non-linear regime). In some of those cases, since we wondered if they could be YSOs, we obtained spectra of them; the resultant spectral type is listed in Table 11 for use by the community in future studies.

B.5. Objects with insignificant IR excesses for which we have spectra

Several objects appeared upon early inspection to have significant IR excesses at Spitzer bands, and thus we obtained spectra of them. However, upon re-examination, we determined that the IR excesses we detect were not significantly above the expected photosphere. Since these objects are no longer YSO candidates, they do not appear in tables in the main body of the text above nor in SEDs below. However, since we obtained spectra for many of them, we still report them here for use by the community. They are listed in Table 11.

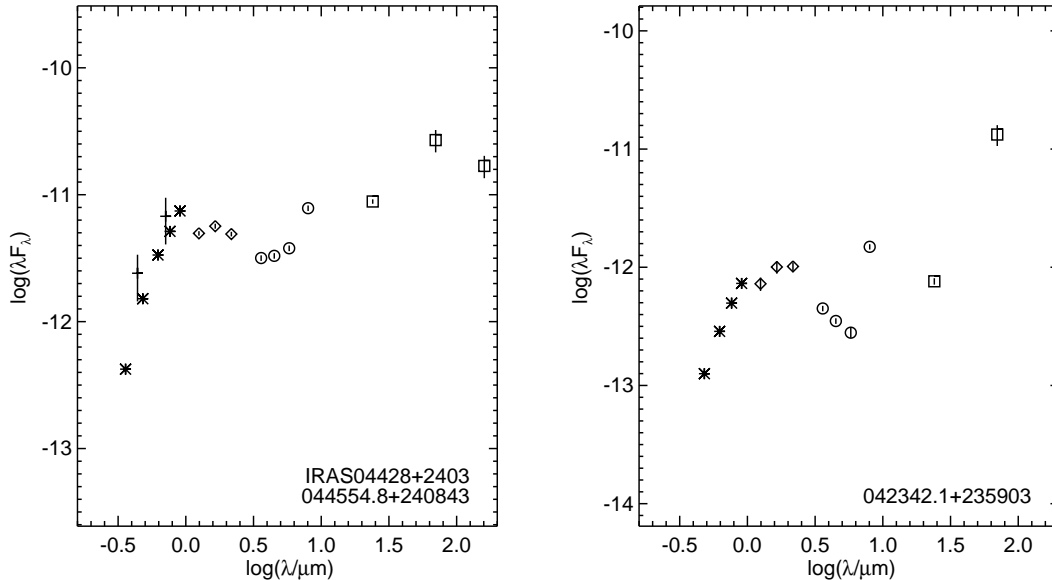


Fig. 13.— Example 8 μm pop-up SEDs for two objects, 044554.8+240843=IRAS 04428+2403 and 042342.1+235903. Notation is as it is for all of the other SEDs in this paper. Both of these objects are likely to be galaxies.

B.6. Extragalactic objects from Luhman et al.

Eight objects show up as having YSO-like colors in at least one of the color spaces we investigated and are reported as spectroscopically confirmed non-members by Luhman et al. (2006, 2009b). Each of these objects are ones that we had independently discarded as likely galaxies based on inspection of our optical imaging: 041916.1+275048, 042754.4+242414, 042336.9+252628, 042535.5+245739, 043027.1+280707, 043401.8+231906, 043502.0+233141, and 044554.8+240843. This further demonstrates the critical importance of high-spatial-resolution optical imaging in refining a YSO candidate list selected based on Spitzer data, before using valuable spectroscopic telescope time to refute or confirm stellar nature and youth.

B.7. IRAS 04428+2403 and other 8 μm pop-up objects

IRAS 04428+2403 (SSTTau 044554.8+240843) appears in Kenyon et al. (2008) listed as a confirmed member of Taurus. However, it appears in two prior papers in the literature, one which identifies it as a galaxy (Chamaraux et al. 1995), and the other which (Kenyon et al. 1994) identifies it as only an unconfirmed Taurus member. By inspection of all our available imaging (prior to identifying it with a literature object), we classified it as a galaxy based on its appearance in the optical images. The SDSS imaging pipeline classified this object as extended. SDSS also obtained a spectrum of this object, and it is a very reddened (due to the Taurus cloud) star-forming galaxy with bright $\text{H}\alpha/\text{N II}$ and S II at a redshift of 0.077. Therefore, we drop this object from our list of previously-identified members.

The SED for IRAS 04428+2403 (seen in Figure 13) resembles those for a class of objects we found in the

process of looking for candidate YSOs. These objects seemed to meet all of our criteria for YSO candidacy (see §3.1.4). This population has SEDs that looked like they could be YSO candidates, but where the 8 μm point in the SED appears significantly above a line connecting the 5.8 and 24 μm points. Several of these objects were targeted for optical spectroscopy, and four of them were actually observed. All of them turned out to be extragalactic objects. Tens if not hundreds of the spatially resolved galaxies in our survey (such as IRAS 04428+2403, but also more obvious resolved galaxies) also have this kind of SED. So, we conclude that even though some of these objects are point sources as far as we can tell, they are extremely likely to be galaxies. An example SED for one of the point-like objects is given in Figure 13. All of the objects that were apparent point sources (e.g., the ones that fooled us) appear in Table 11. The ones that are confirmed extragalactic objects are indicated.

The most likely origin of the 8 micron popup is the polycyclic aromatic hydrocarbon (PAH) emission feature near 8 μm . Geers et al. (2009) have found that low-mass young stars almost always lack PAH emission features at 11 μm in Spitzer spectra or at 3.3 μm in ground-based spectra. Thus we do not expect faint cloud members to show this feature. However, these features are common in lower luminosity galaxies (Weedman & Houck 2009). PAH features are seen around luminous young stellar objects such as the Ae star HD 100546 (Malfait et al. 1998), where strong stellar ultraviolet fluxes can excite PAH emission. All of the 8 micron pop-up sources detected in the Taurus survey, if located at the cloud distance of 137 pc, would have low luminosities strongly inconsistent with an early spectral type. Thus we conclude that none of the 8 micron pop-up sources found in the Taurus survey field are consistent with low-luminosity Taurus members, and we have excluded them from the list of candidates.

C. Literature non-members regarded as potential new members

Several objects listed in the literature as non-members (e.g., assumed but not spectroscopically confirmed background objects) appear as having colors consistent with YSOs. In several cases, the literature regarded them as non-members not because of spectroscopic confirmation, but because of optical properties. Since we investigated their infrared properties for the first time, and found them to have infrared excesses, we have at least for the time being promoted them back to being YSO candidates rather than non-member candidates. These objects are all identified in the relevant tables above (including Table 11), and since they are still YSO candidates, their SEDs appear in Appendix A.

Shenoy et al. (2008) use the data from our Taurus-1 survey (as reported by Luhman et al. 2006) combined with 2MASS to create a catalog of objects they believe to be background objects. Several of the objects they report as candidate background objects are based on 2MASS-only measurements (no IRAC). Now, with the addition of the MIPS-24 data (as well as the IRAC data for the rest of the survey), many of them show up as likely YSO candidates in at least one of our color spaces we investigated. We have promoted several of the objects reported in Shenoy et al. (2008) to potential members; they are listed and identified in the relevant tables in the main body of the paper, but listed in Table 11 as just “Shenoy et al. object.” Most of these objects do not have obvious signs of youth in the spectra we have, so additional data are needed to determine if they are members.

A few objects merit special discussion. The first, 041810.7+251957 ([GBM90] L1506 1), is listed by Goodman et al. (1990) as one of the objects for which the authors measured polarimetry, and therefore they assumed was a background object, but is not called out as anything remarkable in any other sense. It appears as a strong YSO candidate in all of the color-magnitude spaces we investigated. We have it listed

in the tables above as a new member, with a spectral type that we determined to be K8-M0, substantial emission lines in the spectrum, and a YSO SED class of II.

The second object of note is 042920.8+274207 (2MASS 04292083+2742074), which appears in Luhman et al. (2009b) as a background giant, M5III. We report it as a possible new member based on all the information we have; our type is M6 with low gravity. It shares many characteristics of young stars, but also those of some post-main-sequence objects. Further investigation is needed.

We wish to thank the Palomar Observatory, Sloan Telescope, CFHT, XMM-Newton, and of course Spitzer staff for their assistance using the telescopes.

We wish to thank the anonymous referee for thoughtful and thorough comments.

This work is based in part on observations made with the Spitzer Space Telescope, which is operated by the Jet Propulsion Laboratory, California Institute of Technology under a contract with NASA. Support for this work was provided by NASA through an award issued by JPL/Caltech.

This research has made use of NASA’s Astrophysics Data System (ADS) Abstract Service, and of the SIMBAD database, operated at CDS, Strasbourg, France. This research has made use of data products from the Two Micron All-Sky Survey (2MASS), which is a joint project of the University of Massachusetts and the Infrared Processing and Analysis Center, funded by the National Aeronautics and Space Administration and the National Science Foundation. These data are served by the NASA/IPAC Infrared Science Archive, which is operated by the Jet Propulsion Laboratory, California Institute of Technology, under contract with the National Aeronautics and Space Administration. This research has made use of the Digitized Sky Surveys, which were produced at the Space Telescope Science Institute under U.S. Government grant NAG W-2166. The images of these surveys are based on photographic data obtained using the Oschin Schmidt Telescope on Palomar Mountain and the UK Schmidt Telescope. The plates were processed into the present compressed digital form with the permission of these institutions. This research has made use of observations obtained with XMM-Newton, an ESA science mission with instruments and contributions directly funded by ESA member states and the USA (NASA).

The research described in this paper was partially carried out at the Jet Propulsion Laboratory, California Institute of Technology, under contract with the National Aeronautics and Space Administration.

M. Audard and C. Baldwin-Saavedra acknowledge support from a Swiss National Science Foundation grant (PP002–110504).

REFERENCES

- Alcalá, J., et al., *A&AS*, 119, 7
Alksnis, A., et al., *Baltic Astronomy*, 10, 1
Allen, L. E., et al. 2004, *ApJS*, 154, 363
Audard, M., et al., 2007, *A&A*, 468, 379
Aumann, H., et al., 1984, *ApJ*, 278, 23
Barrado y Navascués, D., & Martín, E., 2003, *AJ*, 126, 2997

- Beichman, C., et al., 1986, ApJ, 307, 337
- Bary, J., et al., BAAS, 21115406
- Bessell, 1979, PASP, 91, 589
- Carpenter, J., et al., 2001, AJ, 121, 3160
- Chamaraux, et al., 1995, A&A, 299 347
- Chen, B., et al., 2004, “OM Calibration Status”, XMM-Newton OM calibration documentation
http://xmm.vilspa.esa.es/sas/7.0.0/watchout/Evergreen_tips_and_tricks/uvflux.shtml
- Cieza, L., & Baliber, N., 2007, ApJ, 671, 605
- Cox, A. N., ed., Allen’s Astrophysical Quantities, Fourth Edition, 2000, Springer-Verlag
- D’Alessio, P., et al., 1999, ApJ, 527, 893
- Edwards, S., et al., 1993, AJ, 106, 372
- Elias, J., 1978, ApJ, 224, 857
- Evans, N. J., et al., 2003, PASP, 115, 965
- Evans, N. J., et al., 2007, c2d delivery document, SSC website
- Evans, N. J., et al., 2009, ApJS, 181, 321
- Fazio, G., et al., 2004, ApJS, 154, 10
- Finkbeiner, D., et al., 2004, AJ 128, 2577
- Flaccomio, E., et al., 2003, A&A, 402, 277
- Furlan, E., et al., 2006, ApJS, 165, 568
- Geers, V., et al., 2009, A&A, 495, 837
- Goldsmith, P., et al., 2008, ApJ, 680, 428
- Goodman, A., et al., 1990, ApJ, 359, 363
- Güdel, M., et al., 2007, A&A, 468, 353
- Güdel, M., Padgett, D., & Dougados, C., 2007, in Protostars and Planets V, eds B. Reipurth, D. Jewitt,
and K. Keil, University of Arizona Press, Tucson, p.329-344
- Gautier, T. N., et al., 2007, ApJ, 667, 527
- Guieu, S., et al., 2006, A&A, 446, 485
- Guieu, S., et al., 2007, A&A, 465, 855
- Guieu, S., 2008, PhD Thesis
- Gutermuth, R., et al., 2008, ApJ, 674, 336

- Gutermuth, R., et al., 2009, ApJS, 184, 18
- Grankin, K., et al., 2008, A&A, 479, 827
- Hartmann, L., et al., 2005, ApJ, 629, 881
- Harvey, P., et al., 2007, ApJ, 663, 1149
- Hawarden, T., et al., 2001, MNRAS, 325, 563
- Herbig, G.H., & Rao, N. Kameswara, 1972, ApJ, 74, 401
- Hernandez, J., et al., 2008, ApJ, 686, 1195
- Jørgensen, J., et al., 2006, ApJ, 645, 1246
- Kenyon, S., et al., 1994, AJ, 108, 251
- Kenyon, S., et al., 2008, in the Handbook of Star Forming Regions, Volume I: The Northern Sky ASP Monograph Publications, Vol. 4. Edited by Bo Reipurth, p.405
- Lowrance, P., et al., 2003, ApJL, 584 95
- Luhman, K., et al., 2006, ApJ, 647, 1180
- Luhman, K., et al., 2009a, ApJL, 691, 1265
- Luhman, K., et al., 2009b, ApJ, 703, 399
- Malfait, et al., 1998, A&A, 332, L25
- Monin, J.-L., et al., 2007, BAAS, 211, 2906
- Monin, J.-L., et al., 2009, submitted
- Morales-Calderon, M., et al. 2009, in press
- Motte, F., & André, P., 2001, A&A, 365, 440
- Ogura, et al., 2002, AJ, 123, 2597
- Oliveira, I., et al., 2009, ApJ, 691, 672
- Padgett, D., et al., 2008, Taurus Legacy Delivery Document (P08), available from <http://ssc.spitzer.caltech.edu/legacy/taurushistory.html>
- Padgett, D., et al., 2009, ApJ, submitted?? (P09)
- Padgett, D., et al., 2008b, ApJ, 672, 1013
- Padmanabhan, N., 2008, ApJ, 674, 1217
- Rebull, L., 2001, AJ, 121, 1676
- Rebull, L., et al., 2007, ApJS, 171, 447
- Rebull, L., et al., 2000, AJ, 119, 3026

- Rebull, L., et al., 2006, ApJ, 131, 2934
- Rebull, L., et al., 2006b, ApJ, 646, 297
- Rieke, G., et al., 2004, ApJS, 154, 25
- Scelsi, L., et al., 2007, A&A, 468, 405
- Scelsi, L., et al., 2008, A&A, 490, 601
- Siess, L., Dufour, E., Forestini, M., 2000, A&A, 358, 593
- Shenoy, S., et al., 2008, ApJS, 176, 457
- Skrutskie, M., et al., 2006, AJ, 131, 1163
- Slesnick, C., et al., 2008, SpJ, 688, 377
- Tobin, J., et al., 2008, ApJ, 679, 1364
- Torres, R., et al., 2007, ApJ, 671, 1813
- Torres, R., et al., 2009, ApJ, 698, 242
- Weedman, D., & Houck, J., 2009, ApJ, 693, 370
- Werner, M., et al., 2004, ApJS, 154, 1
- Wolk, S., et al., 2006, AJ, 132, 1100

